

c. Strains in Cladding by Bending Operation

From simple geometry, a cylindrical tube of 0.5 in diameter bent around a wheel of 5.5 in. diameter will be subjected to a tensile strain ϵ_o in its outer surface, and

$$\epsilon_t = \frac{(\pi \times 6.5) - (\pi \times 6.0)}{(\pi \times 5.75)} \times 100\%$$

where 6.0 is the diameter at the neutral axis of the tube; i.e. $\epsilon_t = 8.33\%$. Similarly the tube will be subjected to a compressive strain ϵ_c at the inner surface, where $\epsilon_c = 8.33\%$.

Thus, a net strain of 8.33% will be imposed on the walls of the cladding within any arc deformed to the same radius as the ram used in this experiment. This strain level may be reduced if the tubing is able to absorb part of the strain in the segments on each side of the bending section; alternatively it can be locally increased above this level if, as may be expected in irradiated Zircaloy, the initial deformation softens the cladding in the deformed region (by annihilation of the radiation damage) thus facilitating further deformation in the same region at reduced load.

Without strain gauges on the surface or a grid system from which measurements could be made*, it was not possible to directly measure local strains in short arcs of the bending tubes. In some of the tests illustrated below, the tube clearly attained the diameter of the wheel over part of its length, and thus reached strains of 8.3% as calculated above. Estimates of strain in deformed areas of each specimen have been made where possible. Also to supplement this information, and to put the results in the context of rod behavior during the 'cask-drop' event under consideration, an arbitrary

*The time scale within which this experiment was carried out did not allow for use of such techniques.

measure of deflection is used; this is the deflection of a rod of length 13 in. having the deformed region starting 1 in. from one end, as shown in Figure V-45.

A value of 13 inches is selected as the maximum half-distance between internal grid supports in PWR bundles which are to be transported in the cask; these bundles will be the most highly stressed should the cask drop event occur.** This deflection thus indicates the capacity of the tubing to bend without rupture within the operating length of interest - and provides a very conservative measure of the available deflection since the deformation in these rods was localized within a length of less than 3 in.

**The 26-inch span is a maximum. The realistic span is the 18-1/2 inches of the basket spacer disks.

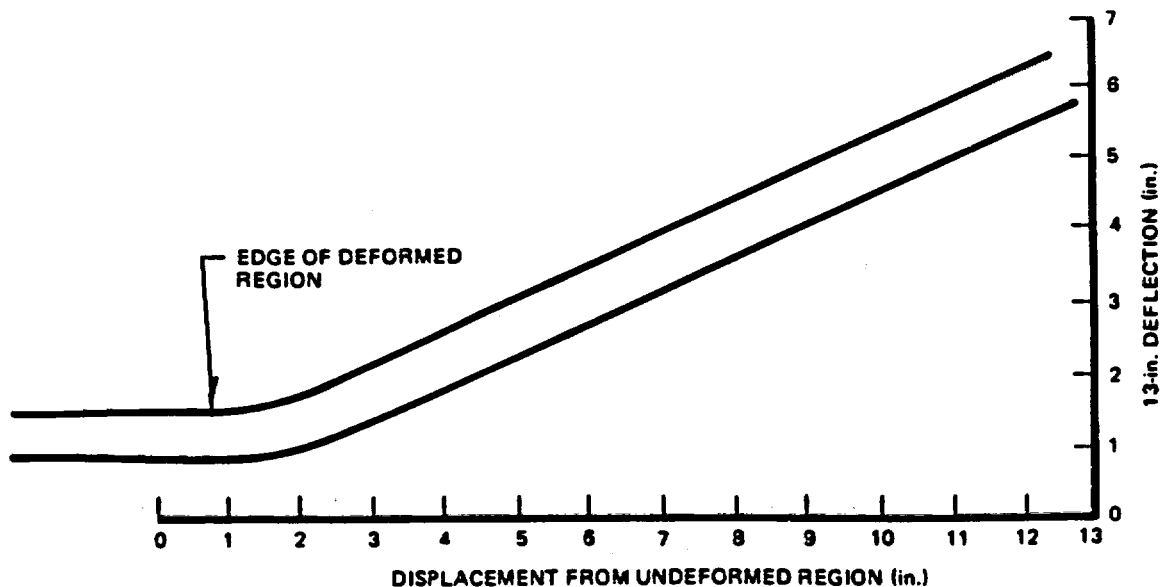


FIGURE V-45. MEASURE OF DEFLECTION

d. Test Results:

A summary of the deflections obtained in eleven specimens strained at rates estimated at 2×10^{-3} - 4×10^{-3} in/in/sec is given in Table V-30. Some specimens were strained further than others, but the objective of the experiment was to show that the rods could all absorb a strain of 3-6%, and that deflections in excess of 2 ins. could be attained within a 13 in. length of the cladding. The Figures V-47 through V-58 show ten of the specimens, including the two which failed under load. All of the specimens tested strained sufficiently that the elastic plus plastic component of the strain at the center of the bend approached, and in eight of the eleven cases certainly reached, the 8.3% stable strain required to fit the 5-1/2" diameter wheel. (Note that the strain in the outer surface reaches 6.7% when the diameter of neutral axis of the clad is 7-1/2".) Thus the strain in the bent section of the one specimen G11/E2-3A which failed at a deflection of 5/8" also exceeded 6.7%, and this tube showed a residual 2-1/8" deflection over 13". The failure mode in this rupture was ductile as indicated in Figure V-46.

In no case was any cracking observed in the nine specimens which were not strained to rupture.

The experiment demonstrates that Zircaloy cladding on high burn-up fuel has ample bending capacity to withstand the deflections and strains imposed in the hypothetical cask drop events.

Table V-30

<u>Specimen No.</u>	<u>Burn-Up MWd/T</u>	<u>Ram Deflection Reached, in.</u>	<u>Estimated Outer Surface Strain %</u>	<u>Residual 13" Deflection in.</u>	<u>Comments</u>	<u>Figure No.</u>
G28/D1-1A	12,000	>2	0.3	90° deflection	Failed	2, 12
G28/D1-1B	12,500	>1	0.3	>5	No cracking	3
G28/D1-2A	14,000	1-1/8	0.3	6	No cracking	4
G38/D1-2B	14,300	1-3/8	0.3	>9	No cracking	5
G28/D1-2C	14,500	1-1/8	0.3	6	No cracking	-
G11/E2-2A	15,500	5/8	6-8	>3	No cracking	6
G11/E2-2B	16,000	1-1/8	0.3	>5	No cracking	7
G11/E2-2C	16,300	1-1/8	0.3	6	No cracking	8
G11/E2-3A	16,500	5/8	6-8	>2-1/8	Failed	12
G11/E2-3B	16,800	1-1/4	0.3	>6	No cracking	9, 10
G11/E2-3C	17,050	5/8	6-8	>2-1/8	No cracking	1, 11

5-134

NEDO-10084-3
September 1984

The strain rate applied in these tests was estimated as $2 \times 10^{-3} - 4 \times 10^{-3}$ in/in/sec.

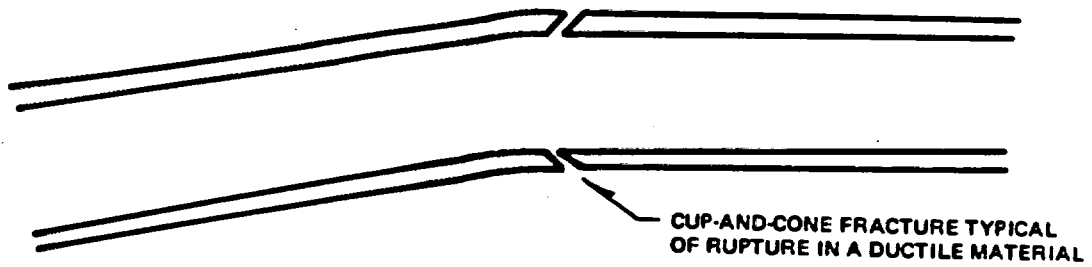


FIGURE V-46. DUCTILE FAILURE-SKETCH

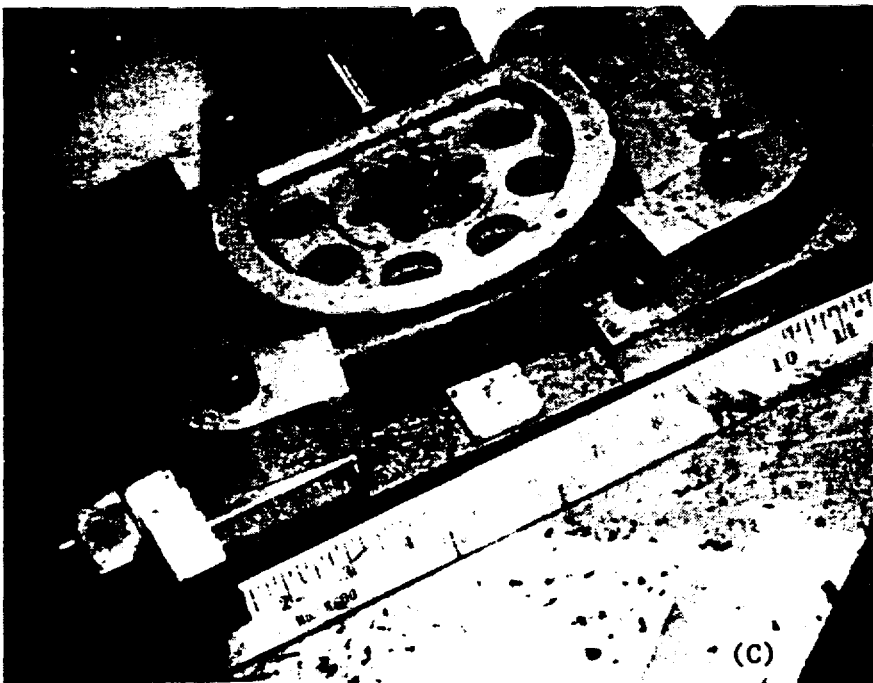
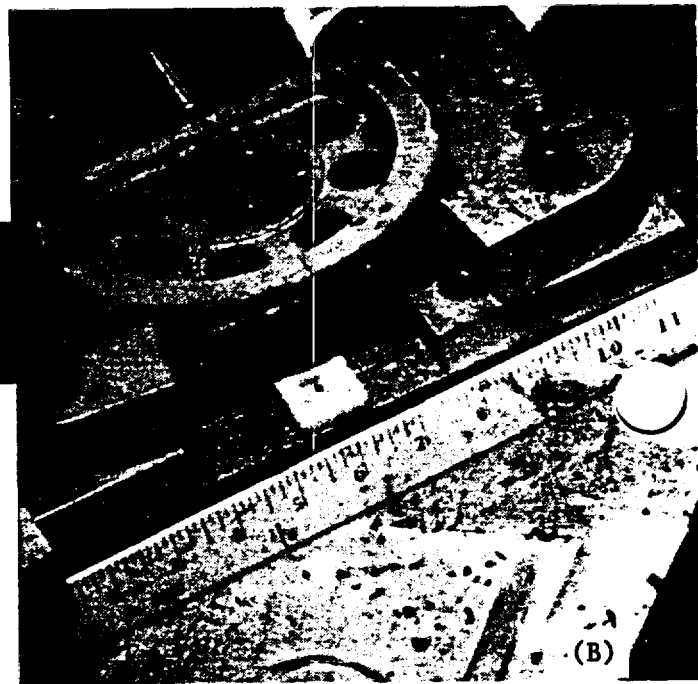
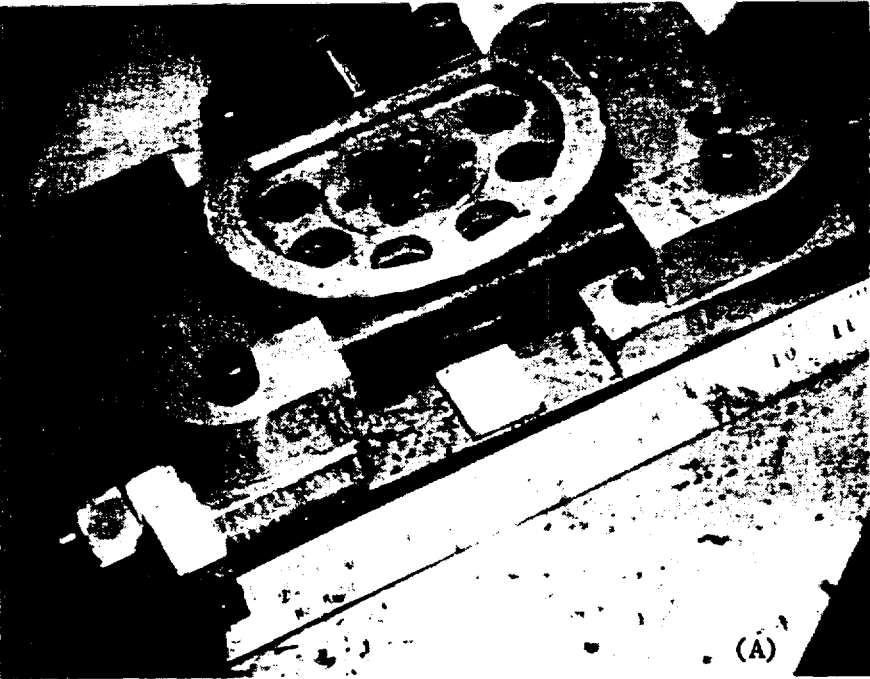
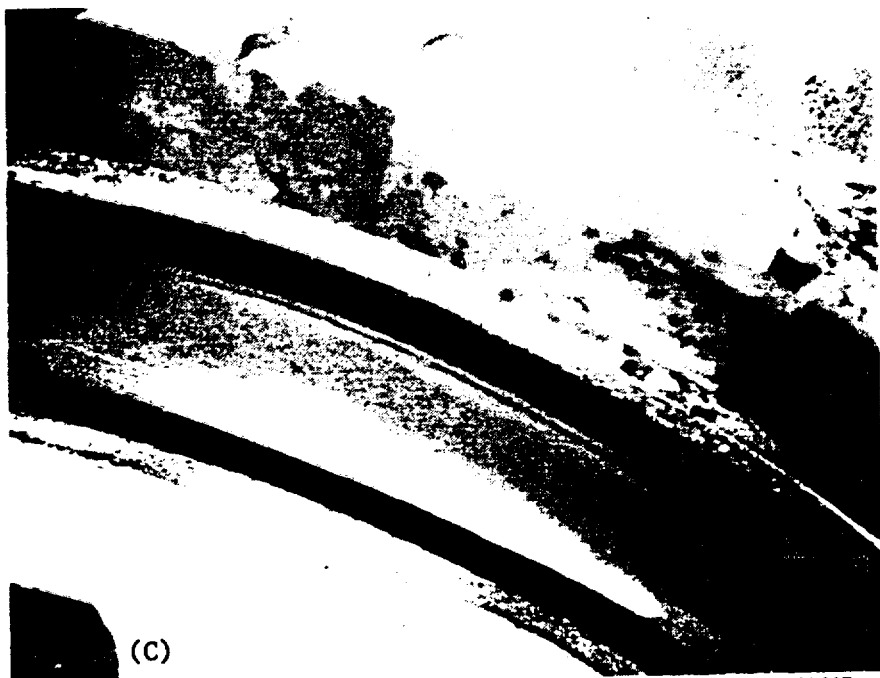
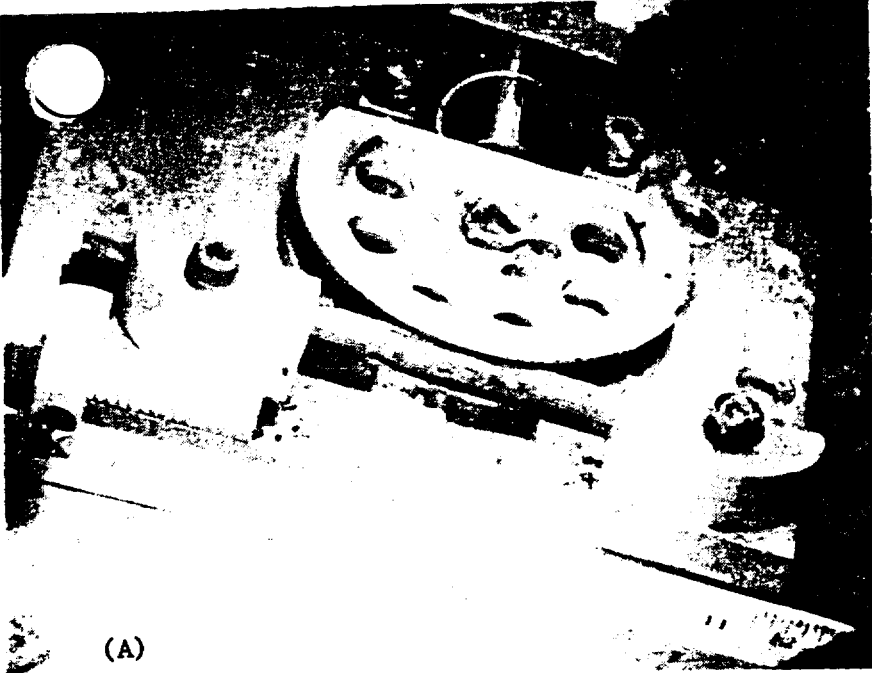
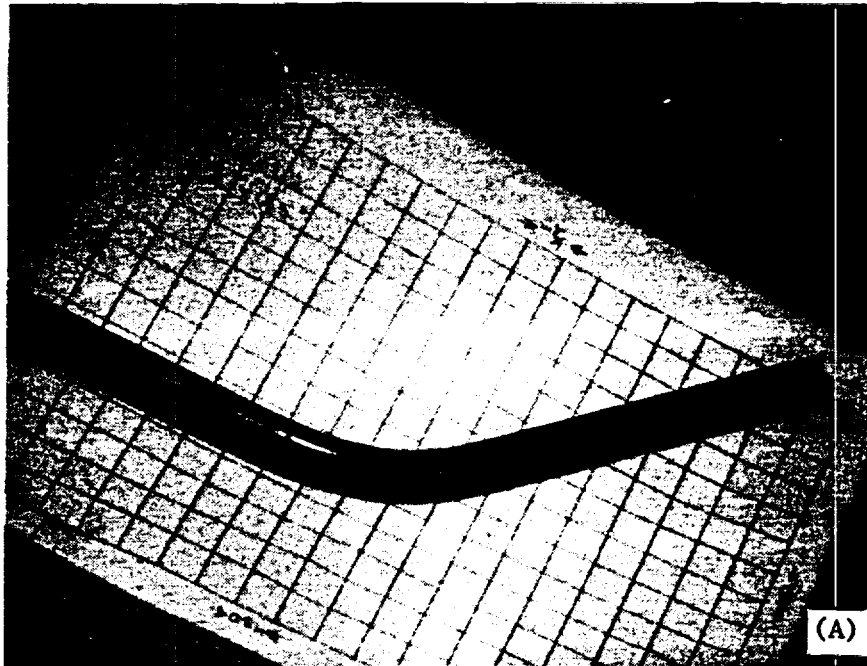


FIGURE V-47. (A) THE TUBE BENDING DEVICE, A PULLEY WHEEL OF 5-1/2" DIAMETER MOUNTED ON A HYDRAULIC RAM. SHOWS SPECIMEN NO. G11/E2-3C, BURN-UP 17,050 MWD/T, LOADED PRIOR TO DEFLECTION. DEFLECTIONS WERE MEASURED BY MEANS OF THE SCALE PERPENDICULAR TO THE ROD. (B) SAME SPECIMEN AFTER DEFLECTION THROUGH 3/8". NOTE THAT THE CRUD LAYER ON THE SURFACE IS BEGINNING TO SPALL AT THE BENT SECTION. (C) SAME SPECIMEN IN POSITION AS UNDER (B), AFTER THE CRUD HAS BEEN REMOVED WITH A WIRE BRUSH. (SEE FIGURE 11 FOR FURTHER DEFLECTION OF THIS SPECIMEN.)



**FIGURE V-48. (A) SPECIMEN NO. G28/D1-1A BURN-UP \sim 12,000 MWD/T AS LOADED
(B) SAME SPECIMEN DEFLECTED 1-1/8". THE SURFACE HAD BEEN WIRE BRUSHED
(C) CLOSE-UP OF BENT SURFACE UNDER LOAD, WITH STRAIN $>$ 8% (SEE TEXT).**



**FIGURE V-49. SPECIMEN NO. G28/D1-1B, BURN-UP $\sim 12,500$ MWD/T
(A) SPECIMEN REMOVED FROM DEVICE AFTER DEFLECTION TO 1". AFTER UNLOADING, 13" DEFLECTION IS ~ 9 ".
(B) OUTER SURFACE OF BENT SECTION. NO CRACKING.
MAGNIFICATION X 4.**

NEDO-10084-3
September 1984

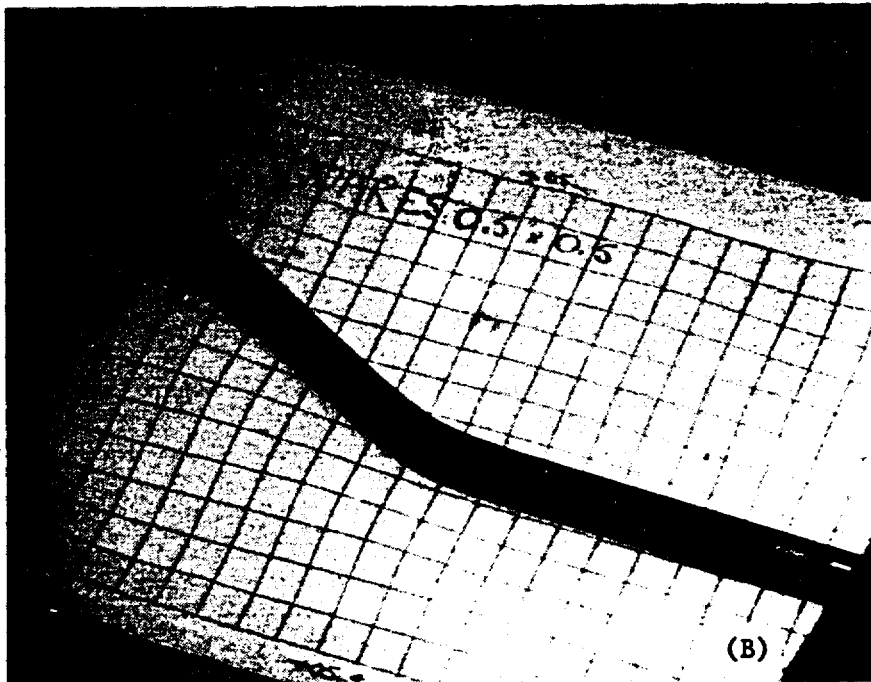
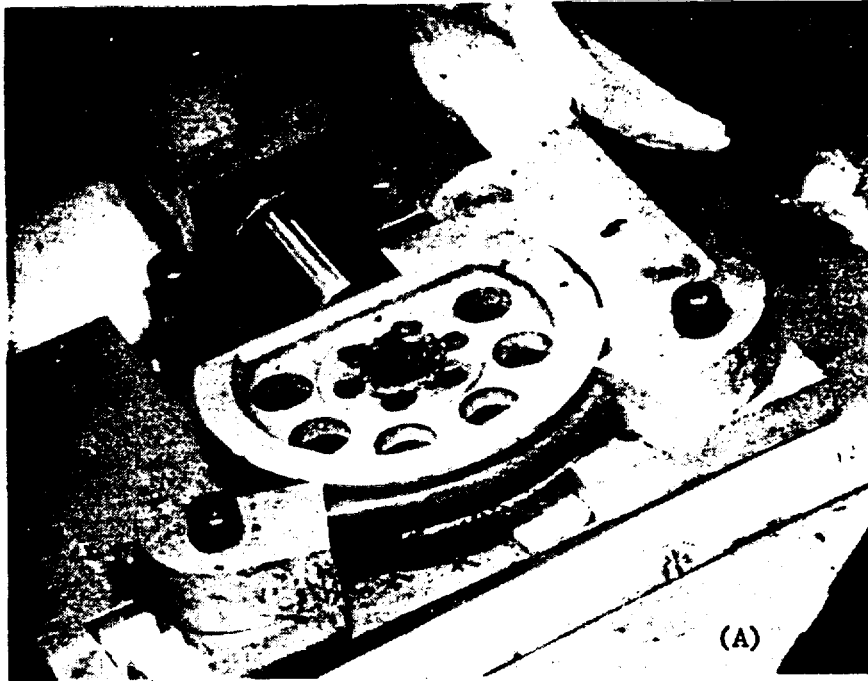


**FIGURE V-50. SPECIMEN NO. G28/D1-2A BURN-UP 14,000 MWD/T
(A) SPECIMEN IN DEVICE DEFLECTED TO 1-1/8"
(B) AFTER UNLOADING TO THIS DEFLECTION;
RESIDUAL 13" DEFLECTION IS 71**

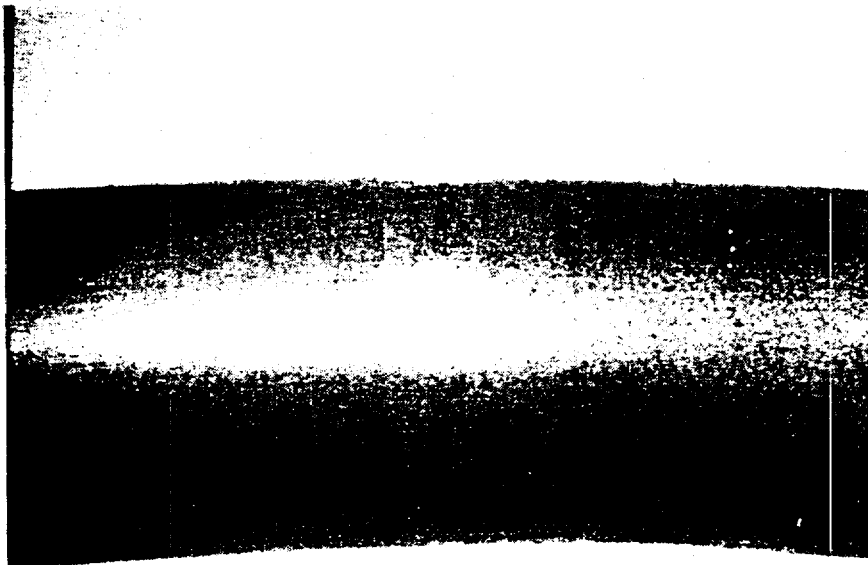
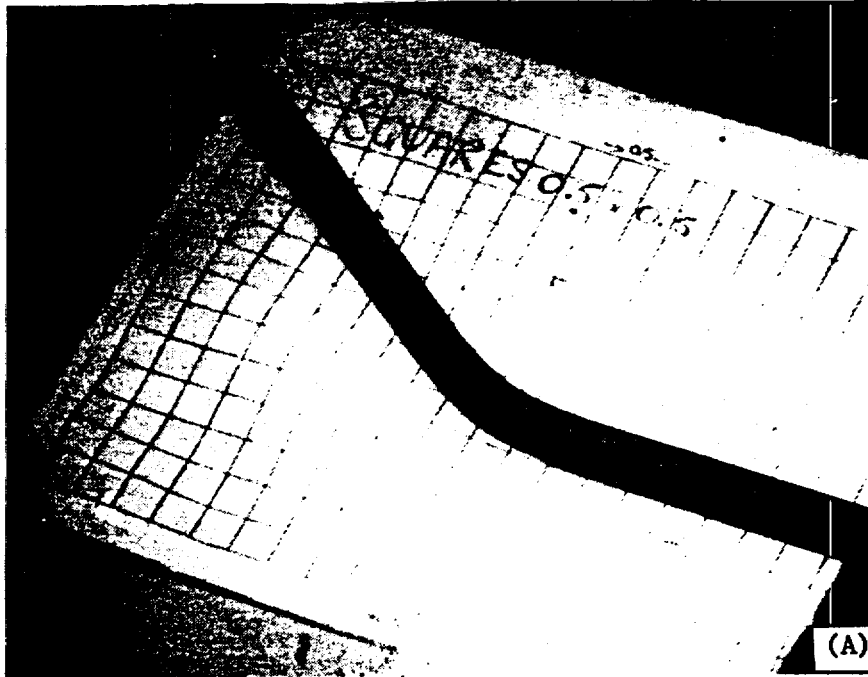


**FIGURE V-51. SPECIMEN NO. G28/D1-2B BURN-UP 14,300 MWD/T
(A) SPECIMEN UNLOADED AFTER DEFLECTION TO 1-3/8". RESIDUAL 13" DEFLECTION ~9"
(B) OUTER SURFACE OF BENT SECTIONS. NO CRACKING. VISIBLE MARKS ARE RESIDUE FROM
PROFILOMETRY. MAGNIFICATION x 3-1/2**

NEDO-10084-3
September 1984

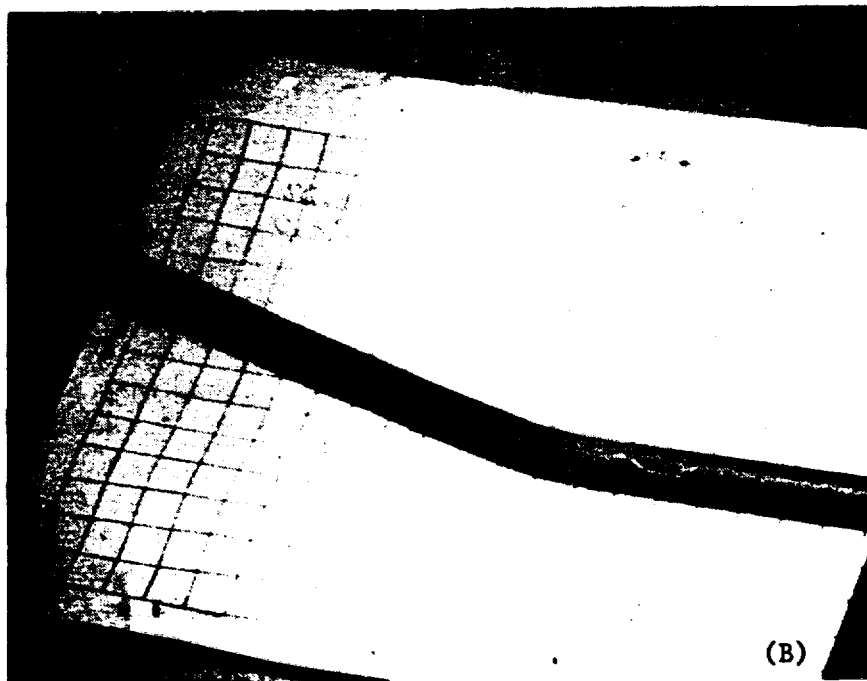
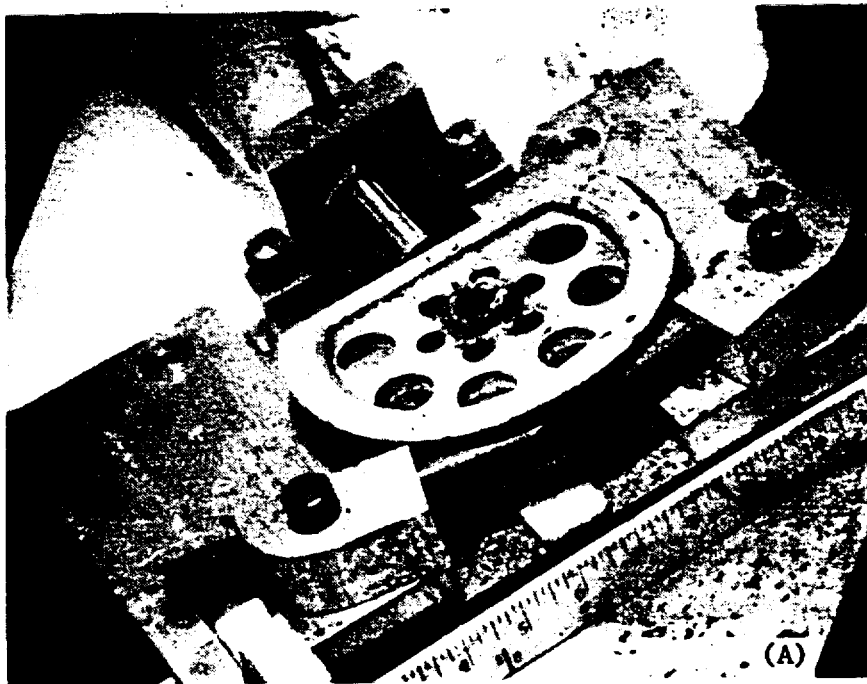


**FIGURE V-52. SPECIMEN NO. G11/E2-2A, BURN-UP 16,500 MWD/T
(A) SPECIMEN IN DEVICE, DEFLECTED TO 5/8".
CRUD LAYER SPALLING AT EDGE OF BENT SECTION
(B) AFTER REMOVAL FROM DEVICE AT THIS DEFLEC-
TION. RESIDUAL 13" DEFLECTION >3".**

NEDO-10084-3
September 1984

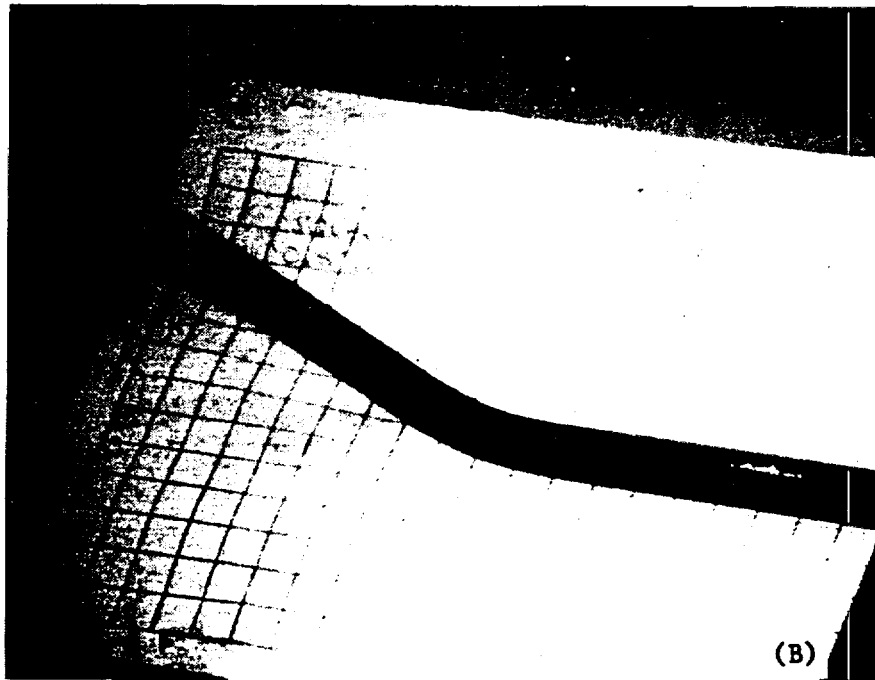
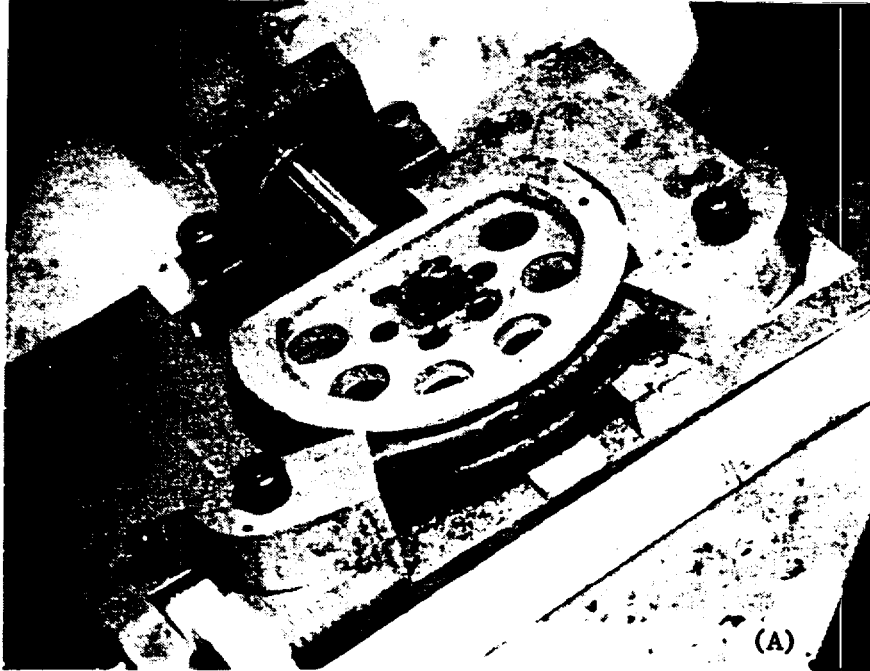


**FIGURE V-53. SPECIMEN NO. G11/E2-2K BURN-UP 16,000 MWD/T
(A) SPECIMEN IN DEVICE AT DEFLECTION TO 1-1/8".
CRUD LAYER IS SPALLING OVER BENT SECTION.
(B) AFTER UNLOADING AT THIS DEFLECTION.
RESIDUAL 13" DEFLECTION ~5".**

NEDO-10084-3
September 1984

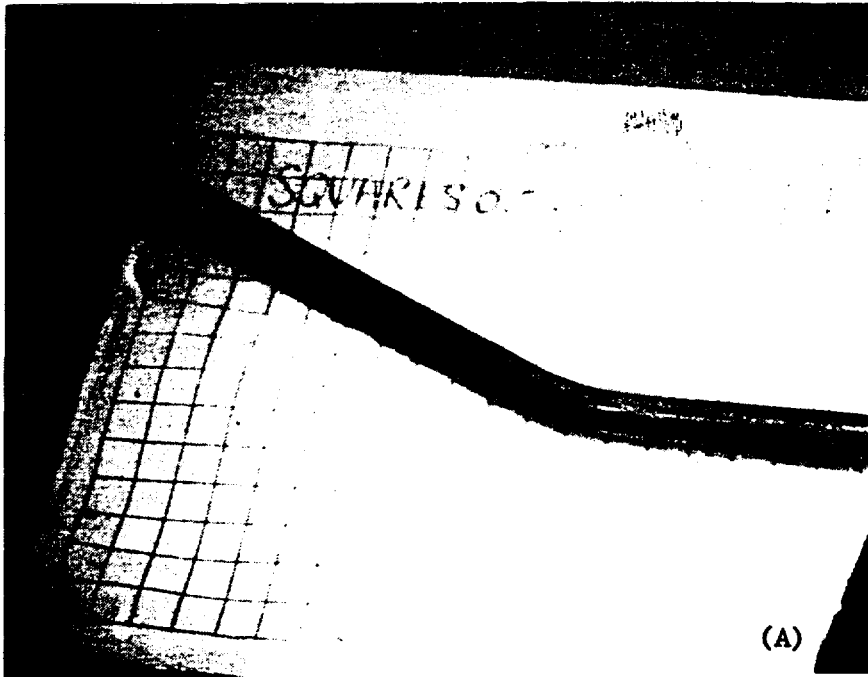


**FIGURE V-54. SPECIMEN NO. G11/E2-2C, BURN-UP \sim 16,300 MWD/T
(A) SPECIMEN AFTER REMOVAL FROM DEVICE AT DEFLECTION OF 1-1/8" RESIDUAL 13" DEFLECTION OF 6"
(B) OUTER SURFACE OF BENT SECTION. NO CRACKING BUT INDICATION OF NECKING. MAGNIFICATION X 4**

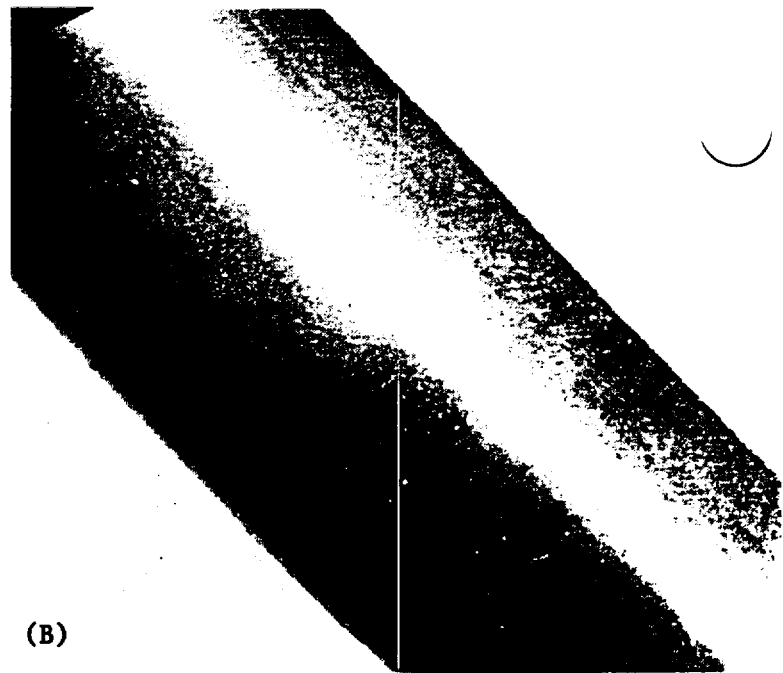
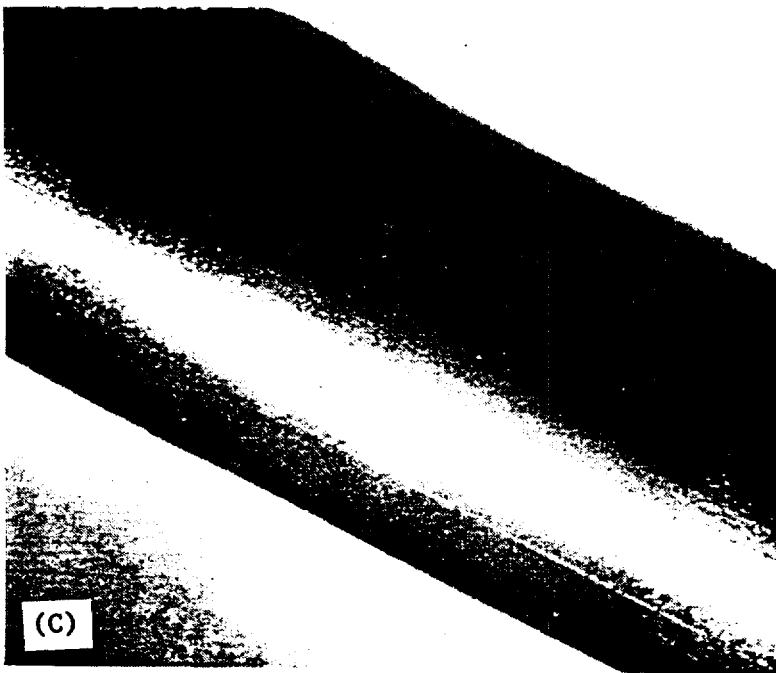
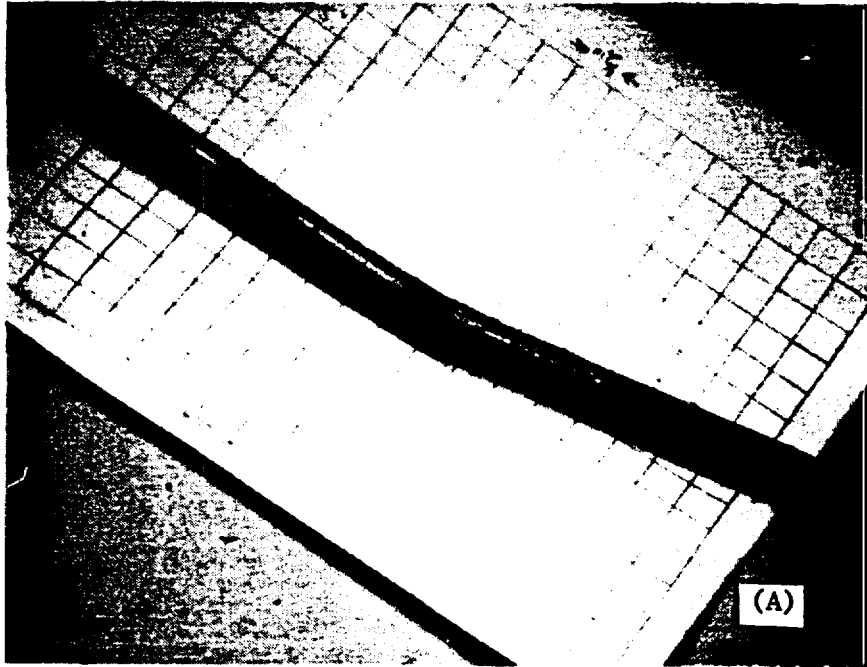
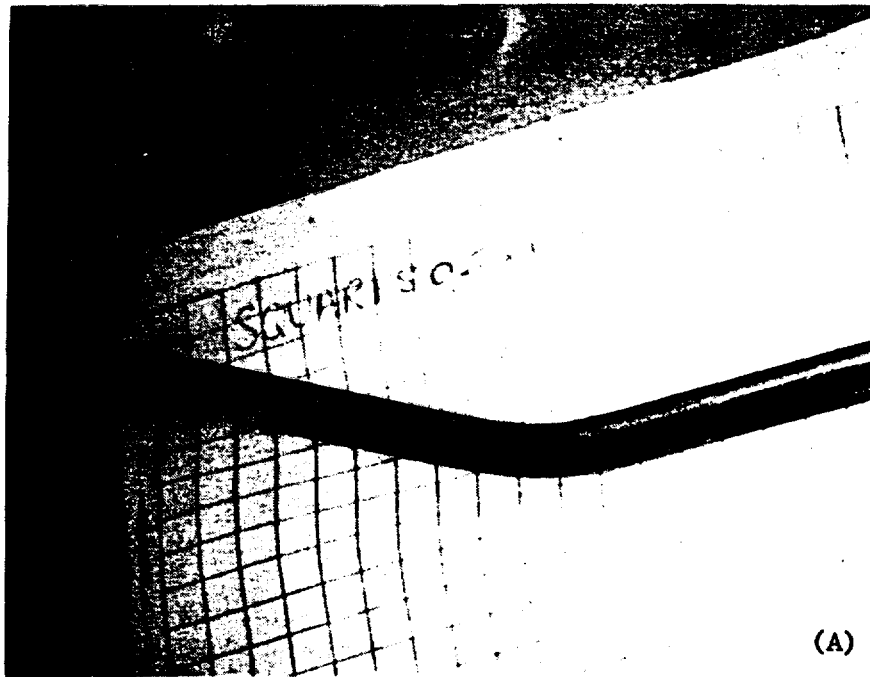
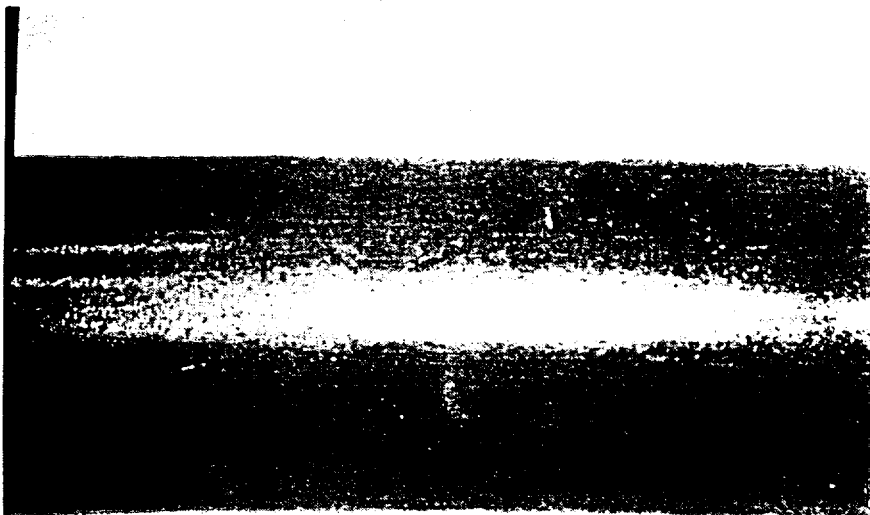


**FIGURE V-55. SPECIMEN NO. G11/E2 - 3B BURN-UP 16,800 MWD/T
(A) SPECIMEN REMOVED FROM DEVICE AFTER DEFLECTION TO 3/4". AFTER UNLOAD-
ING 13" DEFLECTION $>2\frac{1}{2}$ ".
(B) OUTER SURFACE OF BENT SECTION. NO CRACKING. MAGNIFICATION X 4.
(C) INNER SURFACE OF BENT SURFACE. NO CRACKING. MAGNIFICATION X 4.
(FOR FURTHER DEFLECTION OF THIS SPECIMEN SEE FIGURE 6.)**



(A)



(B)

**FIGURE V-56. SPECIMEN G11/E2-3B BURN-UP 16,800 MWD/T
(A) SPECIMEN REMOVED FROM DEVICE AFTER DEFLECTION TO $>1\frac{1}{4}$ ". AFTER UNLOADING 13" DEFLECTION IS >6 ".
(B) OUTER SURFACE OF BENT SECTION. NO CRACKING. MAGNIFICATION X 3-1/2.**

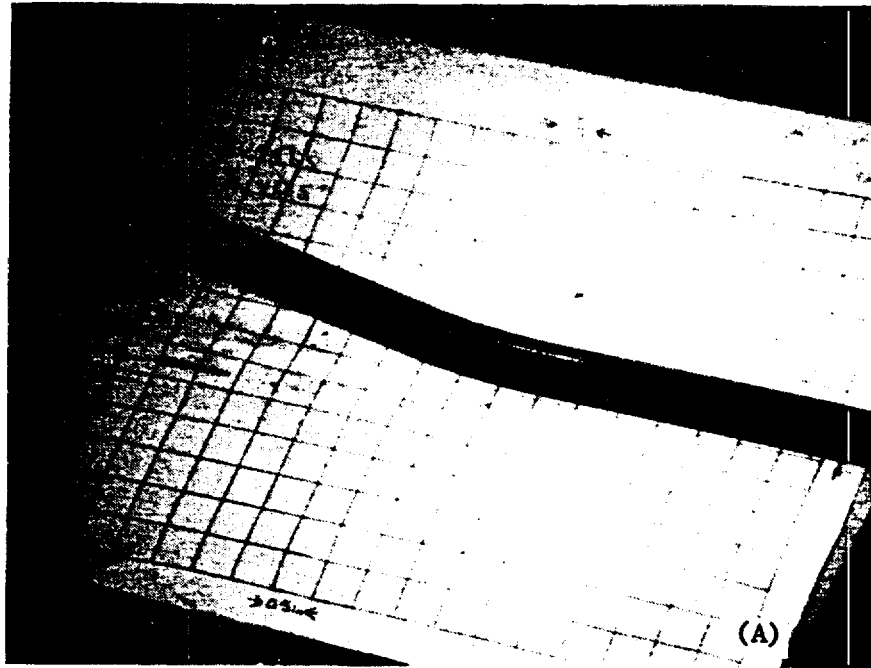


**FIGURE V-57. SPECIMEN NO. G11/E2 - 3C BURN-UP 17,050 MWD/T
(A) SPECIMEN REMOVED FROM DEVICE AFTER DEFLECTION TO 5/8". AFTER UNLOAD-
ING 13" DEFLECTION >2-1/8".
(B) OUTER SURFACE OF BENT SECTION. NO CRACKING. MAGNIFICATION X 4.5
(C) SIDE VIEW OF BENT SECTION. NO CRACKING. MAGNIFICATION X 3**

NEDO-10084-3
September 1984

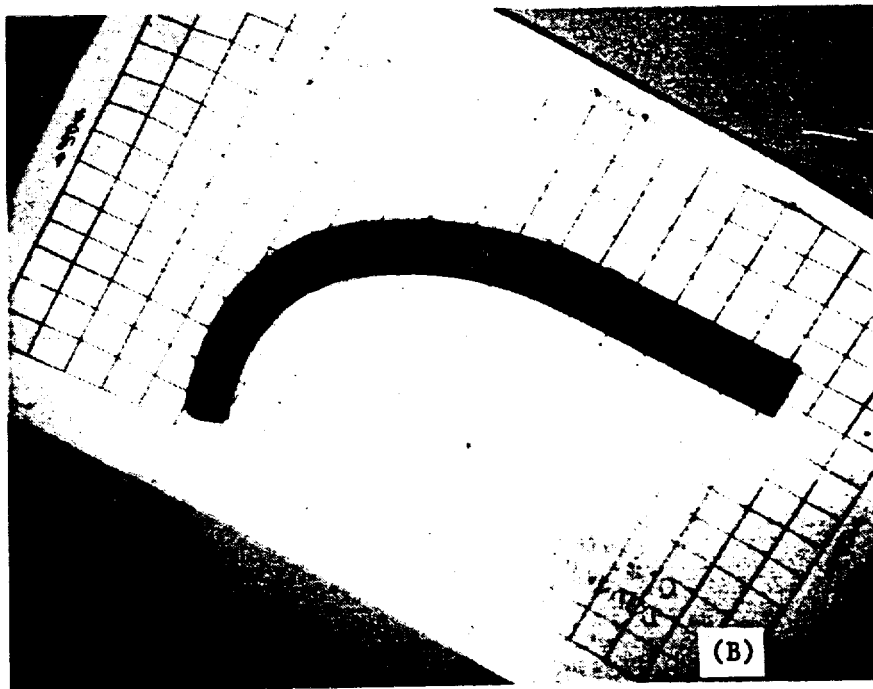
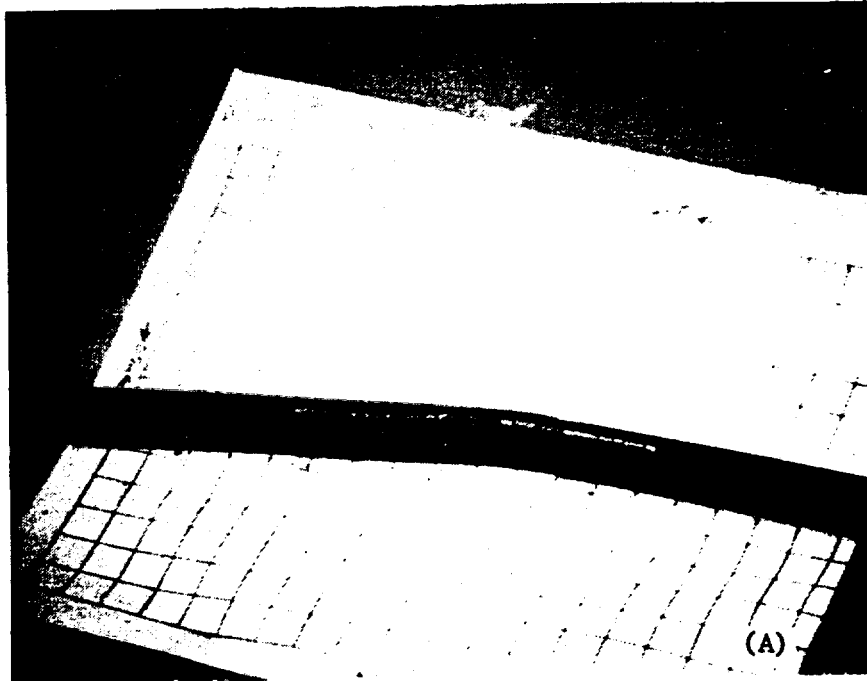


FIGURE V-58. (A) SPECIMEN NO. G11/E2-3A BURN-UP 16,000 MWD/T. THIS SPECIMEN RUPTURED AT THE EDGE OF THE BENT SECTION AFTER DEFLECTION TO $5/8$ ". RESIDUAL 13 " DEFLECTION $>2-1/8$ ". (B) SPECIMEN NO. G28/D1-1A BURN-UP 12,000 MWD/T. THIS SPECIMEN RUPTURED AFTER DEFLECTION >2 " AND AT LEAST 4 " OF ITS LENGTH HAS BEEN STRAINED $>6\%$.

5.6.5.A.4 Generic Side Drop Model - Group I Fuel

Table V-31 shows cladding and pellet parameters for a variety of fuel bundle types. The most highly stressed fuel rod is that described as the Point Beach 15 x 15 pressurized water reactor bundle. The stress level is primarily a result of the 26 inch span of the fuel rod between bundle grid spacers. This configuration was chosen as the "worst case" for modeling purposes. In addition the same fuel rod with an 18-1/2 inch span (typical of fuel basket support disc spacing) was modeled to calculate its reaction assuming it was unsupported between the basket support discs.

a. Model Description

The single fuel rod is modeled by a series of short rigid massless beams and concentrated weights connected by shear and moment springs. Spring properties represent the geometric and physical parameters of the fuel cladding (no credit is taken for the supporting effect of the contained uranium pellets). The mass terms represent the weight of the cladding plus the weight of the fuel pellets. Subsection 5.6.5.A.5 contains a detailed derivation of the bases for this dynamic model called "DYREC" by its author at Stearns-Roger Corporation. The model handles both elastic and plastic behavior of materials through a bilinear analysis.

The functioning of the model is similar to that of an earthquake analysis whereby the supports are accelerated and the structure examined for its response. After initial starting conditions the problem proceeds at some time-step applying the deceleration to the supports and examining the progressive response of each spring-mass element. The predictor-corrector routine takes the response parameters of the two preceding time steps and predicts the behavior of the system in the succeeding time interval. It then enters the shear-shear strain and moment-curvature plots to verify that the prediction

Table V-31
TYPICAL FUEL PROPERTIES

CLADDING											
Fuel Type	Material	P lb/in. ³	o.d. (in.)	t (in.)	i.d. (in.)	A (in. ²)	I (in. ⁴)	W ₁ lb/in.	Grid Span L (in.)	Grid Span Typical Reactor/Array	
1	GE-BWR	Zircaloy	0.237	0.562	0.032	0.498	5.32x10 ⁻²	1.885x10 ⁻³	1.261x10 ⁻²	19.5	Browns Ferry 7x7
2	CE-PWR	Zircaloy	0.237	0.440	0.026	0.388	3.38x10 ⁻²	7.27 x10 ⁻⁴	8.01 x10 ⁻³	18.0	Calvert Cliffs 15x15
	PWR	Zircaloy	0.237	0.413	0.024	0.365	2.93x10 ⁻²	5.57 x10 ⁻⁴	6.95 x10 ⁻³	18.0	Palisades 15x15
3	B&W-PWR	Zircaloy	0.237	0.430	0.0265	0.377	3.36x10 ⁻²	6.87 x10 ⁻⁴	7.96 x10 ⁻³	21.0	Rancho Seco 15x15
4	W-PWR	304 SST	0.290	0.422	0.0165	0.389	2.1 x10 ⁻²	4.32 x10 ⁻⁴	6.09 x10 ⁻³	18.5	Connecticut Yankee 15x15
	PWR	Zircaloy	0.237	0.422	0.0243	0.3734	3.03x10 ⁻²	5.99 x10 ⁻⁴	7.18 x10 ⁻³	26.0	Point Beach 15x15
	PWR	Zircaloy	0.237	0.422	0.0243	0.3734	3.03x10 ⁻²	5.99 x10 ⁻⁴	7.18 x10 ⁻³	18.5	Diablo Canyon 15x15
	PWR	304 SST	0.290	0.402	0.013	0.376	1.59x10 ⁻²	3.01 x10 ⁻⁴	4.6 x10 ⁻³	18.5	San Onofre 1 14x14
	PWR	304 SST	0.290	0.3415	0.012	0.3175	1.24x10 ⁻²	1.69 x10 ⁻⁴	3.6 x10 ⁻³	10.7	Indian Point 1 14x14

PELLETS						ROD
	Fuel Type	Diameter (in.)	A (in. ²)	P lb/in. ³	W ₂ lb/in.	Wt=W ₁ t+W ₂ lb/in.
1	GE-PWR	0.488	1.87x10 ⁻¹	0.40	7.48x10 ⁻²	8.74x10 ⁻²
2	CE-PWR	0.382	1.14x10 ⁻¹	0.40	4.58x10 ⁻²	5.38x10 ⁻²
	PWR	0.359	1.01x10 ⁻¹	0.40	4.05x10 ⁻²	4.75x10 ⁻²
3	B&W-PWR	0.362	1.03x10 ⁻¹	0.40	4.11x10 ⁻²	4.91x10 ⁻²
4	W-PWR	0.3835	1.16x10 ⁻¹	0.40	4.62x10 ⁻²	5.23x10 ⁻³
	PWR	0.3604	1.02x10 ⁻¹	0.40	4.08x10 ⁻²	4.80x10 ⁻²
	PWR	0.3604	1.02x10 ⁻¹	0.40	4.08x10 ⁻²	4.80x10 ⁻²
	PWR	0.370	1.08x10 ⁻¹	0.40	4.30x10 ⁻²	4.76x10 ⁻²
	PWR	0.313	7.74x10 ⁻²	0.40	3.1 x10 ⁻²	3.44x10 ⁻²

NEDO-10084-3
 September 1984

is consistent with the physical conditions. Corrections are made to the projection based on this comparison.

b. Model Basis

The basic of the model is a single degree of freedom vibratory system when the general equation of motion is given by:

$$M\ddot{X} + C\dot{X} + KX = F_0 \sin \omega t.$$

For an undamped system such as this "C" = 0; "K" is the spring constant term which is a measure of stiffness. The shear and moment stiffnesses are given by the shear-shear strain and moment-curvature relationships. The "K" value for the two spring terms is the slope of the V- γ , and M- ϕ curves. In this bilinear analysis there are two values of "K" bending, one for the elastic portion and one for the plastic portion of the material behavior. Since shear always remains elastic (in this analysis), there is only one "K" value. The actual values are shown in Subsection 5.6.5.A.7. Programs similar to this have been used for nuclear power plant pipe-whip analyses.

c. Exact Solution

If the assumption is made that the fuel rod response remains elastic then an exact solution to the problem can be obtained by model superposition. The derivation and results of this model are contained in Subsection 5.6.5.A.6. Input to the exact solution is in the form of a square-wave time-acceleration plot applied to the rod supports.

5.6.5.A.5 Computer Program - "DYREC"

The following discussion of S-R Computer Program "Dyrec" will be limited to a description of the program features relevant to the problem at hand, i.e., beam vibration.

a. Model

"Timoshenko Beam" theory (Ref 20) is applied, i.e., the effects of shear deformation and rotary inertia are considered. The program uses a discrete model approach. The model used to represent the beam consists of rigid bars connected by "Moment Springs" and "Shear Springs." A diagrammatic representation of the model is shown in Figure V-59.

The program assumes bilinear hysteretic materials with kinematic strain hardening. Knowing γ_{ij} and ϕ_{ij} , the shear and moment in the springs can be determined from Figure V-60(a), considering the loading history. Equation of motion for mass "j" and forces acting on mass "j" are diagrammed in Figure V-60(b) and (c), respectively.

B_{ij} = Deformation of shear spring

$$= Y_j - Y_i - \frac{\ell_{ij}}{2} (\ddot{\theta}_i + \ddot{\theta}_j)$$

α_{ij} = Rotation of moment spring

$$= \theta_j - \theta_i$$

γ_{ij} = Shear strain

$$= B_{ij} / \ell_{ij}$$

ϕ_{ij} = Curvature

$$= \alpha_{ij} / \ell_{ij}$$

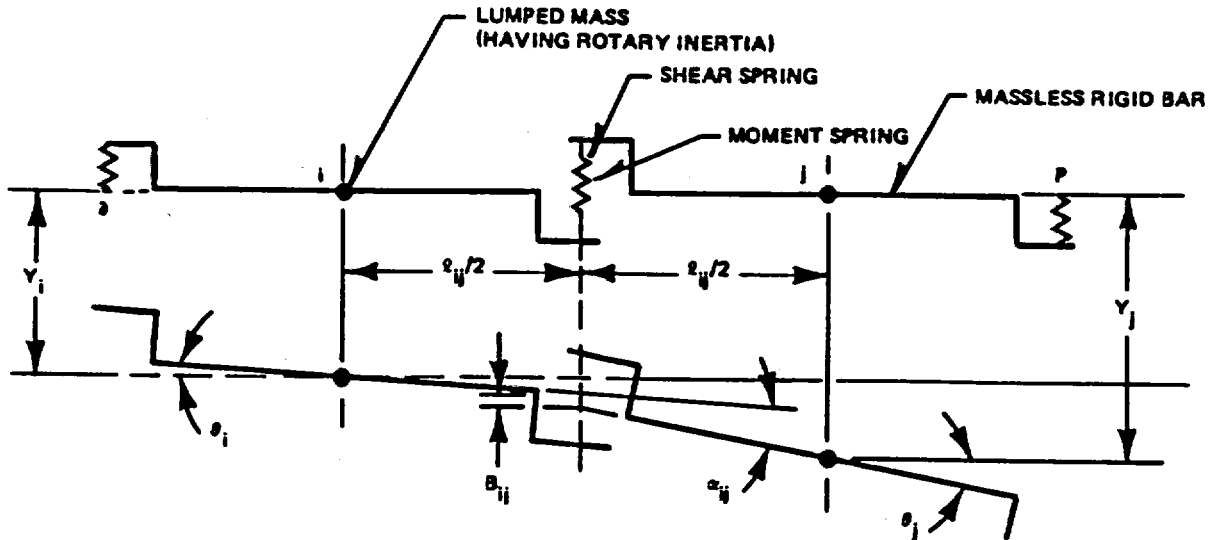


FIGURE V-59. BEAM MODEL AND GEOMETRY OF DEFORMATION

b. Equations of motion:

$$m_j \ddot{Y}_j + Q_{ij} - Q_{jk} = P_j$$

$$I_j \ddot{\theta}_j + M_{ij} - M_{jk} - Q_{ij} \left(\frac{l_{ij}}{2} \right) - Q_{jk} \left(\frac{l_{jk}}{2} \right) = T_j$$

The above equations can be re-written as:

$$I. \quad \ddot{Y}_j = \frac{1}{m_j} (P_j - Q_{ij} + Q_{jk})$$

$$II. \quad \ddot{\theta}_j = \frac{1}{I_j} \left[T_j - M_{ij} + M_{jk} + Q_{ij} \left(\frac{l_{ij}}{2} \right) + Q_{jk} \left(\frac{l_{jk}}{2} \right) \right]$$

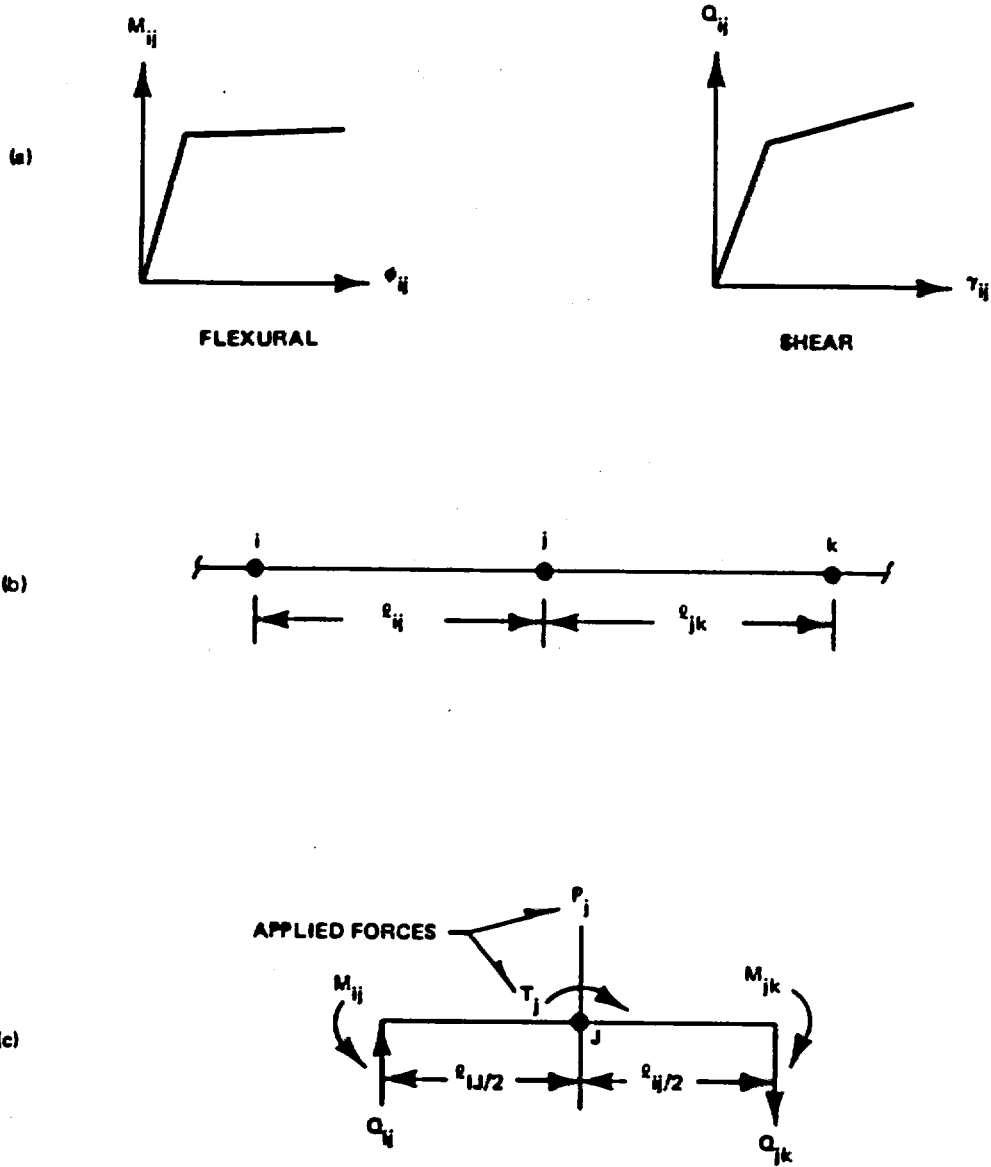


FIGURE V-60(a),(b),(c). DIAGRAMS REFERENCED IN SECTION 5.6.5.5, a.

Numerical integration of equations of motion:

The following recurrence formulas are used:

$$Y_j^{(s+1)} = 2Y_j^{(s)} - Y_j^{(s-1)} + \Delta t^2 \ddot{Y}_j^{(s)}; \text{ similarly for } \theta_j^{(s+1)}$$

$$\dot{Y}_j^{(s+1)} = \dot{Y}_j^{(s)} + \frac{\Delta t}{2} \left[3\ddot{Y}_j^{(s)} - \ddot{Y}_j^{(s-1)} \right]; \text{ similarly for } \dot{\theta}_j^{(s+1)}$$

The above equations assume linear acceleration between t_s and t_{s+1} .

Once the displacements and velocities have been obtained by the above recurrence formulas, the accelerations are calculated by using Eq's I and II above.

It should be noted that the recurrence formulas used are not self-starting. The solution is started using a predictor - corrector technique.

1. Predictor

$$Y_j^{(1)} = Y_j^{(0)} + \Delta t \dot{Y}_j^{(0)} + \frac{\Delta t^2}{2} \ddot{Y}_j^{(0)}; \text{ similarly for } \theta_j^{(1)}$$

$$\dot{Y}_j^{(1)} = \dot{Y}_j^{(0)} + \dot{\theta}_t Y_j^{(0)} \text{ similarly for } \dot{\theta}_j^{(1)}$$

2. Solve for $\ddot{Y}_j^{(1)}$ and $\ddot{\theta}_j^{(1)}$ using Eq's I and II.

3. Corrector (Newmark B-method with $B = 1/6$)

$$Y_j^{(1)} = Y_j^{(0)} + \Delta t \dot{Y}_j^{(0)} + \frac{\Delta t^2}{3} \ddot{Y}_j^{(0)} + \frac{\Delta t^2}{6} \ddot{Y}_j^{(1)}; \\ \text{similarly for } \theta_j^{(1)}$$

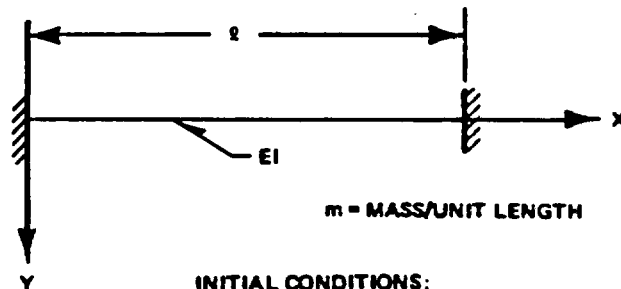
$$\dot{Y}_j(1) = \dot{Y}_j(0) + \frac{\Delta t}{2} \left[\ddot{Y}_j(0) + \ddot{Y}_j(1) \right] ; \text{ similarly for } \dot{\theta}_j(1)$$

Repeat steps (2) and (3) until solution has converged.

5.6.5.A.6 Derivation and Results of "Exact" Elastic Solution for PWR and BWR Fuel Rods - 30 Foot Drop Group I Fuel

As discussed in 5.6.5.A.4, if it is assumed that the response of the fuel rod to the side load impulse remains elastic then the problem can be solved by model superposition. The results will be used for those cases which remain elastic. The results will also be compared to the elastic portion of the "DYREC" bilinear model as a double check on calculational accuracy. The following is the exact solution derivation:

a. Derivation

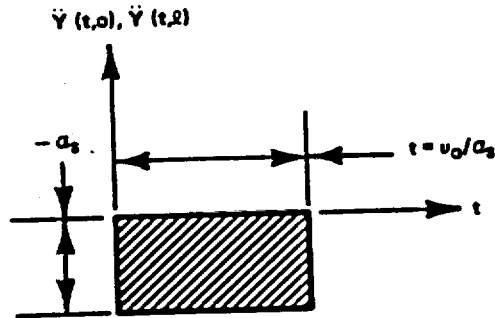


INITIAL CONDITIONS:

$$Y(0, x) = 0$$

$$\dot{Y}(0, x) = v_0$$

SUPPORT ACCELERATION:



Differential equation of motion:

$$m \frac{\partial^2 v}{\partial t^2} + EI \frac{\partial^4 u}{\partial x^4} = 0$$

u = Displacement of beam relative to supports
 $= Y - Y_s$; where Y_s = support displacement

$$\dot{u} = \dot{Y} - \dot{Y}_s; \quad \ddot{u} = \ddot{Y} - \ddot{Y}_s$$

Re-write D.E. of Motion:

$$m(\ddot{u} + \ddot{Y}_s) + EIu^{IV} = 0$$

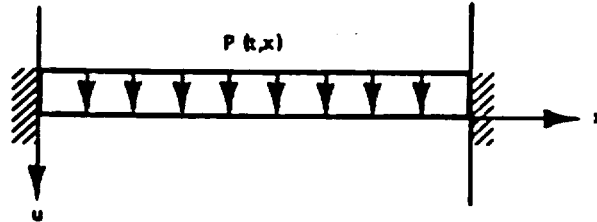
or

$$\ddot{m}u + EIu^{IV} = -m\ddot{Y}_s$$

Initial conditions:

$$u(0,x) = \dot{u}(0,x) = 0$$

EQUIVALENT SYSTEM:



D.E.:

$$m \ddot{u} + E I u^{IV} = p(t,x)$$

where

$$p(t,x) = m a_s \quad 0 \leq t \leq t_1$$

$$p(t,x) = 0 \quad t > t_1$$

Dynamic Deflection, u :

$$u = \sum_{n=1}^{\infty} \phi_n(x) A_n$$

Modal Eq. of motion:

$$A_n + W_n^2 A_n = \frac{f(t) \int_0^l P_1(x) \dot{\phi}_n(x) dx}{m \int_0^l \phi_n^2(x) dx}$$

$$P_1(x) = m a_s$$

$$f(t) = 1; \quad 0 \leq t \leq t_1$$

$$= 0; \quad t > t_1$$

Modal static deflection:

$$A_{nst} = \frac{\int_0^{\ell} P_1(x) \phi_n(x) dx}{W_n^2 m \int_0^{\ell} \phi_n^2(x) dx}$$

$$A_n = A_{nst} - DLF_n$$

$$\text{Where } DLF_n = 1 - \cos W_n t; \quad t \leq t_1$$

$$= \cos w_n (t - t_1) - \cos W_n t; \quad t > t_1$$

Mode shapes, $\phi_n(x)$:

$$\phi_n(x) = \cosh \beta_n x - \cos \beta_n x + \alpha_n (\sinh \beta_n x - \sin \beta_n x)$$

Where

$$\alpha_n = (\cos \beta_n \ell - \cosh \beta_n \ell) / (\sinh \beta_n \ell - \sin \beta_n \ell)$$

Frequencies, W_n :

$$W_n = (\beta_n \ell)^2 \sqrt{\frac{EI}{m \ell^4}}$$

Value of integrals:

$$\int_0^{\ell} P_1(x) \phi_n(x) dx = m a_s (\gamma_u \ell) = \gamma_n M a_s$$

Where

$$\gamma_n = \frac{2 (\cosh \beta_n l - \cos \beta_n l - \sin \beta_n l \sinh \beta_n l)}{\beta_n l (\sinh \beta_n l - \sin \beta_n l)}$$

$$\int_0^l \phi_n^2(x) dx = l \quad \text{For all modes}$$

$$\therefore A_{nst} = \frac{\gamma_n M a_s}{W_n^2} = \frac{\gamma_n a_s}{W_n^2} \quad n$$

$$u(x,t) = \sum_n^{\infty} \frac{\gamma_n a_s}{W_n^2} (DLF_n) [\cosh \beta_n x - \cos \beta_n x + \alpha_n (\sinh \beta_n x - \sin \beta_n x)]$$

MOMENTS

$$M = -EI \frac{\partial^2 u}{\partial x^2}$$

$$= \frac{-EI}{l^2} \sum_n^{\infty} \gamma_n \frac{(\beta_n l)^2 a_s}{W_n^2} (DLF_n) [\cosh \beta_n x + \cos \beta_n x + \alpha_n$$

$$(\sinh \beta_n x + \sin \beta_n x)]$$

Values of $\beta_n l$:

n	$\beta_n l$
1	4.7300408
2	7.8532046
3	10.9956078
4	14.1371655
5	17.2787596

$n > 5 \quad \beta_n l = (n + 0.5)\pi$ to at least 7 decimal places.

For PWR Fuel Rod:

$$\begin{aligned}
 a_s &= 47257 \text{ "/sec}^2 \\
 v_o &= 527.45 \text{ "/sec} \\
 t_1 &= v_o/a_s = 1.1161 \times 10^{-2} \text{ sec} \\
 EI &= 5.6484 \text{ k - in}^2 \\
 l &= 18.5" \text{ (unsupported span)} \\
 m\ddot{l} &= \frac{18.5\pi[(0.211^2 - 0.1867^2) \times 0.237 + 0.1802^2 \times 0.4]}{386.4 \times 1000} \\
 &= 2.298187 \times 10^{-6} \text{ k - sec}^2/\text{in}
 \end{aligned}$$

For BWR Fuel Rod: (Browns Ferry fuel rod)

$$\text{Cladding: } R_o = 0.281" \quad R_i = 0.249" \quad \delta = 0.237 \text{ \#/in}^3$$

$$\text{Pellets: } R = 0.244" \quad \delta = 0.4 \text{ \#/in}$$

$A_s, N_o,$ and t_1 same as for PWR fuel

$$E = \frac{\sigma_y}{\epsilon_y} = \frac{75}{0.008} = 9375 \text{ ksi}$$

$$EI = 9375\pi (0.281^4 - 0.249^4) / 4 = 17.6031 \text{ k - in}^2$$

$$\begin{aligned} \ell &= 19.5'' \\ m\ell &= 19.5\pi [(0.281^2 - 0.249^2) \times 0.237 + 0.244^2 \times 0.4] / 286400 \\ &= 4.412876 \times 10^{-6} \text{ k - sec}^2/\text{in} \end{aligned}$$

In the summation for u and M, the first 30 modes were used.

A short time-sharing computer program was written to perform the calculations described above.

b. Results - Elastic Solution/30 Foot Side Drop

1. PWR Fuel Rod:

Unsupported span, $\ell = 18.5$ in

Max. Moment = $0.3265''^k$ @ $t = 0.0068$ sec (fixed end).

Referring to M - δ curve Figure V-61 this moment is only very slightly above the calculated curve.

\therefore the assumption that the rod remains elastic is for all intents and purposes valid.

$$\phi = 0.3265 / 5.6484 = 0.0578 \text{ in}^{-1}$$

$$\text{Max. strain, } \epsilon = 0.211 \times 0.0578 = 0.0122$$

$$\text{Max. center relative deflection} = 0.637'' \text{ @ } t = 0.0072 \text{ sec.}$$

The results of the 26 inch span exact solution showed the rod to exceed its yield value; a non-linear analysis is necessary for evaluation. See Section 5.6.5.A.7.

2. BWR Fuel Rod:

Unsupported span, $\ell = 19.5$ in.

$$\text{Max. moment} = 0.6566''^k \text{ @ } t = 0.0056 \text{ sec (fixed end).}$$

$$\text{Max. strain, } \epsilon = R_o \phi = 0.281(0.6566) / 17.6031 = 0.01048.$$

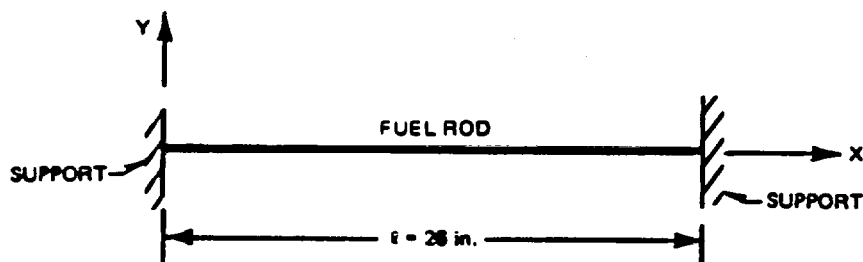
This exceeds $E_y = 0.008$ by only a slight amount and therefore the assumption of elastic behavior is justified.

Max. center relative deflection = 0.459" @ $t = 0.006$ sec.

5.6.5.A.7 Side Drop Analysis - 30 Foot/Bi-Linear - Group I Fuel

The exact solution of the 26 inch span showed that permanent deformation would occur therefore a non-linear dynamic analysis was performed on the Point Beach fuel rods using the "DYREC" code described in 5.6.5.A.5 (they have the lowest factor of safety of all the Zircaloy clad fuels).

a. Analysis

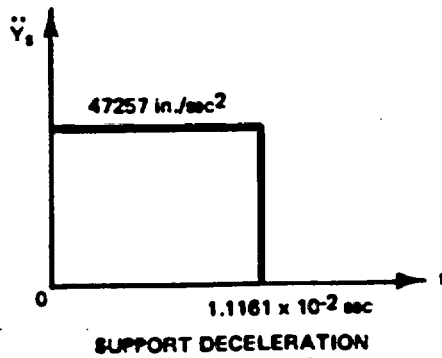


The dynamic loading consists of the sudden deceleration of the fuel pin supports due to the cask impact. This deceleration is assumed constant over a time interval $t_1 = v_o / \ddot{Y}_s$, where $v_o =$ Impact velocity and $\ddot{Y}_s =$ deceleration.

$$\text{Max. } \ddot{Y}_s = 122.3 \times 386.4 = 47257 \text{ "/sec}^2$$

$$v_o = \sqrt{2gH} = \sqrt{2 \times 386.4 \times 360} = 527.45 \text{ "/sec}$$

$$t_1 = \frac{527.45}{47257} = 1.1161 \times 10^{-2} \text{ sec. (11.161 milliseconds)}$$



The fuel rod segment is represented by a 26-inch long built-in beam. For analytical purposes only half the span was considered with one end built-in and the other end constrained from rotating but permitted to move vertically thus simulating mid-span conditions. Ten masses are distributed along the 13 inch length and are equivalent to the actual rod linear weight distribution.

Properties of dynamic model:

Masses

Cladding: $R_o = 0.211''$ $R_i = 0.1867''$ $\gamma = 0.237 \text{ \#/in}^3$
 Pellets: $R = 0.1802''$ $\gamma = 0.4 \text{ \#/in}^3$

Masses 2 through 10:

$$M_T = \frac{1.3 \pi [(0.211^2 - 0.1867^2) \times 0.237 + 0.1802^2 \times 0.4]}{386.4 \times 1000}$$

$$= 1.6149 \times 10^{-7} \text{ k-sec}^2/\text{in}$$

Masses 1 and 11:

$$M_T = 8.0745 \times 10^{-8} \text{ k-sec/in}$$

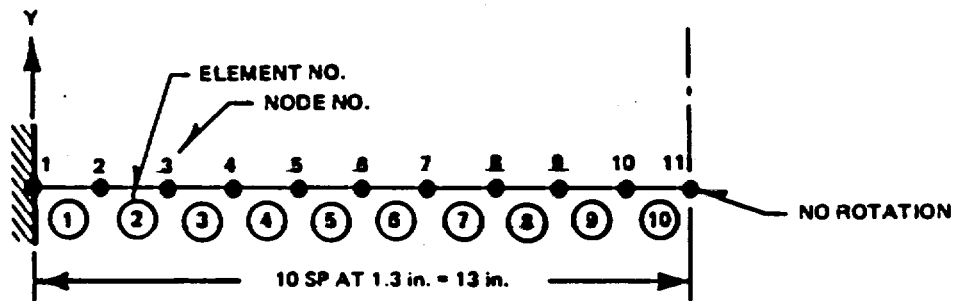
Rotary Masses: (Masses 1 and 11 immaterial since no rotation at these nodes)

Masses 2 through 10:

$$M_R = \Sigma I \rho \Delta x$$

$$= \frac{1.3 \pi [(0.211^4 - 0.1867^4) \times 0.237 + 0.1802^4 \times 0.4]}{4 \times 386.4 \times 1000}$$

$$= 1.5949 \times 10^{-9} \text{ k-in-sec}^2$$



MULTI-MASS DYNAMIC MODEL

Shear Stiffness:

$$E = 75/0.008 = 9375 \text{ ksi}$$

$$G = E/[2(1 + \nu)] = 9375/[2(1 + 0.3)] = 3606 \text{ ksi}$$

$$A_s G = 0.01518 (3606) = 54.739 \text{ kips}$$

$$t_y = 0.577 \times 75 = 43.275 \text{ ksi}$$

$$V_y = 0.01518 (43.275) = 0.657^k \text{ shear}$$

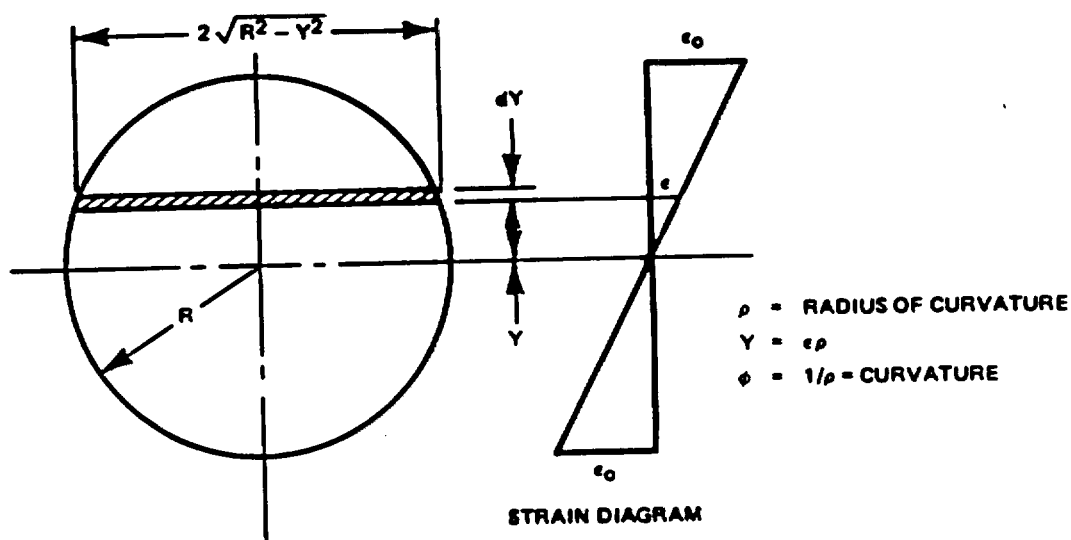
$$\gamma_y = 43.275/3606 = 0.012 \text{ shear strain}$$

Determination of Spring Properties:

Fuel Rod

Find moment-curvature relationship using stress-strain curve shown in 5.6.5.A.2.

FOR A CIRCULAR CROSS-SECTION



$$dM = 2\sigma Y \sqrt{R^2 - Y^2} dY$$

$$dY = \rho d\epsilon$$

$$dM = 2\sigma \rho^2 \epsilon \sqrt{R^2 - \epsilon^2 \rho^2} d\epsilon$$

$$M = 4\rho^2 \int_0^{R/\rho} \sigma \epsilon \sqrt{R^2 - \epsilon^2 \rho^2} d\epsilon$$

$$= 4\rho^3 \int_0^{\epsilon_0} \sigma \epsilon \sqrt{\epsilon_0^2 - \epsilon^2} d\epsilon$$

$$= \frac{4\phi R^4}{\epsilon_o^4} \int_0^{\epsilon_o} \sigma \epsilon \sqrt{\epsilon_o^2 - \epsilon^2} d\epsilon$$

For an annular cross-section,

r = inner radius

R = outer radius

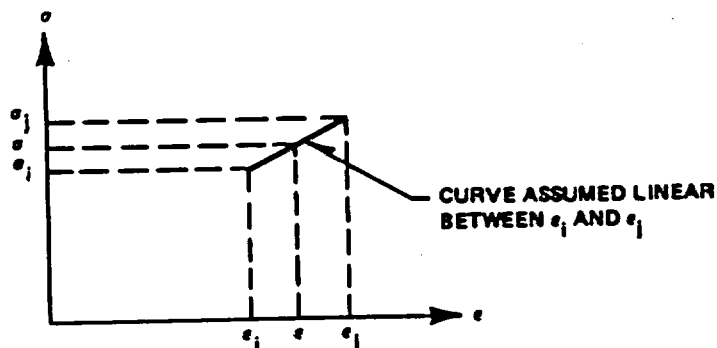
$$\epsilon_{oi} = r \epsilon_o / R$$

$$\phi = \epsilon_o / R$$

$$M = \frac{4\phi R^4}{\epsilon_o^4} \int_0^{\epsilon_o} \sigma \epsilon \sqrt{\epsilon_o^2 - \epsilon^2} d\epsilon - \frac{4\phi r^4}{\epsilon_{oi}^4} \int_0^{\epsilon_{oi}} \sigma \epsilon \sqrt{\epsilon_{oi}^2 - \epsilon^2} d\epsilon$$

$$= \frac{4R^3}{\epsilon_o^3} \left[\int_0^{\epsilon_o} \sigma \epsilon \sqrt{\epsilon_o^2 - \epsilon^2} d\epsilon - \int_0^{\epsilon_{oi}} \sigma \epsilon \sqrt{\epsilon_{oi}^2 - \epsilon^2} d\epsilon \right]$$

Numerical integration of above equation:



$$\sigma = \sigma_1 + \frac{(\epsilon - \epsilon_1)}{(\epsilon_j - \epsilon_1)} (\sigma_j - \sigma_1)$$

Define $E_t = (\sigma_j - \sigma_i) / (\epsilon_j - \epsilon_i)$

$$\sigma = \sigma_i - E_t \epsilon_i + E_t \epsilon$$

$$\begin{aligned} & \int_{\epsilon_i}^{\epsilon_j} \sigma \epsilon \sqrt{(\epsilon_o^2 - \epsilon^2)} d\epsilon \\ &= (\sigma_i - E_t \epsilon_i) \int_{\epsilon_i}^{\epsilon_j} \epsilon \sqrt{(\epsilon_o^2 - \epsilon^2)} d\epsilon + E_t \int_{\epsilon_i}^{\epsilon_j} \epsilon^2 \sqrt{(\epsilon_o^2 - \epsilon^2)} d\epsilon \\ &= (\sigma_i - E_t \epsilon_i) \left[-\frac{(\epsilon_o^2 - \epsilon^2)^{3/2}}{3} \right]_{\epsilon_i}^{\epsilon_j} + E_t \left[\frac{-\epsilon (\epsilon_o^2 - \epsilon^2)^{3/2}}{4} \right. \\ & \quad \left. + \frac{\epsilon_o^2 \epsilon (\epsilon_o^2 - \epsilon^2)^{1/2}}{8} + \frac{\epsilon_o^4}{8} \sin^{-1} \left(\frac{\epsilon}{\epsilon_o} \right) \right]_{\epsilon_j}^{\epsilon_i} \\ &= (\sigma_i - E_t \epsilon_i) \left[\frac{(\epsilon_o^2 - \epsilon_i^2)^{3/2}}{3} - \frac{(\epsilon_o^2 - \epsilon_j^2)^{3/2}}{3} \right] \\ & \quad + E_t \left\{ \frac{\epsilon_i (\epsilon_o^2 - \epsilon_i^2)^{3/2}}{4} - \frac{\epsilon_j (\epsilon_o^2 - \epsilon_j^2)^{3/2}}{4} + \frac{\epsilon_o^2}{8} \right. \\ & \quad \left. \left[\frac{\epsilon_j (\epsilon_o^2 - \epsilon_j^2)^{1/2}}{4} - \frac{\epsilon_i (\epsilon_o^2 - \epsilon_i^2)^{1/2}}{4} \right] \right. \\ & \quad \left. + \frac{\epsilon_o^4}{8} \left[\sin^{-1} (\epsilon_j / \epsilon_o) - \sin^{-1} (\epsilon_i / \epsilon_o) \right] \right\} \end{aligned}$$

For evaluation of $\int_{\epsilon_i}^{\epsilon_j} \sigma \epsilon \sqrt{(\epsilon_o^2 - \epsilon^2)} d\epsilon$, substitute ϵ_{o1} for ϵ_o in above equation.

A computer program was written to evaluate the above integrals.

b. Results - 30 Foot Side Drop/Bi-Linear Analysis

Summary of computer results for the 26 inch span using $M - \phi$ and $V - \gamma$ relationships derived from dynamic stress-strain curve.

1. Max. moment = 0.433" @ $t = 0.012965$ sec.
Curvature, $\phi = 0.11709 \text{ in}^{-1}$
Strain, $G = R_o \phi = 0.211 \times 0.11709 = 0.0247$
Referring to Figure V-34, this strain corresponds to a stress of 125 ksi. The above moment occurs at the fixed end of the fuel rod.
2. Max. shear force = 0.1027^k @ $t = 0.012037$ sec @ fixed end of rod. Since $0.1027^k < 0.657^k$, no yielding occurs.
3. Max. strain rate = 5.965 in/in/sec at fixed end of pin @ $t = 0.024807$ sec.

These results are shown on Figure V-61. Also shown are the exact solution results for the eighteen and one half inch span PWR. Based on the exact solution, the BWR fuel was determined to remain elastic under the 30 foot drop conditions, therefore, a bi-linear analysis was considered unnecessary.

5.6.5.A.8 Confirmation of Model

Three separate evaluations were performed to assure that the model selected and analyzed in 5.6.5.A.7 was correct and represented the "worst" case.

The first analysis consists of demonstrating the stability of the time step used in the numerical integration procedure for solving the equations of motion for the model shown in 5.6.5.A.8. The original time step used was 10^{-6} sec. The computer analysis was re-run using a time step of 0.5×10^{-6} sec. A comparison of the results of the first analysis with the results of the second

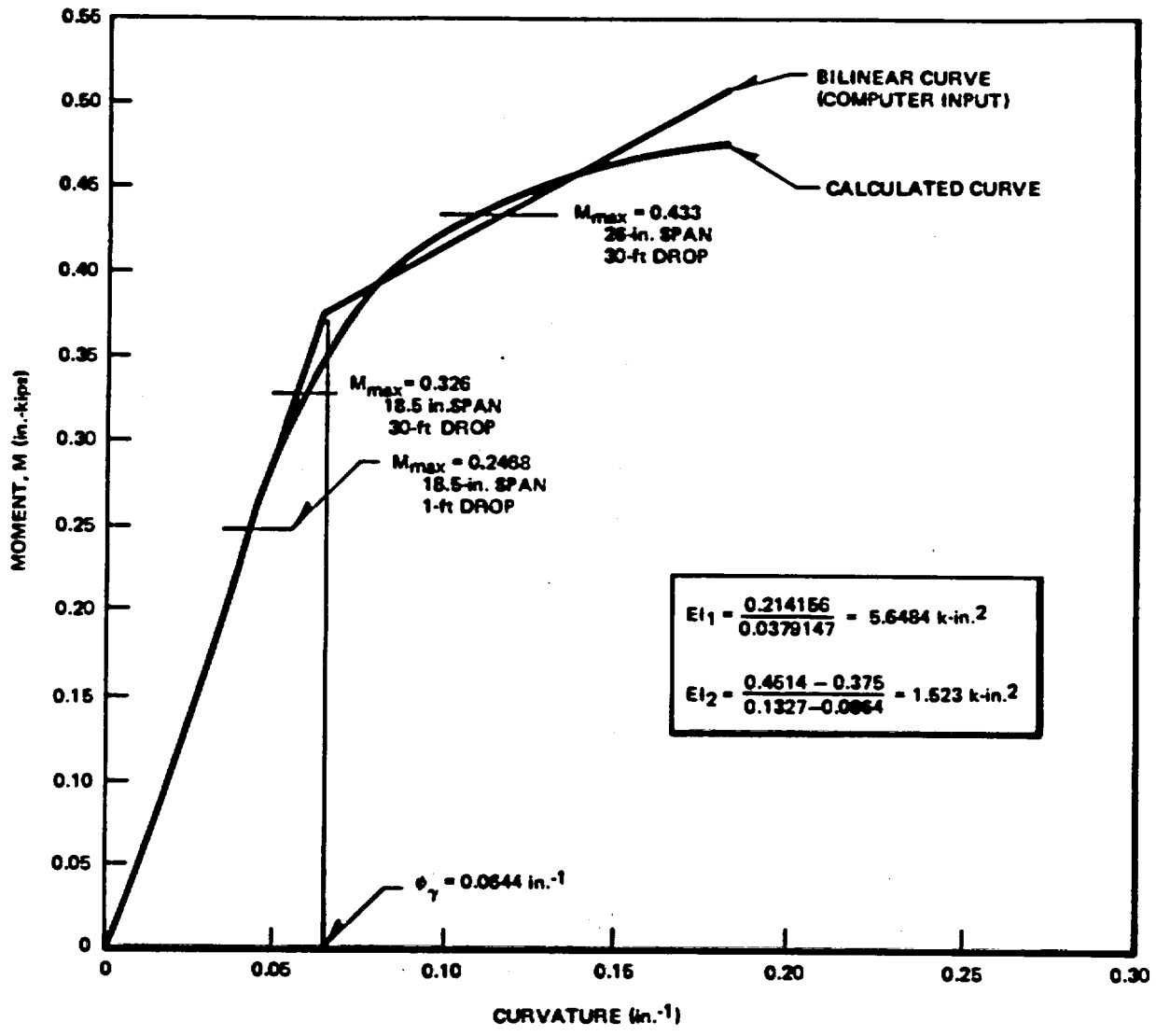
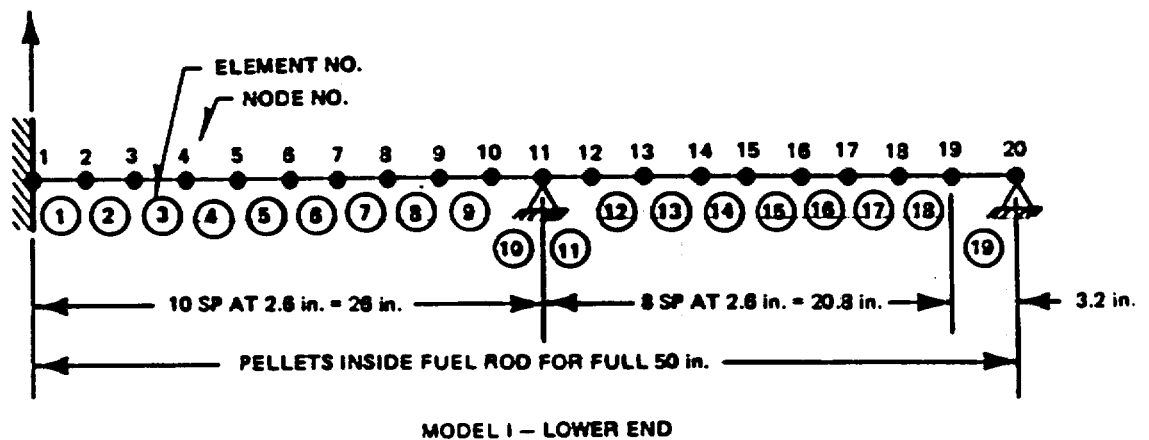


FIGURE V-61. MOMENT VS CURVATURE

analysis shows essentially no difference in the solution. This verified that the model converged on the correct solution.

The next two analyses consist of investigating what effect different boundary conditions have on the problem. Two models will be used for this purpose. The first model is a representation of the lower end of a fuel rod, the second model is the upper end.



Use same support deceleration moment-curvature as model in 5.6.5.A.7.

Translation Masses:

Mass No.	Mass
1	1.6149×10^{-7} k-sec ² /in
2-18	3.2299×10^{-7} k-sec ² /in
19	3.6026×10^{-7} k-sec ² /in
20	1.9876×10^{-7} k-sec ² /in

Rotary Masses:

Mass No.	Mass
1	Immaterial (no rotation)
2-18	3.1898×10^{-9} k-in-sec ²
19	3.5578×10^{-9} k-in-sec ²
20	1.9629×10^{-9} k-in-sec ²

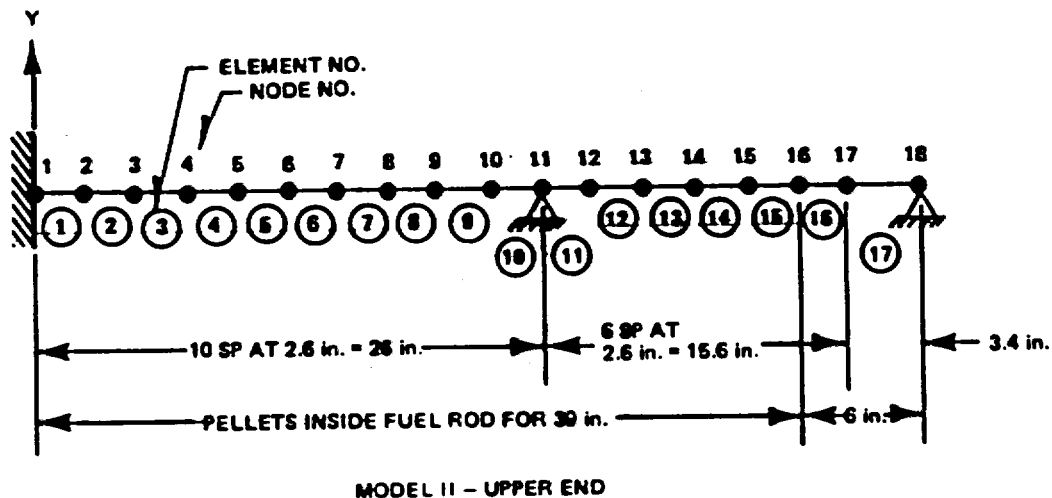
Use $\Delta t = 1 \times 10^{-6}$ sec.

Max. moment = $0.3377 \text{ }^{\text{''}}\text{k}$ in element 16 @ $t = 0.013083 \text{ sec.}$

Curvature, $\phi = 0.0831 \text{ in}^{-1}$

Strain, $\epsilon = R_o \phi = 0.211 \times 0.0831 = 0.01754$

These results are less than those obtained for the fixed-end model.



Translational Masses:

Mass No.	Mass
1	$1.6149 \times 10^{-7} \text{ k-sec}^2/\text{in}$
2-15	$3.2299 \times 10^{-7} \text{ k-sec}^2/\text{in}$
16	$1.8570 \times 10^{-7} \text{ k-sec}^2/\text{in}$
17	$5.5866 \times 10^{-8} \text{ k-sec}^2/\text{in}$
18	$3.1657 \times 10^{-8} \text{ k-sec}^2/\text{in}$

Rotary Masses:

Mass No.	Mass
1	Immaterial
2-15	$3.1898 \times 10^{-9} \text{ k-in-sec}^2$
16	$2.0753 \times 10^{-9} \text{ k-in-sec}^2$
17	$1.1086 \times 10^{-9} \text{ k-in-sec}^2$
18	$6.2822 \times 10^{-10} \text{ k-in-sec}^2$

Use $\Delta t = 1 \times 10^{-6} \text{ sec.}$

Max. moment = $0.3207 \text{ }^{\text{k}}$ in element 14 @ $t = 0.02714$ sec.

Curvature, $\phi = 0.0596 \text{ in}^{-1}$

Strain, $\epsilon = R_o \phi = 0.211 \times 0.0596 = 0.0126$

These results are less than those obtained for the fixed-end model.

5.6.5.A.9 Summary of 30 Foot Side Drop Analyses and Discussion of Conservatism

a. Results Summary

1. The significant parameter in evaluating cladding under these conditions is ductility. It is recognized that under one-of-a-kind accident conditions such as this that some degree of permanent fuel rod deformation may occur. The real criterion for fuel acceptability under such conditions is not the amount of deformation sustained but rather, cladding integrity as a result of the loading. This can only be determined through a comparison of model results with cladding physical properties, particularly its capacity for elongation.
2. The base-case model described in 5.6.5.A.7 was run under the 122.3 "g" loading with the resulting maximum strain of 2.47 percent (elastic plus plastic). This strain occurred at the built-in end 12.965 milliseconds after cask impact. Displacement of the mid-span is 2.35 inches relative to the built-in ends.
3. The results of the two alternative fuel configuration cases showed that maximum moments and strains were less than those of the base case under similar loadings thus demonstrating that the built-in assumption is the "worst" case.
4. The convergence check at one-half the time-step of the initial convergence (0.5 microsecond vs. 1.0 microsecond) showed essentially no difference between the two base case runs thus establishing the validity of convergence.

5. Comparison to exact solution - to verify the functioning of the spring-mass dynamic model, an exact solution time-sharing program was written for the elastic portion of the fuel rod behavior. A comparison of the results of the two programs showed identical values to four decimal places. The exact solution program will not function beyond the elastic portion of the rod response. This elastic response matching does, however, indicate the correct functioning of the spring-mass system.
6. Exact solution output - the 18.5 inch span PWR cask where basket restraint is considered and the 19.5 inch span BWR case were found to be elastic under 30-foot side drop conditions. The PWR case produced a maximum strain of 1.22% while the BWR case produced a maximum strain of 1.048%.

The exact solution was also used to check on fuel rod behavior under one-foot drop conditions. The 2 millisecond, 210 g input pulse resulted in a maximum strain of 0.922% for the 18.5 inch span PWR case. This will be discussed in a later section.

b. Discussion of Conservatism

1. As mentioned above, the fuel rod properties used in the spring-mass and exact solution models took no credit for the presence of the fuel pellets contained therein. Discussions with the fuel designers indicate that high-fired pellets will in fact contribute quite a bit to the rigidity of the rod, although it is difficult to quantify since this is not a parameter usually associated with bundle design.

2. Another conservative feature of this analysis is the presence of water in the cask cavity during the drop accident. Since all rods displace during the drop then an equal volume of water must also be displaced. The damping or resistance to movement provided by the surrounding water will reduce the displacements, moments and hence strains in the cladding. As in 1., above, this term is difficult to incorporate into the model but its presence and effect cannot be ignored.

3. An examination of the fuel basket shows that there are physical constraints provided by the basket spacer disks and guide channels which prohibit any significant deflections on a large percentage of the fuel rods. Contact will occur between the lowest row of rods and the guide channel. Each subsequent row will deflect and contact the row beneath it until the maximum deflection distance is achieved. This action can be seen by envisioning the bundle on a flat table top. The table represents the constraining effect of the basket. Clearly the row of rods closest to the table top can only deflect a short distance (0.223") until contact. The second row can deflect the same amount as the first row plus the distance between the two rows (0.141"). The third row deflection is the first row deflection plus two row-to-row gaps. This process continues through the bundle, with each row having an available deflection distance 0.141" greater than the previous row before rod-to-rod contact. Once the available deflection reaches the maximum rod deflection based on the drop model, then all remaining rows will deflect the full amount (2.35 inches). A simple calculation shows that none of the rows in the 15 x 15 bundle will deflect the full 2.35". The maximum deflection of Row 15 is 2.197". Considering some deflection in the channel, row 15 may be strained the maximum amount.

4. At the large deflections experienced in this problem, the bending analysis becomes quite conservative. The shape of the fully deflected fuel rod is that of a catenary. In fact whenever a rod is deflected more than six rod depths, the restraining force becomes that of a catenary (e.g. tension along the rod, not bending). The load under these conditions is carried by the cladding more in tension than bending with a subsequent reduction in stress level. Experiments conducted by Stearns-Roger stress analyst at the University of Michigan demonstrated this phenomenon. A hydrostatically loaded flat circular plate obeyed the laws of bending mechanics until deflections were such that the plate became a membrane in tension. Based on a bending stress calculation the plate should have failed, yet it did not due to the deflection-produced switch from bending to tension for load carrying purposes. A similar thing occurs with the fuel rod.
5. Based on the four discussed points of conservatism, it is clear that the single PWR rod, 26 inch span, unrestricted model is truly the "worst" case evaluation. The likely case of a 18.5 inch span, as established by basket spacer disc distances, shows that the cladding yield value is not exceeded under 30 foot drop conditions. Likewise the BWR fuel rod remains elastic during the 30 foot drop loading.

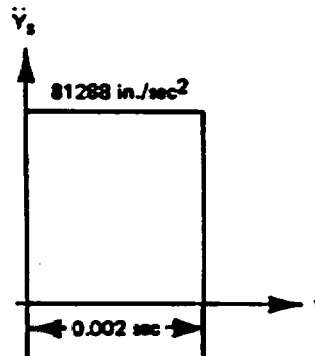
5.6.5.A.10 Normal Conditions - 1 Foot Side Drop

Subsection 5.11.3 discusses the behavior of the cask, tiedowns and skid when dropped a distance of one foot in the normal transport orientation. This analysis shows that the cask model node #7 experiences a peak deceleration of 210 g's for a time duration of approximately 1 millisecond. To check on the behavior of the PWR fuel assembly under these conditions, the 18.5 inch span model (exact solution) was run with a support deceleration of 210 g's applied for two milliseconds.

a. Analysis

Due to the high peak acceleration of the cask ($81288 \text{ "/sec}^2 = 210 \text{ g's}$) during the 1' drop, some estimate of the fuel rod response must be calculated.

The actual acceleration vs. time graph of Node 7 of the cask model is shown below. As an estimate of the fuel rod response, the following support acceleration will be applied to the PWR Fuel Rod:



For results (@ fixed end):

Max. Moment = 0.2468 "k @ $t = 0.0042 \text{ sec}$.

Max. Strain = 0.211 ($0.2468/5.6486 = 0.00922$).

This strain is slightly higher than $E_y = 0.008$.

b. Conclusion

The maximum moment is less than that for the 30 foot drop loading. Referring to Figure V-61, it can be seen that the rod behaves elastically.

5.6.5.A.11 End Drop Analysis - 30 Foot Drop

As mentioned in 5.6.5.A.1, the fuel bundles are not totally restrained in the axial direction to allow for some axial thermal expansion. Since there is some small gap between the end of the bundle and the end of the cask, there will be an impact once the gap is closed during cask deceleration.

The stresses in the fuel pellet stack and the cladding are best evaluated using a stress-wave propagation analysis. This analysis is derived as follows:

a. Derivation

Figure V-62 shows a simplified model of the system.

1. Conditions at Impact

Due to impact, waves of stress will travel along the fuel rods at a velocity, $V = \sqrt{E/\rho}$ where E = Young's modulus and ρ = mass density.

If the cask is assumed to be infinitely rigid, the particles on the end of the fuel rod will assume the velocity of the cask. Let the cask velocity = $v(t)$ which is seen to be time dependent because of the forces acting on it. Velocity of particles on the end of the fuel rod relative to the unstressed portion of the rod = $U_0 - v(t)$.

Let f = Force on end of fuel rod due to relative particle velocity

$$= A \sqrt{\rho E} (U_0 - v) \quad (\text{Note: } v = v(t))$$

The foregoing equations for V and f can be found in Timoshenko's "Theory of Elasticity," Chapter 12, 1st Edition.

The fuel rods are comprised of UO_2 pellet surrounded by a Zirconium alloy tube. The total force acting on the fuel rod will be the force acting on the pellets (f_p) plus the force acting on the

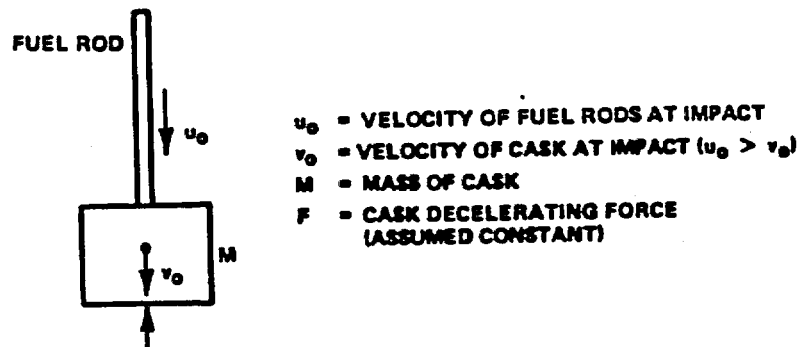


FIGURE V-62. FUEL ROD IMPACT MODEL

cladding (f_c). The pellets act as a solid rod since all loading is in compression.

$$f_p = A_p \sqrt{(\rho E)_p (U_o - v)}$$

$$f_c = A_c \sqrt{(\rho E)_c (U_o - v)}$$

Referring to Reactor Handbook, Vol. I, pages 293-294, 711 (Ref. 1)

$$\rho_p = \frac{10.96 \times 0.0361}{386.4} = 1.024 \times 10^{-3} \text{ lb-sec}^2/\text{in.}^4$$

$$E_p = 23 \times 10^6 \text{ psi}$$

$$\rho_c = \frac{6.55 \times 0.0361}{386.4} = 6.12 \times 10^{-4} \text{ lb-sec}^2/\text{in.}^4$$

$$E_c = 13 \times 10^6 \text{ psi}$$

Modulus of Elasticity was chosen at a fuel rod temperature of 300°F.
(normal operating condition)

2. Velocity of Stress Waves Through Pellets and Cladding:

$$V_p = \sqrt{\frac{23 \times 10^6}{1.024 \times 10^{-3}}} = 1.498 \times 10^5 \text{ in./sec}$$

$$V_c = \sqrt{\frac{13 \times 10^6}{6.12 \times 10^{-4}}} = 1.458 \times 10^5 \text{ in./sec}$$

Assume $V_c = V_p = V = 1.48 \times 10^5$ in./sec. Revise E_p & E_c to 22.45×10^6 and 13.4×10^6 psi respectively to be consistent with value of V .

3. Equation of Motion for Cask:

$$(1) \quad M \frac{dv}{dt} = f_p + f_c - F$$

$$(2) \quad f_p + f_c = (A_p \sqrt{(\rho E)_p} + A_c \sqrt{(\rho E)_c}) (U_o - v)$$

Differentiating both sides of Eq. (2) W.R.T. t

$$\frac{df_p}{dt} + \frac{df_c}{dt} = -\beta \frac{dv}{dt}$$

Substituting into Eq. (1):

$$-\frac{M}{\beta} \frac{d}{dt} (f_p + f_c) = f_p + f_c - F$$

Letting $f_p + f_c = f'$

$$(3) \quad \frac{df'}{dt} + Bf' = BF \quad \text{Where } B = \beta/M$$

4. Solution to Differential Equation:

$$(4) \quad f' = (f'_0 - F)e^{-Bt} + F$$

$$\text{Where } f'_0 = \beta(U_0 - v_0)$$

Let l = length of fuel rod

Total time that fuel rod is in contact with cask =

$$T = \frac{2l}{v} = 1.352 \times 10^{-5} \text{ s.}$$

$$(5) \quad f_p = \sqrt{\frac{A_p (\rho E)_p}{\beta}} f'$$

$$(6) \quad f_c = \sqrt{\frac{A_c (\rho E)_c}{\beta}} f'$$

5. Determine Velocities of Fuel Rods and Cask at Any Time t :

$$(0 \leq t \leq T)$$

$$M \frac{dv}{dt} = f' - F = (f'_0 - F)e^{-Bt}$$

$$M \int_{v_0}^{v_t} dv = \int_0^t (f'_0 - F)e^{-Bt} dt$$

$$M(v_t - v_0) = \frac{f'_0 - F}{B} (1 - e^{-Bt})$$

$$(7) \quad v_t = v_0 + \frac{f'_0 - F}{MB} (1 - e^{-Bt})$$

6. Equation of Motion For Pellets:

$$M_p \frac{dU_p}{dt} = -f_p$$

$$M_p \int_{U_0}^{U_{pt}} dU_p = \left(\frac{-A_p \sqrt{(\rho E)_p}}{\beta} \right) \int_0^t \left[(f'_0 - F)e^{-Bt} + F \right] dt$$

$$M_p (U_{pt} - U_o) = \frac{A_p \sqrt{(\rho E)_p}}{\beta} \left[\frac{f'_o - F}{B} (e^{-Bt} - 1) - Ft \right]$$

$$(8) U_{pt} = U_o - \frac{A_p \sqrt{(\rho E)_p}}{M_p \beta} \left[\frac{f'_o - F}{B} (1 - e^{-Bt}) + Ft \right]$$

By a similar process:

$$(9) U_{ct} = U_o - \frac{A_c \sqrt{(\rho E)_c}}{M_c \beta} \left[\frac{f'_o - F}{B} (1 - e^{-Bt}) + Ft \right]$$

NOTE: U_{pt} and U_{ct} are average velocities of the pellets and cladding respectively. Since it is assumed that $V_p = V_c$, U_{pt} and U_{ct} will be equal.

7. Determination of v_o & U_o :

Let H = Drop height = 360"

D_c = Distance external fins crush = 1.54"

D_p = Gap between fuel pins and cask cavity prior to cask impact on unyielding surface.

g = 386.4 in./sec²

8. Equations of Motion of Cask After Impact With Unyielding Surface But Prior to Being Impacted by Fuel Rods: (Subscript 'c' here refers to cask)

$$\ddot{X}_c = -a = \frac{-H}{D_c} g$$

$$\dot{X}_c = \frac{-Hg}{D_c} t + \sqrt{2gH}$$

$$X_c = \frac{-Hg t^2}{2 D_c} + \sqrt{2gH} t$$

9. Equations of Motion of Fuel Rods: (Subscript 'p' here refers to fuel pins)

$$\ddot{x}_p = g$$

$$\dot{x}_p = gt + \sqrt{2gH}$$

$$x_p = \frac{gt^2}{2} + \sqrt{2gH} t$$

Solve for Time When Fuel Rods Impact Cask:

$$D_p + x_c - x_p = 0$$

$$D_p - \frac{Hg t^2}{2D_c} + \sqrt{2gH} t - \frac{g t^2}{2} - \sqrt{2gH} t = 0$$

$$t = \sqrt{\frac{2 D_p D_c}{g(H+D_c)}}$$

Substituting this value of t in the equations for x_c and x_p , the values of v_o and U_o are obtained respectively.

$$v_o = \sqrt{2gH} \left(1 - \sqrt{\frac{HD_p}{D_c(H+D_c)}} \right)$$

$$U_o = \sqrt{2gH} \left(1 + \sqrt{\frac{D_p D_c}{H(H+D_c)}} \right)$$

b. Computations

Four fuel types were examined, the one BWR and three select PWR's. The PWR's were (1) the B&W Zircaloy cladding bundle, (2) the Westinghouse Zircaloy cladding bundle, and (3) the Westinghouse 14 x 14 stainless steel bundle. These four bundles are a representative cross-section of the two generic fuel types.

Based on a comparison of the safety factors it is clear that the side drop is the more severe orientation for the fuel rods. Hence, those parameters governing resistance to side loading are the limiting criteria for the fuel integrity under the 30-foot drop.

A computer program was written to determine the pellet stress (f_p/A_p), cladding stress (f_c/A_c), cask velocity (v) and average fuel rod velocity (U) at intervals in time ranging from 0 to T.

The input parameters for the four fuel types are shown in Table V-32. The results of the computed solution are shown in Table V-33. Safety factors are based on dynamic ultimate strengths. All of the representative fuels are more than able to sustain the end drop without failure.

Table V-32
FUEL ROD INPUT PARAMETERS

<u>Fuel Bundle</u>	<u>A_p (in.²)</u>	<u>A_c (in.²)</u>	<u>l (in.)</u>	<u>M_p (lb-sec²/in.)</u>	<u>M_c (lb-sec²/in.)</u>	<u>D_p (in.)</u>	<u>Material</u>
GE BWR	164.8	46.9	161	27.17	4.62	0.75	Zr
B&W PWR	162.0	50.7	154	25.55	4.78	0.75	Zr
W PWR	160.5	47.7	150	24.65	4.38	0.50	Zr
PWR	148.2	21.8	130	19.85	2.12	0.50	SST

$$M = \frac{127,600}{386.4} = 330 \text{ lb-sec}^2/\text{in.}$$

$$F = 140,000 \times 234 = 3.28 \times 10^7 \text{ lb}$$

Table V-33
FUEL END DROP RESULTS

<u>Fuel Type</u>	<u>Max. Cladding Stress, psi</u>	<u>SF*</u>	<u>Material</u>
GE-BWR	45,370	2.1	Zircaloy
B&W-PWR	44,900	2.1	Zircaloy
W-PWR	39,600	2.4	Zircaloy
W-PWR	60,360	1.4	304 SST

* σ_{UD} = 93.75 ksi Zircaloy
= 82.50 ksi Stainless Steel

c. Confirmation of Calculations:

The impact between the fuel rods and the cask has been idealized as shown in Figure V-63.

This idealization should yield conservative results since in reality when the fuel assemblies come into contact with the cask, the fuel rods themselves do not make immediate contact, but rather appurtenances (such as lifting bales, etc.) do, which will absorb some of the shock and reduce the stresses in the fuel rods due to impact.

As a check on the cask and fuel rod velocities after impact, the following equation should be satisfied.

$$\int_{t_1}^{t_2} F dt = \left(\sum mv \right)_f - \left(\sum mv \right)_i$$

Using the BWR calculations as an example:

$$\begin{aligned} -3.28 \times 10^7 \times 2.176 \times 10^{-3} &= [330 \times 28.1] + [31.79 \times (-345)] - [330 \times 160.15] - [31.79 \times 529] \\ -7.14 \times 10^4 &= -7.14 \times 10^4 \quad \text{Checks} \end{aligned}$$

5.6.5.B Fuel Bundles - Group II

The Group II BWR and PWR fuels were analyzed for the limiting accident cases, viz. 30-ft side drop and 30-ft end drop. The analyses are summarized in Appendix V-2. Although more precise and detailed modeling techniques were used to analyze the Group II fuels, the results are similar to those for Group I fuels. Based on allowable limits, no fuel or basket failures occur in the 30-foot drop.

5.6.6 Cask Shells and Shielding at 122.3 g Side Drop

When the cask impacts during the 30-foot side drop, the body acts as a beam supported at either end by the structural rings and acted upon by the 122.3 g maximum deceleration. The shear and moment diagrams for this loading condition are shown on Figure V-64. The following analysis examines the stress levels in the shells for bending, internal shear and external shear (punching action).

5.6.6.1 Assumptions

- a. Only the inner and outer shells resist the bending stresses. No credit will be taken for reinforcement by the uranium.

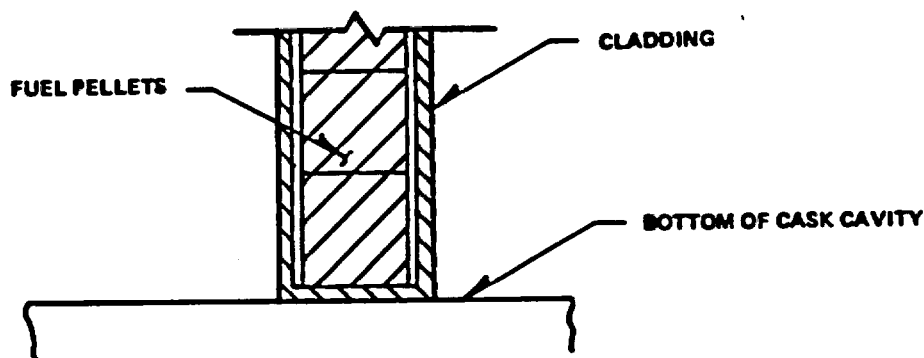


FIGURE V-63. IMPACT MODEL DETAIL

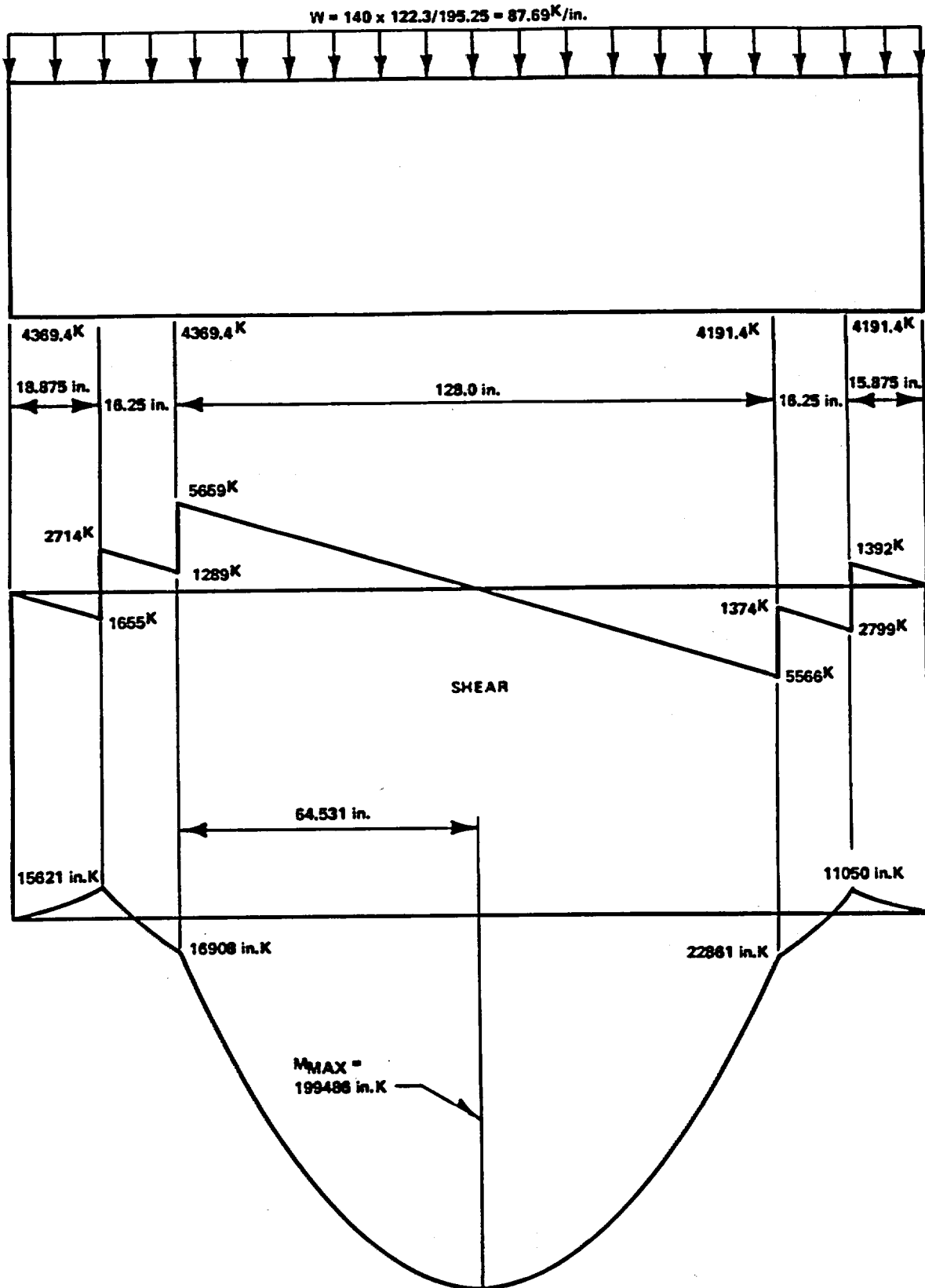


FIGURE V-64. CASK BODY SHEAR AND MOMENT DIAGRAM

- b. The inner and outer shells will deflect the same under load. Therefore, the load each carries will be proportional to its moment of inertia.
- c. Under high strain-rate conditions, the dynamic yield stresses may be taken as 125% of the static yield value.

5.6.6.2 Dynamic Yield Stresses (Normal Conditions)

- (a) 317 or 216 SST Inner Shell (@ 283°F)

$$\sigma_y = (1.25) (41.2) = 51.5 \text{ ksi}$$

$$\sigma_\gamma = (0.577) (51.5) = 29.7 \text{ ksi}$$

- (b) 317 SST Outer Shell (@ 230°F)

$$\sigma_y = (1.25) (47.9) = 59.9 \text{ ksi}$$

$$\sigma_\gamma = (0.577) (59.9) = 34.6 \text{ ksi}$$

5.6.6.3 Moment of Inertia and Section Moduli

- (a) Inner Shell

$$I = \pi (19.25^4 - 18.75^4)/4 = 10,776 \text{ in.}^4$$

$$S = 10,776/19.25 = 560 \text{ in.}^3$$

- (b) Outer Shell

$$I = \pi (24.75^4 - 23.25^4)/4 = 65,208 \text{ in.}^4$$

$$S = 65,208/24.75 = 2,635 \text{ in.}^3$$

Based on assumption (b):

$$\text{Inner shell load \%} = 10,776/75,984 = 14.18\%$$

$$\text{Outer shell load \%} = 65,208/75,984 = 85.82\%$$

5.6.6.4 Bending Stresses

From Figure V-64, the maximum bending moment is 199,486 in.-kips. The bending stress is given by:

$$\sigma_B = \frac{fM}{S}$$

where: f = shell load fraction
M = Moment, in.-kips
S = Section modulus, in.³

(a) Inner Shell

$$\sigma_B = \frac{(0.1418)(199486)}{560} = 50.5 \text{ ksi} < 51.5 \text{ ksi}$$

(b) Outer Shell

$$\sigma_B = \frac{(0.8582)(199486)}{2635} = 65.0 \text{ ksi} > 59.9 \text{ ksi}$$

As can be seen, the outer fiber stress level of the outer shell exceeds yield. This will be examined in more detail to quantify the extent of permanent strain. This is done to determine if permanent deformation can produce a radiation streaming problem by separating the uranium ring joints.

5.6.6.5 Outer Shell Permanent Strain Analysis

Referring to the shear and moment diagram Figure V-64, we must first determine how much of the outer shell, axially, is stressed beyond the dynamic yield point. This can be determined as follows:

$$\frac{fM'}{S} = \sigma_y$$

$$\frac{0.8582 M'}{2635} = 59.9$$

$$M' = 183,900 \text{ in.-kips}$$

Thus, any outer shell section subjected to a bending moment less than M' will remain elastic. The axial extent of the shell above the dynamic yield value measured from the point of maximum moment is given by

$$\begin{aligned} X &= \sqrt{\frac{2(M-M')}{W}} \\ &= \sqrt{\frac{2(199,486 - 183,900)}{87.69}} \\ &= 18.85 \text{ in. (above and below } M_{\max}) \end{aligned}$$

Figure V-65 is the stress-strain diagram for modified 317 stainless steel. Scale B is the curve as normally seen extending to ultimate strength. Scale A is an enlargement of that portion of Scale B around the yield strength. From Scale A it can be seen that at a stress level of 65 ksi the permanent strain is only 0.0041. This value is not significantly different from 0.002 strain used to define yield point.

Using an average strain of 0.003 and applying it to the total affected length of $2 \times 18.85 = 37.7$ inches yields a maximum elongation of 0.113 inches over that length. There is no uranium joint at the point of maximum moment. The closest joint is 7-13/16 inches away which makes the corresponding outer shell strain somewhat less than 0.0041. However, using this maximum strain value and applying it to the effective maximum uranium joint length of 1/2 inch (see Figure V-66) yields a maximum uranium face separation of

$$S = (0.0041) (0.5) = 0.002 \text{ inch}$$

Gamma probe measurements at various joint gaps using a Cobalt 60 source, indicate that a 0.002-inch face separation has an insignificant affect on radiation shielding.

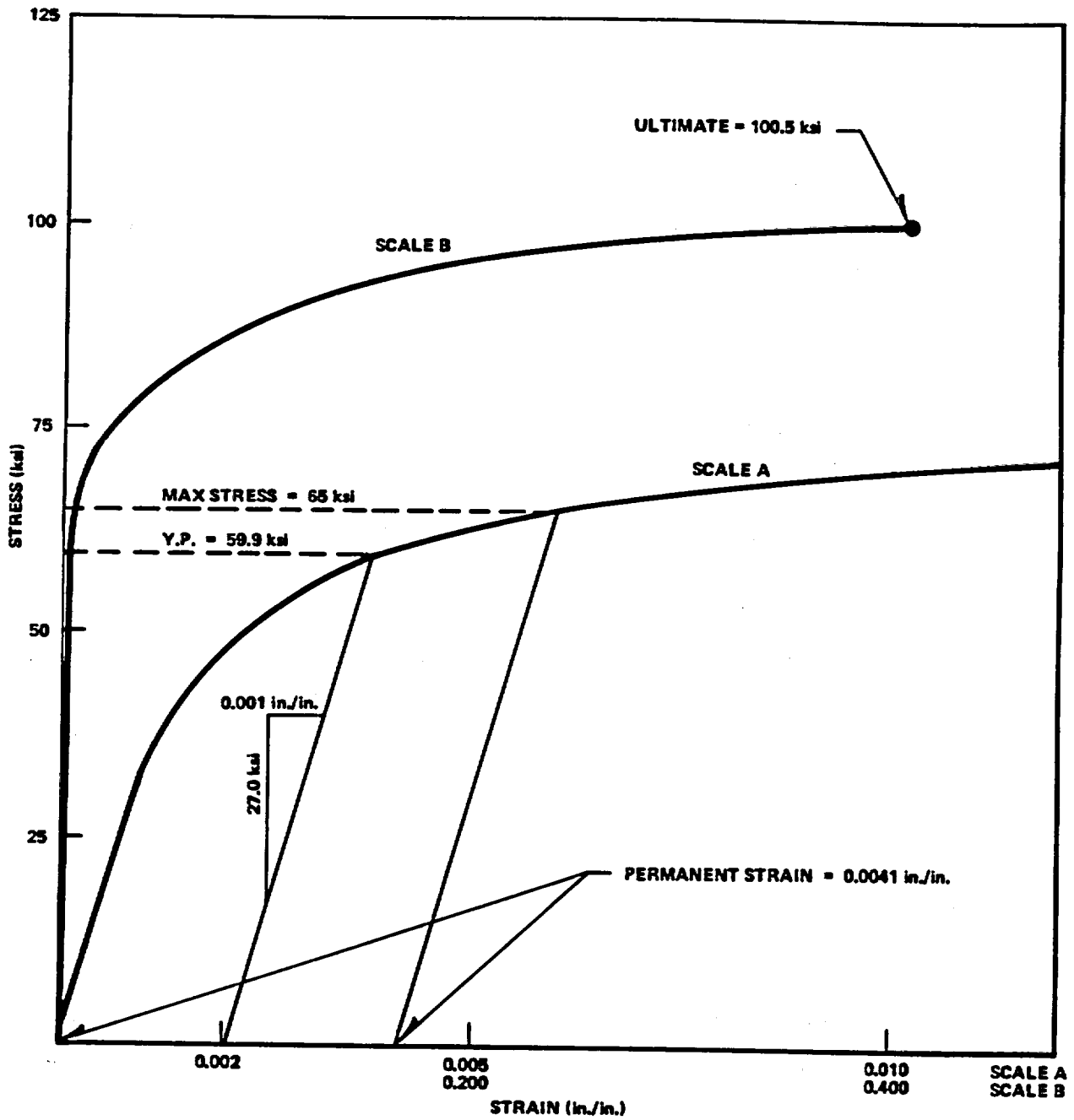


FIGURE V-65. DYNAMIC STRESS-STRAIN CURVE FOR MOD TYPE 317 STAINLESS STEEL

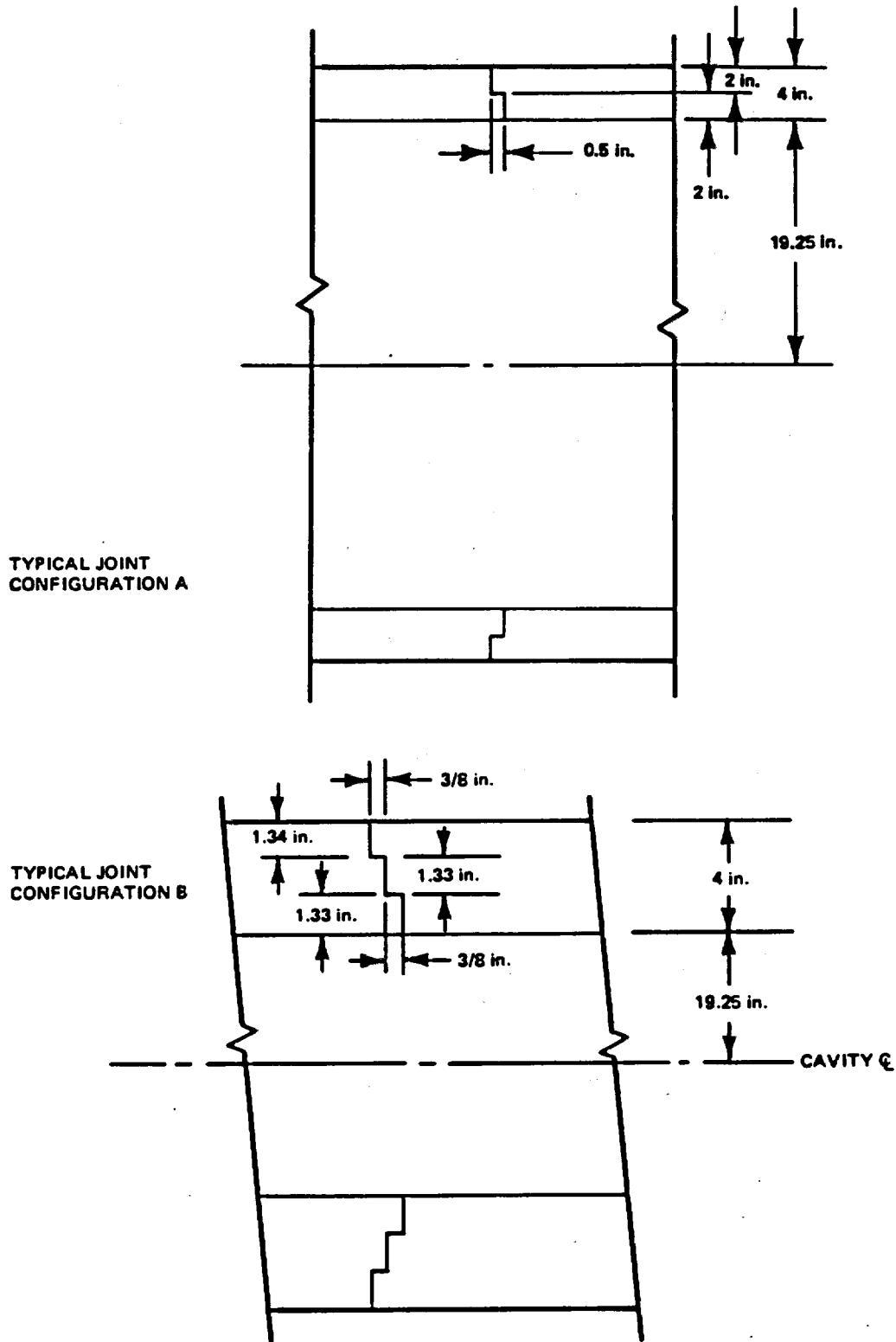


FIGURE V-66. URANIUM JOINT CONFIGURATIONS

5.6.6.6 Shear Force in Shells

Because of the contact pressure between the shell and the uranium cylinder, a friction force, f , exists between the shell and the uranium due to the relative movement arising from the stretching and compressing of the shell fibers in bending. This friction force acts on the inner surface of the outer shell and on the outer surface of the inner shell.

Referring to Figure V-67:

M = Bending Moment @ x

$M + dM$ = Bending Moment @ $x + dx$

P_1 = Contact Press. Between Outer Shell and Uranium

P_2 = Contact Press. Between Inner Shell and Uranium

μ = Coeff. of Friction Between Shells and Uranium

For Outer Shell ($r = 23.25$ in., $R = 24.75$ in.)

$$f = \pi \mu r p_1 dx$$

$$Y_2 = 2r/\pi$$

For Inner Shell ($r = 18.75$ in., $R = 19.25$ in.)

$$f = \pi \mu R P_2 dx$$

$$Y_2 = 2r/\pi$$

$$I = \frac{\pi(R^4 - r^4)}{4}$$

$$F = \frac{2}{3} \frac{M}{I} (R^3 - r^3) = \frac{8M(R^3 - r^3)}{3\pi(R^4 - r^4)}$$

$$F + dF = \frac{2}{3} \frac{(M+dM)}{I} (R^3 - r^3) = \frac{8(M+dM)(R^3 - r^3)}{3\pi(R^4 - r^4)}$$

$$Y_1 = \frac{3\pi(R^4 - r^4)}{16(R^3 - r^3)}$$

Solve for V_L & V_R :

$$1) \quad F_v = 0 = V_L - Wdx - V_R$$

$$2) \quad M_{,0}'' = 0 = V_L dx + 2F_{Y_1} + 2f_{Y_2} - W \frac{dx^2}{2} - 2(F + dF)Y_1$$

$W \frac{dx^2}{2}$ may be neglected because it is quite small.

Substituting in the appropriate values and solving for V_L & V_R , the following is obtained:

Outer Shell:

$$V_L = \frac{dM}{dx} - 4\mu r^2 P_1 = V - 4\mu r^2 P_1 \quad \text{Where } V = \text{shear @ } x$$

$$V_R = V - 4\mu r^2 P_1 - Wdx$$

Inner Shell:

$$V_L = V - 4\mu R^2 P_2$$

$$V_R = V - 4\mu R^2 P_2 - Wdx$$

Referring to Figure V-68:

$$\sum F_H = 0 = 2(R-r) \tau dx + F + f - (F + dF)$$

$$\text{or, } 2(R-r) \tau dx = dF - f$$

Solving for τ :

Outer Shell:

$$\tau = V \left[\frac{4(R^2 + Rx + r^2)}{3\pi(R^4 - r^4)} \right] - \frac{\pi\mu r P_1}{2(R-r)}$$

The first term in the expression for τ is nothing more than $\frac{VQ}{Ib}$. Thus, the shear stress is reduced by the friction between the shell and the uranium.

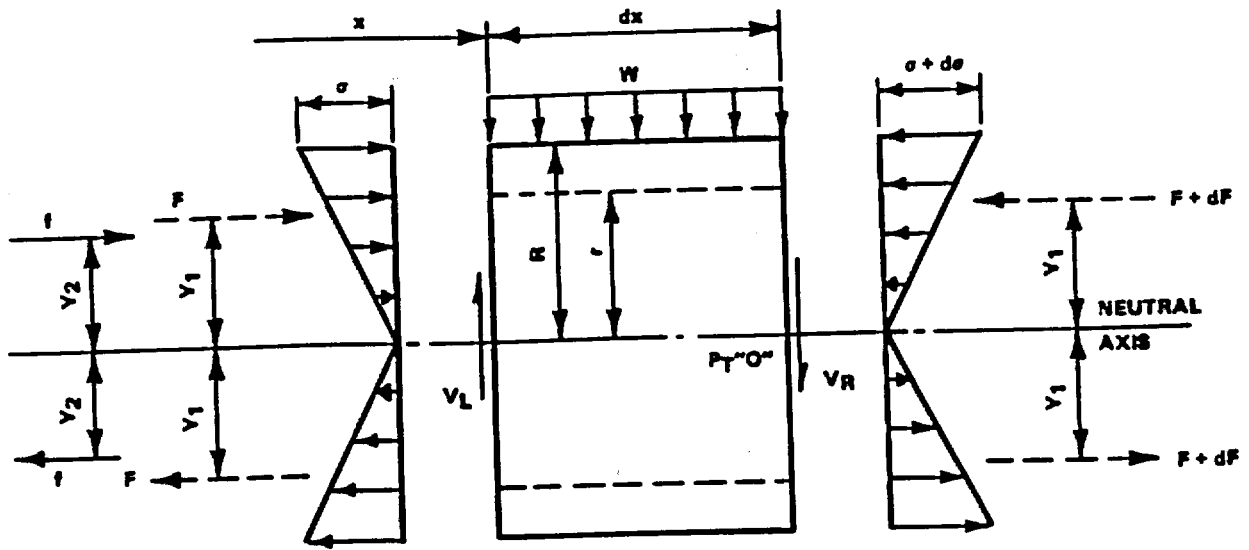


FIGURE V-67. FORCES ACTING ON A LENGTH dx OF SHELL

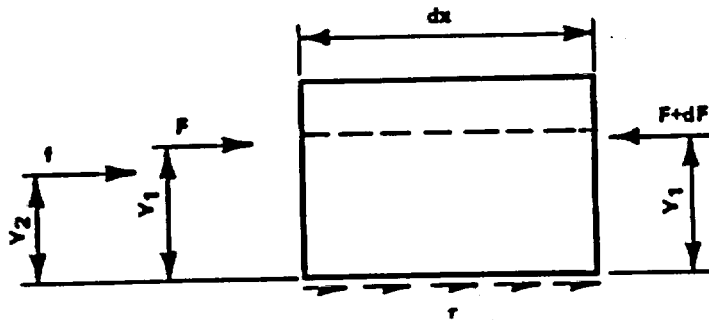


FIGURE V-68. HORIZONTAL SHEAR STRESS AT NEUTRAL AXIS OF SHELL

Inner shell:

$$\tau = v \left[\frac{4(R^2 + Rr + r^2)}{3\pi(R^4 - r^4)} \right] - \frac{\pi \mu R P_2}{2(R-r)}$$

Contact pressures between shells and uranium: The minimum possible contact pressures between the shells and the uranium for the normal operating condition will be used. This corresponds to an internal pressure of 55 psi and the minimum interference fits specified, i.e., zero inches between inner shell and uranium and 0.005 inches between outer shell and uranium.

Solving the equations for the contact pressures:

$$P_1 = 456 \text{ psi}; P_2 = 299 \text{ psi (see Section 5.4)}$$

Coefficient of Friction, μ :

The inner surface of the outer shell and the outer surface of the inner shell are to be copper plated. Mark's "Mechanical Engineers' Handbook," 6th Edition, pages 3-40, gives a coefficient of friction of 0.53 for copper on mild steel. Since uranium exhibits properties similar to mild steel, a value of $\mu = 0.5$ will be used.

Shear stress in Outer Shell:

$$v = 0.8582 \times 5659 = 4857k$$

$$\tau = 4857 \left[\frac{4(24.75^2 + 24.75 \times 23.25 + 23.25^2)}{3 \times \pi (24.75^4 - 23.25^4)} \right] - \frac{\pi \times 0.5 \times 23.25 \times 0.456}{2 (24.75 - 23.25)}$$

$$= 43.0 - 5.55 = 37.45 \text{ ksi} > 34.6$$

Shear Stress in Inner Shell:

$$v = 0.1418 \times 5659 = 802k$$

$$\tau = 802 \left[\frac{4(19.25^2 + 19.25 \times 18.75 + 18.75^2)}{3 \times \pi (19.25^4 - 18.75^4)} \right] - \frac{\pi \times 50.5 \times 19.25 \times 0.299}{2 (19.25 - 18.75)}$$

$$= 26.9 - 9.04 = 17.86 \text{ ksi} < 29.7$$

It can be seen that the shear stress in the outer shell (37.45 ksi) slightly exceeds the shear yield stress (34.6 ksi). Again, as in the case of the bending stress at the center of the cask, only slight permanent shear deformation will occur at the structural rings. This will cause no problem as far as radiation shielding integrity is concerned.

5.6.6.7 Shear Forces in Uranium

Based on the shell analysis of the previous subsection, there will be a shearing force carried by the uranium. This force is resisted by either a uranium section or a uranium joint depending on the location of the force. Referring to Figure V-69, the magnitude of the force is as follows:

$$f_1 = \pi \times 0.5 \times 19.25 \times 0.299 = 9.04k$$

$$f_2 = \pi \times 0.5 \times 23.25 \times 0.456 = 16.65k$$

$$V = 9.04 \times 24.5 + 16.65 \times 29.6 = 714k$$

If V is resisted by internal shear the stress level is very low

$$\tau = \frac{714}{\pi(23.25^2 - 19.25^2)} = 1.34 \text{ ksi}$$

The most highly stressed section is the uranium joint shown on Figure V-66 and of the two joints shown, Configuration A has the smaller shear area.

If V is resisted by the uranium joint:

$$\text{Shear yield stress of uranium} = 1.25 \times 29 \times 0.577 = 20.9 \text{ ksi}$$

$$\text{Min. shear area} = \frac{714}{20.9} = 34.1 \text{ in.}^2$$

Load must be resisted along an arc length = $\frac{34.1}{2.0} = 17.05$ in.

Angle = $17.05/21.25 = 0.8025$ rad = 46°

It is reasonable to assume that the 714k force will spread out 23° each side of the centerline.

5.6.6.8 Bending Stress in Uranium Jt:

$$M = 714 \times 0.25 = 178.5 \text{ in. k}$$

$$S = \frac{17.05 \times 2^2}{6} = 11.37 \text{ in.}^3$$

$$\sigma = \frac{178.5}{11.37} = 15.7 \text{ ksi} < 29 \times 1.25 = 36.25$$

$$SF = \frac{36.25}{15.7} = 2.31$$

5.6.6.9 External Shear at Impact Rings

There is a "punching" action directly under each of the four impact rings. (See Figure V-64) - Shear and Moment Diagram). Figure V-70 shows the conservatively assumed area which must resist the 4369.4 kip reaction in double shear.

Shear capacity of the shaded area:

$$= 27.16 (1.5 \times 34.6 + 4 \times 20.9 + 0.5 \times 29.7) \times 2$$

$$= 8170 \text{ kips}$$

$$SF = \frac{8170}{4369.4} = 1.87$$

5.6.6.10 Conclusion

The above analyses have shown the cask inner shell, outer shell, and uranium shielding pieces capable of sustaining the shear and bending forces associated with the 122.3 g side drop deceleration without loss of integrity or reduction of shielding ability.

FIGURE WITHHELD UNDER 10 CFR 2.390

FIGURE V-70. EXTERNAL SHEAR RESISTANCE AREA

5.7 40-INCH DROP PUNCTURE

This analysis examines the cask outer shell and the cavity valve box lid under the loading conditions imposed by a 40-inch drop on a 6-inch diameter pin.

5.7.1 Outer Shell

The significance of puncturing the outer shell on a uranium shielded cask is minor compared to that of a lead shielded cask. A punctured lead cask could result in shielding loss due to leakage during the 30-minute fire. This cannot occur with a uranium cask since the shielding melting point is much greater than the fire temperature (MP = 2071°F). Nevertheless, the determination of the outside shell thickness is based on a formula developed for a lead-shielded cask, and is therefore, considered to be quite conservative.

$$t = \left(\frac{W}{\sigma_u} \right)^{0.71} \quad (\text{ref 21, page 12})$$

where

W = Cask wt in kips

σ_u = ultimate tensile strength of outside shell (ksi)

t = outside shell thickness (in.)

solving

$$t = 1.35 \text{ in.}$$

The actual IF 300 outer shell is 1.5 inches thick resulting in a puncture safety factor of 1.11.

5.7.2 Valve Box

Maximum damage to the valve box will occur when the 6-inch diameter pin strikes the valve box as illustrated in Figure V-71 below.

5.7.2.1 Loss of KE and Impulsive Reaction

When the cask and pin contact, the resulting impact can be considered "perfectly plastic." The KE analysis is as follows:

$$M = \frac{W}{g}$$

I = Mass moment of inertia of cask about center of mass

V_1 = Linear velocity of CM before impact.

$$= \sqrt{2gH}$$

$$H = 40 \text{ in.}$$

V_2 = Linear velocity of CM after impact.

ω_2 = Angular velocity of CM after impact.

$$K^2 = \frac{I}{M}$$

Using the principle of impulse and momentum for a rigid body:

$$(\text{System momenta})_1 + (\text{System Ext. Impulse}) = (\text{System Momenta})_2$$

Figure V-72 shows graphically the above relationship:

Taking moments about CM:

$$0 + r (F\Delta t) - I_{\omega} = MK^2\omega$$

considering vertical components:

$$MV_1 - F\Delta t = MV_2$$

after impact vertical velocity at "A" must be zero.

$$\text{Therefore, } V_A = 0 = V_2 - r\omega$$

then,

$$\omega = \frac{V_2}{r}$$

FIGURE WITHHELD UNDER 10 CFR 2.390

NEDO-10084-3
September 1984

solving for $F\Delta t$, V_2 and ω ,

$$F\Delta t = MV_1 \left(\frac{K^2}{r^2 + K^2} \right)$$

$$V_2 = V_1 \left(\frac{r^2}{r^2 + K^2} \right)$$

$$\omega = V_1 \left(\frac{r}{r^2 + K^2} \right)$$

The difference between the post-impact KE, and the pre-impact KE must be dissipated in the valve box.

$$\begin{aligned} \Delta KE &= \frac{1}{2} MV_1^2 - \left(\frac{1}{2} MV_2^2 + \frac{1}{2} I\omega^2 \right) \\ &= \frac{1}{2} MV_1^2 \left(\frac{k^2}{r^2 + k^2} \right) = \left(KE_1 \frac{k^2}{r^2 + k^2} \right) \end{aligned}$$

This ΔKE must be absorbed by crushing the fins on the valve box lid.

5.7.2.2 Mass Moment of Inertia of the Cask:

An inspection of the formulas for $F\Delta t$ and ΔKE , above, shows that the higher the value of the radius of gyration, K , the higher also will be the impulsive reaction and the change in KE. Therefore, in determining K , the cask will conservatively be assumed to have all its mass concentration in a hollow cylinder with the following dimensions (Figure V-73):

- a, inside radius = 18.75 in.
- b, outside radius = 24.75 in.
- ℓ, length = 192.25 in.

$$I = \frac{M}{12} \left[3(b^2 + a^2) + \ell^2 \right]$$

$$\begin{aligned} K^2 &= \frac{3(b^2 + a^2) + \ell^2}{12} \\ &= 3420 \text{ in.}^2 \end{aligned}$$

$$M = \frac{140}{3864} = 0.362 \text{ k-sec}^2/\text{in.}$$

$$KE = 40 \times 140 = 5600 \text{ in-k}$$
$$r^2 = 70.625^2 = 4990 \text{ in.}^2$$

$$\Delta KE = 5600 \left(\frac{3420}{4990+3420} \right)$$
$$= 2275 \text{ in.-k}$$

$$V_1 = \sqrt{2 \times 386.4 \times 40}$$
$$= 175.8 \text{ in./sec}$$

$$\Delta t = 0.362 (175.8) \left(\frac{3420}{4990+3420} \right)$$
$$= 25.9 \text{ kip-sec.}$$

5.7.2.3 Fin Bending:

The 6 in. ϕ piston could strike either two or three fins; both cases are examined. It is assumed that the fins bend along their entire (14 in.) length.

a. Case I - Two Fins

$$\Delta KE = 2275 \text{ in.-k} = 2 \times 55 \times 14 \times 0.5625^2 \times \theta$$

Solving:

$$\theta = 4.67 \text{ rad}$$

Using the fin bending correlation

$$\frac{\delta}{h} = 0.67$$

$$\text{then, } \delta = (7 \text{ in.}) (0.67) = 4.69 \text{ in.}$$

$$F = \frac{2275}{4.69} = 485 \text{ k}$$

$$\Delta t = \frac{25.9}{485} = 0.0534 \text{ sec}$$

Since this lid and box loading is less than that of the 30-foot drop condition, no further analysis is required.

b. Case II - Three Fins

$$2275 = 3 \times 55 \times 14 \times 0.5625^2 \times \theta$$

$$\theta = 3.11 \text{ rad}$$

$$\frac{\delta}{h} = 0.335$$

$$\text{then, } \delta = 7 \times 0.335 = 2.345 \text{ in.}$$

$$F = \frac{2275}{2.345} = 970 \text{ k}$$

$$\Delta t = \frac{25.9}{970} = 0.0267 \text{ sec.}$$

5.7.2.4 Component Stresses (Figure V-74)

Maximum stress in valve box lid occurs when the pin impacts fin numbers 3, 4 and 5. Assuming that the 970 k load is uniformly distributed over an area of:

$$12.5 \times 32.75 \tan 12^\circ$$

yields a value:

$$W = \frac{970}{(12.5 \times 6.96)} = 11.14 \text{ ksi}$$

conservatively assuming that the lid is simply supported on all four sides, find the value of W_u , the ultimate load the plate can carry.

Rotation of yield lines:

$$\theta = 2 \times \left(\frac{1}{8.84} \right) = 0.226$$

$$M = 58.4 \text{ in.-k/in. (from 30 ft drop analysis)}$$

$$\begin{aligned} W_1 &= 2 \times 17.68 \times 58.4 \times 0.226 \\ &= 467 \text{ in.-k} \end{aligned}$$

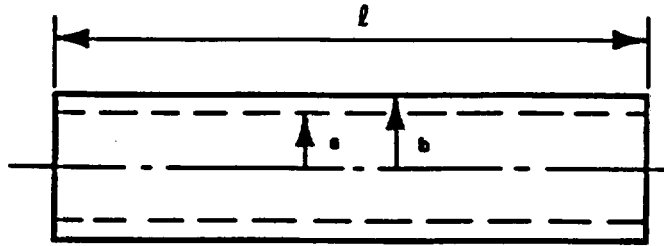


FIGURE V-73. BODY MODEL

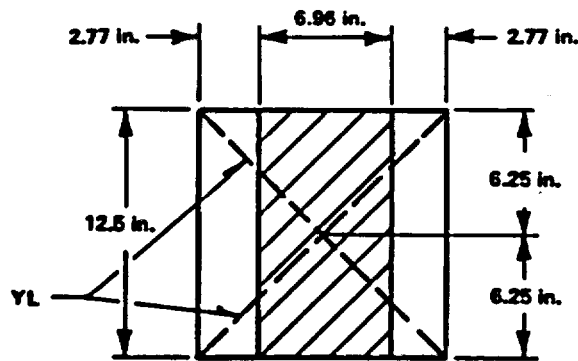


FIGURE V-74. LOADING DISTRIBUTION

External Work:

$$\begin{aligned}W_e &= 2 \times W_u \times 6.96 \times 2.77 \times 1.385/6.25 \\ &\quad + 4 \times W_u \times 3.48^2 \times 3.93/6.25 \\ &= 39.05 W_u\end{aligned}$$

Since, by virtual work theorem:

$$W_i = W_e$$

$$W_u = \frac{467}{39.05} = 11.95 \text{ ksi}$$

$$\therefore \text{Lid SF} = \frac{11.95}{11.14} = 1.073$$

Checking stresses in wall #1:

$$P = 11.14 \times (6.96 \times 2.77 \times 3.48^2) = 350\text{k}$$

$$\sigma = \frac{350}{1 \times 12.5} = 28 \text{ ksi}$$

$$\text{SF} = \frac{58}{28} = 2.07$$

Checking axial stresses in wall #3:

Assume: Pin centerline strikes directly over fin #1.

$$P = 970\text{k}$$

$$\sigma = \frac{970}{1.5 \times 12.5} = 51.7 \text{ ksi}$$

$$\text{SF} = \frac{58}{51.7} = 1.13$$

5.7.2.5 Conclusion

The analyses of this section demonstrate that the cavity valve box is capable of sustaining the 40-inch puncture without losing integrity (SF > 1.0) or damaging the contents.

5.8 CASK TIEDOWN AND LIFTING

5.8.1 Materials

5.8.1.1 Saddle, cradle, cradle pedestals and tipping cradle trunnions are A516 GR 70 steel.

Min. Yield = 38.0 ksi

Ult. Tensile = 70.0 to 85.0 ksi

5.8.1.2 Block Pin A1S1 4340

Heat treated to Min. Yield = 125.0 ksi

5.8.1.3 Structural rings are Type 216 stainless steel

Yield = 58.4 ksi @ 70°F

5.8.1.4 Cask outer shell is CG-8M, modified 317 stainless steel:

Yield = 47.4 ksi @ 235°F

5.8.2 Cask-to-Skid Tiedown Properties and Stresses During Transport

Figure V-75 shows the cask in its horizontal shipment position. The cask is supported at the front by a saddle and at the rear by a pivot cradle held between two pedestals. Acting through the cask center of gravity are the 10 g axial and 2 g vertical forces prescribed in the regulations. Also acting through the CG but not shown on the figure is the regulatory 5 g lateral force.

The reactions at the supports are given by:

$$R_B = \frac{19.6H - 93.125V}{163.75} = 0.1197H - 0.569V = .059W$$

$$R_C = \frac{19.6H + 70.625V}{163.75} = -0.1197H - 0.432V = -2.061W$$

$$R_H = H = 10W$$

Solving for all combinations of H and V yields the data in Table V-34.

FIGURE WITHHELD UNDER 10 CFR 2.390

NEDO-10084-3
May 1985

Table V-34
SUPPORT REACTIONS

ALL LOADS IN KIPS				
<u>H</u>	<u>V</u>	<u>R_s</u>	<u>R_c</u>	<u>R_H</u>
+1400.0	+280.0	+ 8.5	-288.5	+1400.0
+1400.0	-280.0	+ 326.9	- 46.9	+1400.0
-1400.0	+280.0	- 326.9	+ 46.9	-1400.0
-1400.0	-280.0	- 8.5	+288.5	-1440.0

The individual support components under the normal shipping loads are discussed in following sections.

5.8.2.1 Front Saddle - Transport

Figure V-76 is Section A-A of Figure V-75 and shows the front saddle configuration. The CG of the bearing area is located as follows:

$$y = R \left(1 - \frac{\sin \alpha}{\alpha} \right)$$

where R = 25.0 in.
 $\alpha = 67.5^\circ (1.178 \text{ rad})$

$$y = 5.40 \text{ in.}$$

Figure V-77 is Section C-C of Figure V-76 and shows the details of the front saddle to cask interface.

Table V-35 shows the structural properties of the composite ring section shown in Figure V-77.

Table V-35
PROPERTIES OF COMPOSITE RING SECTION

<u>Part</u>	<u>A</u>	<u>Y</u>	<u>AY</u>	<u>AY²</u>	<u>I_{o-x}</u>
Rings	17.50	3.50	61.3	215	71.5
Shell	34.50	7.75	267.4	2072	6.5
Flg.	9.56	9.63	92.1	887	4.0
Σ	61.56	6.83	420.8	3174	82.0

FIGURE WITHHELD UNDER 10 CFR 2.390

FIGURE V-78. SADDLE CONFIGURATION

5-210

FIGURE WITHHELD UNDER 10 CFR 2.390

FIGURE V-77. SADDLE-CASK INTERFACE

$$I_x = 3174 + 82.0 - 61.56 \times 6.83^2 = 380 \text{ in.}^4$$

The following calculations define the section properties of the saddle base:

$$I_{xx} = 0.0833 (14 \times 60^3 - 11 \times 57^3) = 82,400 \text{ in.}^3$$

$$I_{yy} = 0.0833 (60 \times 14^3 - 57 \times 11^3) = 7390 \text{ in.}^3$$

$$A = (14 \times 60) - (11 \times 57) = 213 \text{ in.}^2$$

$$C_x = 30.0 \text{ in.}, C_y = 7.0 \text{ in.}$$

Stress Analysis

$$\begin{aligned} \text{Saddle lateral load} &= H_s \\ W_L &= 5W = 5 \times 140 = 700\text{k} \end{aligned}$$

$$H_s = 0.569 W_L = 398 \text{ kips}$$

$$\text{Saddle vertical load} = R_s$$

$$R_s = 326.9 \text{ kips}$$

$$\text{Saddle longitudinal load} = R_H$$

$$R_H = 1400 \text{ k}$$

Moments:

$$M_x = 40 H_s = 40 \times 398 = 15,920 \text{ in.-kips}$$

$$M_y = 20.4 R_H = 20.4 \times 1400 = 28,560 \text{ in.-kips}$$

Bending stress:

$$\begin{aligned}\sigma_{\max} &= \frac{R_s}{A} + \frac{M_x C_x}{I_x} + \frac{M_y C_y}{I_y} \\ &= \frac{326.9}{213} + \frac{15920 \times 30}{82400} + \frac{28560 \times 7}{7390} \\ &= 1.53 + 5.80 + 27.03 \\ &= 34.36 \text{ ksi (combined stress at base)}\end{aligned}$$

and

$$SF = \frac{38.0}{34.36} = 1.11$$

Bearing stress @ saddle from R_H :

Length of bearing area, $L_B = 2R_\alpha$

$$\begin{aligned}&= 2 \times 25.0 \times 1.178 \\ &= 58.9 \text{ in.}\end{aligned}$$

$$p = \frac{R_H}{L_B} = \frac{1400}{58.9} = 23.8 \text{ kips/in.}$$

$$A_B = 0.50 \text{ in.}^2/\text{in.}$$

Therefore:

$$\sigma_B = \frac{23.8}{0.5} = 47.6 \text{ ksi}$$

and

$$SF = \frac{38.0}{0.6 \times 47.6} = 1.33$$

Weld stresses - bearing element to vessel shell:

$$I_{\text{Weld}} = \frac{1.0 \times 2.0^3}{12} = 0.07 \text{ in.}^4/\text{in.}$$

$$c = 1.0 \text{ in.}$$

$$A_w = 2.0 \text{ in.}^2/\text{in.}$$

$$M = 0.25 p = 5.95 \text{ in.-kips/in.}$$

then:

$$\sigma_{\text{Bending}} = \frac{5.95 \times 1.0}{0.67} = 8.88 \text{ ksi}$$

$$SF_B = \frac{47.4}{8.88} = 5.34$$

and

$$\tau = \frac{23.8}{2} = 11.9 \text{ ksi}$$

$$SF_s = \frac{(47.4)(0.577)}{11.9} = 2.4$$

Shell moment as a result of saddle bearing forces:

The bearing surface is that region between the structural rings.
The solution follows case 15 of Reference 3, Table XIII.

$$M = 1.0p = 1.0 \times 23.8 = 23.8 \text{ in.-kips/in.}$$

$$M_o = M/2 = 11.9 \text{ in.-kips/in.}$$

$$M_x = M_o e^{-\lambda x} (\cos \lambda x + \sin \lambda x)$$

$$\lambda = \left(0.78 \sqrt{rt}^{-1}\right) = 0.214$$

when: $M_x = 0$

$$\cos \lambda x + \sin \lambda x = 0$$

$$\lambda x = 135^\circ = 2.356 \text{ rad}$$

$$x = \frac{2.356}{\lambda} = 11.0 \text{ in.}$$

therefore influence of top flange on M_o can be neglected.

Shell bending stress

$$\sigma_B = \frac{6M_o}{t^2} = \frac{6 \times 11.9}{1.5^2}$$

$$= 31.75 \text{ ksi}$$

$$SF = \frac{47.4}{31.75} = 1.5$$

Note that outside of the bearing surface, M_o is directly resisted by the top flange with minimal effect on the shell.

5.8.2.2 Pivot Cradle - Transport

Figure V-75 shows the cradle in its shipping position. Figure V-78 below is the cradle cross-section. Table V-36 gives the properties of this section.

Table V-36

PROPERTIES OF PIVOT CRADLE SECTION

<u>Part</u>	<u>A</u>	<u>X</u>	<u>AX</u>	<u>AX²</u>	<u>I_{o-y}</u>	<u>Y</u>	<u>AY</u>	<u>AY²</u>	<u>I_{o-x}</u>
Top Flg.	5.0	2.5	12.5	31.25	10.42	23.5	117.5	2761.25	0.42
CTR. "	3.0	2.5	7.5	18.75	2.25	15.0	45.0	675.00	0.25
BTM. "	5.0	2.5	12.5	31.25	10.42	0.5	2.5	1.25	0.42
Outside Web	22.0	0.5	11.0	5.50	1.83	12.0	264.0	3168.00	887.33
Inside Web	22.0	4.5	99.0	445.50	1.83	12.0	264.0	3168.00	887.33
Σ	57.0	2.50	142.5	532.25	26.75	12.16	693.0	9773.50	1775.75

$$I_y = 532.25 + 26.75 - 57.0 \times 2.50^2 = 203 \text{ in.}^4 \quad C_y = 2.50 \text{ in.}$$

$$I_x = 9773.50 + 1775.75 - 57.0 \times 12.16^2 = 3125 \text{ in.}^4 \quad C_x = 12.16 \text{ in.}$$

In the normal transport position, the pivot cradle is acted upon by the 2g load as shown in Figure V-79. The value of 2p is R_c which from Table V-34 is 288.5 kips.

FIGURE WITHHELD UNDER 10 CFR 2.390

FIGURE V-78. PIVOT CRADLE CROSS-SECTION

FIGURE WITHHELD UNDER 10 CFR 2.390

FIGURE V-79. VERTICAL LOADING OF PIVOT CRADLE (CASK IN HORIZONTAL POSITION)

Figure V-80 shows the transport loads imposed on the pivot cradle pedestal during shipment. Once again, the values of H_c and R_c from Table V-34 are 302.4 kips and 288.5 kips, respectively.

Figure V-81 is a detail of one cradle pedestal. Section properties at various elevations are shown in Table V-37.

Table V-37
PEDESTAL PROPERTIES
AND MOMENTS

SECT. NO.	Y	e_x	e_y	M O M E N T S			S E C T. P R O P E R T I E S		
				$H_c Y$	$R_c e_x$	$R_c e_y$	A	I_x	I_y
1	16.0	4.33	0	4840	575	0	75.1	4385	540
2	21.0	5.67	1.07	6360	753	142	88.3	6563	1146
3	26.0	7.02	2.14	7870	933	284	101.4	9352	2068
4	31.0	8.38	3.21	9380	1113	427	114.7	12835	3369
5	37.0	10.00	4.50	11200	1328	598	130.5	17992	5522
6	43.0	10.00	4.50	13020	1328	598	130.5	17992	5522

Stress Analysis

Pivot cradle ring:

From Figure V-80, $R_c = 288.5^k = 2p$

Using case 4, $\theta = \frac{\pi}{2}$ plus case 7, $\theta = \frac{\pi}{2}$

from Reference 3, Table VIII yields:

$$M_o = 6.50P = 938 \text{ in.-kips.}$$

$$M_{x=0} = 0.1365 M_o - 0.50 PR$$

$$= -2272 \text{ in.-kips}$$

$$T_{x=0} = 0.637 \frac{M_o}{R} + 0.3183 P$$

$$= + 64 \text{ kips}$$

Maximum tensile stress on outside ring.

FIGURE WITHHELD UNDER 10 CFR 2.390

FIGURE Y-80. PEDESTAL LOADS

FIGURE WITHHELD UNDER 10 CFR 2.390

NEDO-10084-3
September 1984

NEDO-10084-3
September 1984

$$\begin{aligned}\sigma_T &= \frac{M_{x=0} X}{I_Y} + \frac{P}{A} \\ &= \frac{2272 \times 2.50}{203} + \frac{64}{57.0} \\ &= 29.07 \text{ ksi}\end{aligned}$$

Maximum compressive stress inside ring:

$$\sigma_c = \frac{2272 \times 2.50}{203} - \frac{64}{57.0} = 26.83 \text{ ksi}$$

Consider 90°,

$$\begin{aligned}M_{x=\frac{\pi}{2}} &= \pm 0.50 M_o + 0.1818 PR \\ &= 1342 \text{ in.-kips or } 404 \text{ in.-kips}\end{aligned}$$

$$\begin{aligned}T_{x=\frac{\pi}{2}} &= 0 + P \\ &= 144.25 \text{ kips}\end{aligned}$$

Stress in ring is maximum at $x = 0$

$$SF = \frac{38.0}{29.07} = 1.31$$

Pivot cradle pedestals:

$$\begin{aligned}W_L &= 700 \text{ kips} \\ \text{Pedestal lateral load} &= H_c \\ H_c &= 0.432 W_L = 302.4 \text{ kips}\end{aligned}$$

$$\begin{aligned}\text{Pedestal vertical loads} &= R_L \text{ \& } R_R \\ R_c &= 288.5 \text{ kips}\end{aligned}$$

$$R_R = \frac{39.75 R_c - 3.0 H_c}{79.5} = 132.8 \text{ kips}$$

$$R_L = 288.5 - 132.8 = 155.7 \text{ kips}$$

Referring to Figure V-81:

$$\sigma_1 = \frac{R_R}{A} ; \sigma_2 = \frac{H_Y C_Y}{I_Y}$$

$$\sigma_3 = \frac{R_R e_Y C_Y}{I_Y} ; \sigma_4 = \frac{R_R e_X C_Y}{I_Y}$$

$$\sigma_T = \sigma_1 + \sigma_2 + \sigma_3 + \sigma_4$$

Properties and moments are shown in Table V-37. Stresses are shown in Table V-38.

Table V-38
PEDESTAL STRESSES

<u>SECTION</u>	<u>STRESSES, ksi</u>				
	σ_1	σ_2	σ_3	σ_4	σ_T
1	1.77	31.40	0	1.62	34.79
2	1.50	25.40	0.57	1.57	29.04
3	1.31	21.45	0.77	1.50	25.03
4	1.16	18.70	0.85	1.42	22.13
5	1.02	16.22	0.87	1.33	19.44
6	1.02	18.85	0.87	1.33	22.07

Maximum stress is at section 1. The safety factor is as follows:

$$SF = \frac{38.0}{34.79} = 1.09$$

Checking the pedestal bolt stresses:

Maximum stress is when R_c is acting upward (Figure V-80):

$$P = \frac{R_L}{2} = \frac{155.7}{2} = 77.8 \text{ k/bolt}$$

$$\text{Root area, } A_R = 1.29 \text{ in.}^2$$

$$\sigma_T = \frac{P}{A_R} = \frac{77.8}{1.29} = 60.2 \text{ ksi}$$

$$\sigma_{YP} = 105.0 \text{ ksi (A320, Gr L7)}$$

$$SF = \frac{105.0}{60.2} = 1.74$$

Pivot cradle trunnions:

These items will be evaluated in the lifting section where they are in their most highly stressed condition.

5.8.2.3 Cask Body and Upper Structural Rings - Transport

The upper structural rings straddle and are pinned to the front saddle. These members resist all of the axial and a portion of the vertical and lateral forces.

The axial forces were examined in the front saddle analysis (subsection 5.8.2.1). The following will cover the vertical and lateral forces imposed on the rings which in turn act on the cask body.

Figure V-82 shows the computer model of the composite cask wall consisting of a stainless steel ring linked to a uranium ring. The forces (F_X, F_Y) are the reactions to H_c and R_c at the pin which connects the structural rings to the front saddle.

This model was run for the following values:

$$R_s = 326.9 \text{ kips}$$

$$H_s = 398.0 \text{ kips}$$

R_s and H_s are transmitted around the stainless steel ring by tangential shear:

$$\tau = \frac{R_s \sin \theta - H_s \cos \theta}{\pi R}$$

NEDO-10084-3
September 1984

FIGURE WITHHELD UNDER 10 CFR 2.390

Model results are used to check on any interferences between the outer shell and the uranium shielding. Also, stress levels at the various nodal points are examined.

Computer output for the two rings are shown in Tables V-39 and V-40.

Table V-39
STAINLESS STEEL RING

NODE	Δ_X	Δ_Y	Δ_R	NODE	Δ_X	Δ_Y	Δ_R
	in. $\times 10^2$	in. $\times 10^2$	in. $\times 10^2$		in. $\times 10^2$	in. $\times 10^2$	in. $\times 10^2$
2	0.622	-0.031	0.622	80	0.621	-0.088	-0.621
4	1.004	-0.042	0.985	78	0.317	-0.121	-0.294
8	1.361	0.003	1.295	74	0.063	-0.184	-0.003
12	1.649	0.082	1.506	70	-0.071	-0.276	0.189
16	1.848	0.166	1.593	66	-0.103	-0.332	0.278
20	1.958	0.223	1.542	62	-0.080	-0.349	0.303
24	1.995	0.234	1.362	58	-0.035	-0.332	0.289
28	1.984	0.188	1.069	54	0.012	-0.292	0.255
32	1.952	0.090	0.689	50	0.050	-0.238	0.211
36	1.921	-0.044	0.257	46	0.074	-0.174	0.160
40	1.904	-0.188	-0.188	42	0.083	-0.105	0.105
44	1.903	-0.318	-0.612	38	0.077	-0.030	0.042
48	1.908	-0.411	-0.980	34	0.055	0.045	-0.026
52	1.905	-0.454	-1.269	30	0.020	0.112	-0.091
56	1.873	-0.445	-1.461	26	-0.022	0.165	-0.146
60	1.798	-0.394	-1.550	22	-0.061	0.196	-0.182
64	1.670	-0.317	-1.537	18	-0.080	0.201	-0.183
68	1.482	-0.230	-1.425	14	-0.056	0.178	-0.131
72	1.234	-0.151	-1.220	10	0.048	0.131	0.005
76	0.939	-0.099	-0.943	6	0.277	0.037	0.268

Table V-40
URANIUM RING

NODE	Δ_X in. $\times 10^2$	Δ_Y in. $\times 10^2$	Δ_R in. $\times 10^2$	NODE	Δ_X in. $\times 10^2$	Δ_Y in. $\times 10^2$	Δ_R in. $\times 10^2$
1	0.622	0.247	0.622	79	0.677	-0.493	-0.677
3	0.824	0.260	0.855	77	0.469	-0.506	-0.384
7	1.011	0.302	1.055	73	0.297	-0.544	-0.114
11	1.160	0.361	1.197	69	0.173	-0.592	0.115
15	1.262	0.419	1.267	65	0.104	-0.630	0.286
19	1.313	0.458	1.252	61	0.085	-0.642	0.394
23	1.318	0.459	1.146	57	0.104	-0.614	0.436
27	1.293	0.410	0.952	53	0.146	-0.540	0.415
31	1.254	0.307	0.679	49	0.192	-0.421	0.341
35	1.220	0.153	0.342	45	0.225	-0.270	0.231
39	1.208	-0.038	-0.038	41	0.236	-0.105	0.105
43	1.227	-0.245	-0.434	37	0.221	0.053	-0.018
47	1.227	-0.444	-0.817	33	0.186	0.192	-0.125
51	1.346	-0.608	-1.153	29	0.137	0.303	-0.208
55	1.413	-0.714	-1.408	25	0.089	0.378	-0.253
59	1.442	-0.748	-1.549	21	0.058	0.412	-0.250
63	1.401	-0.712	-1.552	17	0.067	0.403	-0.183
67	1.285	-0.640	-1.435	13	0.136	0.360	-0.042
71	1.111	-0.566	-1.232	9	0.260	0.306	0.153
75	0.899	-0.513	-0.968	5	0.428	0.264	0.381

Plotting these data yields Figure V-83. The mutual plot shows any interference to be insignificant hence the model simulates the actual loading. (Interference of any significance cannot physically occur.)

Examining the Stresses

Stainless Steel:

Maximum stress occurs at node 10:

M = 114.1 in-kips (tension on inside)

P = 180.1 kips (compression)

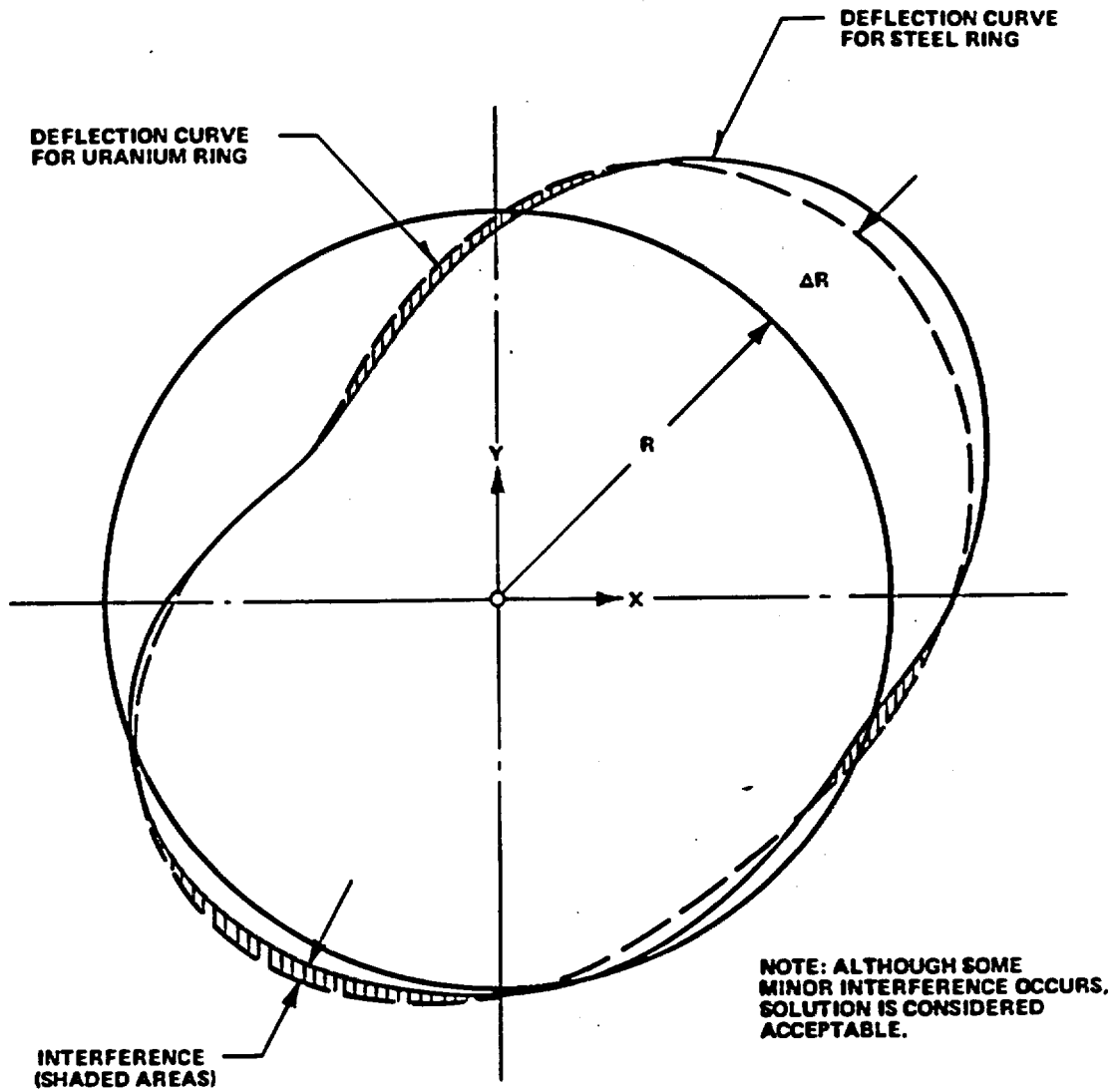


FIGURE V-83. RADIAL DEFLECTION CURVES FOR STEEL AND URANIUM RINGS

At node 10 a 3 in. diameter pin hole is provided to engage the saddle. Therefore, the section properties must be adjusted from those in Table V-33. These revised properties are as follows:

$$A = 61.56 - 2 \times 1.25 \times 3.0 = 54.06 \text{ in.}^2$$

$$\bar{Y} = \frac{420.8 - 7.50 \times 3.5}{54.06} = 7.30 \text{ in.}$$

$$\begin{aligned} I &= 3174 + 82 - 7.50 \times 3.5^2 \\ &\quad - \frac{2 \times 1.25 \times 3.0^3}{12} - 54.06 \times 7.30^2 \\ &= 278 \text{ in.}^4 \end{aligned}$$

$$\begin{aligned} \sigma_c &= \frac{180.1}{54.06} + \frac{114.1 \times 12 \times 7.3}{278} \\ &= 39.34 \text{ ksi} \end{aligned}$$

$$\text{and, SF} = \frac{47.4}{39.34} = 1.2$$

Uranium:

Maximum stress occurs at node 59:

$$M = 20.94 \text{ in.-kips (tension on inside)}$$

$$P = 3.54 \text{ kips (compression)}$$

$$\begin{aligned} \sigma_c &= \frac{3.54}{80.0} + \frac{20.94 \times 12}{53.35} \\ &= 4.75 \text{ ksi} \end{aligned}$$

$$\text{and, SF} = \frac{30.0}{4.75} = 6.31$$

3 in. ϕ Pin:

Maximum stress occurs at node 81:

$$I_x = 182 \text{ kips ; } F_y = 228 \text{ kips}$$

$$R = (182^2 + 228^2)^{1/2} = 292 \text{ kips}$$

$$\text{Shear on pin, } V = \frac{R}{2} = 146 \text{ kips}$$

NEDO-10084-3
September 1984

$$\tau = \frac{146}{\pi \times 1.5^2} = 20.7 \text{ ksi}$$

$$SF = \frac{125 \text{ ksi} \times 0.577}{20.7} = 3.48$$

Bending stresses:

$$M = 146 \times 1.875 \text{ in.} = 274 \text{ kips}$$

$$\sigma_B = \frac{4 \times 274}{\pi \times 1.5^3} = 103.2 \text{ ksi}$$

$$SF = \frac{125}{103.2} = 1.21$$

Pin bearing stresses:

$$\sigma_{Brg.} = \frac{146}{3.0 \times 1.25} = 38.95 \text{ ksi}$$

$$SF = \frac{58.4}{0.6 \times 38.95} = 2.50$$

Structural Ring:

Shear out from pin:

Maximum shear out force occurs at node 82:

$$F_X = 215 \text{ kips} ; F_Y = 98 \text{ kips}$$

$$F = F_X (\cos 18^\circ) - F_Y (\sin 18^\circ) = 174 \text{ kips}$$

$$A_s = 5.84 \text{ in.}^2$$

$$\therefore \tau = \frac{174}{5.84} = 29.8 \text{ ksi}$$

$$SF = \frac{58.4 \times 0.577}{29.8} = 1.13$$

Fin Loading - 5 G Lateral Load:

Figure V-84 shows a single lower impact fin assuming that the total transverse load, H_c , is transferred to the cradle by this fin:

$$H_c = 4.5 (\sigma_1 + \sigma_2)$$
$$4.5 + D = 3 \left(\frac{2\sigma_2 + \sigma_1}{\sigma_2 + \sigma_1} \right)$$

Solving for σ_1 and σ_2 , check the buckling stress on a 1" length of fin:

$$P_c = \frac{1}{2} \left(\sigma_2 + \sigma_2 - \frac{\sigma_2 - \sigma_1}{9} \right)$$
$$= \frac{1}{2} \left[2(4.03) - \left(\frac{40.3 - 26.8}{9} \right) \right]$$
$$= 39.55 \text{ ksi}$$

Buckling strength of fin:

$$\frac{k\ell}{r} = \frac{2.0 (6.0)}{0.289(1.125)} = 36.9$$

$$\sigma_{cr} = 46.0 \text{ ksi}$$

$$\text{and SF} = \frac{46.0}{39.55} = 1.16$$

5.8.2.4 Aluminum Enclosure - Transport

The personnel barrier which surrounds the cask (Section 4.0) during shipment weighs approximately 2300 pounds. This structure is fastened to the equipment skid with 93 9/16-inch diameter bolts. The total bolting area is approximately 15 square inches. The average shearing stress in the bolts under the combined horizontal loads of 10g axial and 5g lateral is under 2000 psi. The 2g vertical load imposes an even lower tensile stress level.

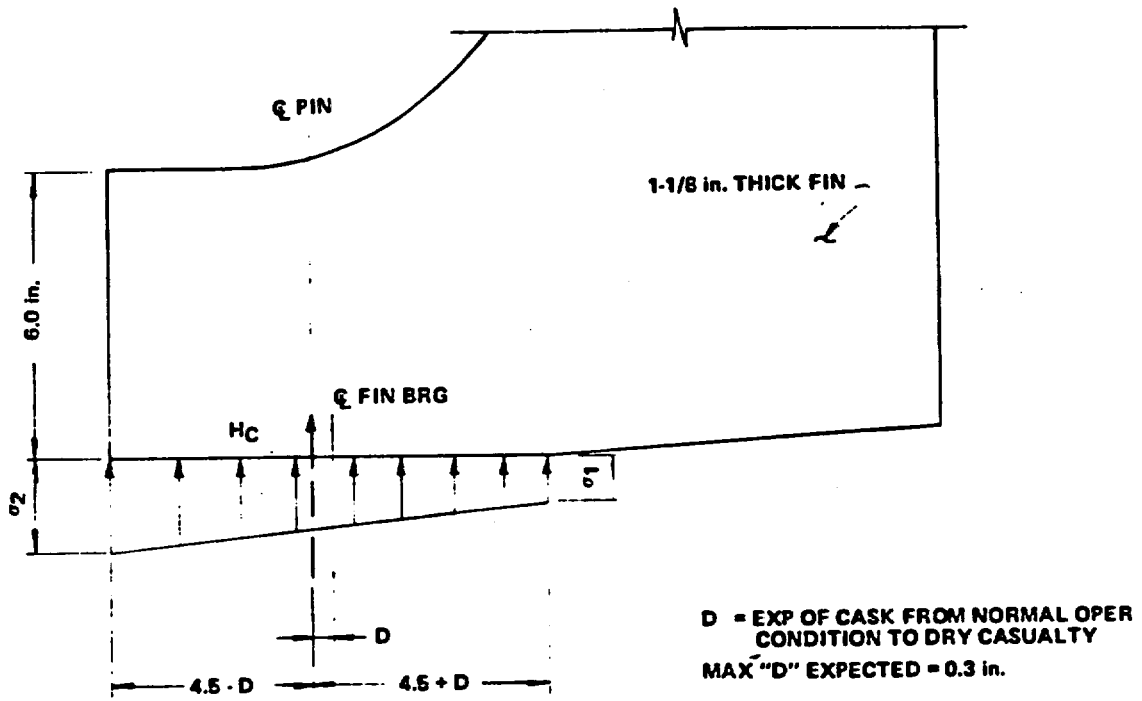


FIGURE V-84. BOTTOM HEAD FIN LATERAL LOADING

5.8.3 Cask and Tiedown Component Properties and Stresses During Lifting

To remove the cask from its skid the 3-inch diameter hold-down pins are removed from the front saddle and used to secure trunnion blocks to the upper pair of structural rings. This is illustrated in Figure V-85.

There are two types of trunnions which may be used on the IF300 Cask. The design shown on Figure V-85 is the symmetrical unit fabricated from AISI 4340 steel and chrome or nickel plated for corrosion protection. The trunnion illustrated in Figure V-86 is the off-set unit which is fabricated from stainless steel (304N or Nitronic 40). The cylindrical bearing surface on the stainless steel trunnion is Stellite coated to a depth of 1/8 inch to preclude galling. Use of the off-set trunnion compensates for the cask valve box weight bias and causes the cask to hang more nearly plumb.

The stainless steel affords better corrosion protection than the plating on the carbon steel trunnions. The off-set trunnion mounts to the cask in the same manner as the symmetrical trunnion. From a strength standpoint the minimum requirements for either trunnion material are:

0.2% yield strength, psi	38,000
Total elongation 2", %	20
Charpy impact at -40°F, ft-lbs	15 (minimum)

The cask lifting yoke engages the trunnions and the cask is rotated to the vertical position. Rotation occurs at the tipping cradle trunnions held in the rear pedestals. The cask is then lifted vertically to disengage it from the cradle.

The following analysis examines the cask body, lifting components and tipping components with the cask in the horizontal and vertical positions. A value of three times the cask weight is used to evaluate the lifting components.

FIGURE WITHHELD UNDER 10 CFR 2.390

FIGURE V-85. CASK LIFTING BLOCK AND PIN

FIGURE WITHHELD UNDER 10 CFR 2.390

FIGURE V-86. OFF SET BLOCK

5.8.3.1 Cask Horizontal
3 in. ϕ Block Pin

From Figure V-87:

$$T_{P1} = \frac{119}{2} = 59.5 \text{ k}$$

$$T_{P2} = \frac{1}{2} \left[\frac{119(6)}{3.5} \right] = 102 \text{ k}$$

$$T_B = T_{P2} = 102 \text{ k}$$

$$T_P = \sqrt{(59.5)^2 + (102)^2}$$
$$= 118 \text{ k}$$

$$M_{\max} = 118 (1.625) = 191.8 \text{ in-kips}$$

$$\sigma_B = \frac{191.8}{2.65} = 72.4 \text{ ksi}$$

$$\text{and SF} = \frac{125}{72.4} = 1.73$$

$$\tau = \frac{118}{7.07} = 16.7 \text{ ksi}$$

$$\text{and SF} = \frac{(125)(0.577)}{16.7} = 4.32$$

Bearing Stress on Outer Shell

$$A_B = 1.0 (14.) = 14 \text{ in.}^2$$

$$\sigma_c = \frac{2 T_B}{A_B} = \frac{2 \times 102}{14}$$

$$= 14.6 \text{ ksi}$$

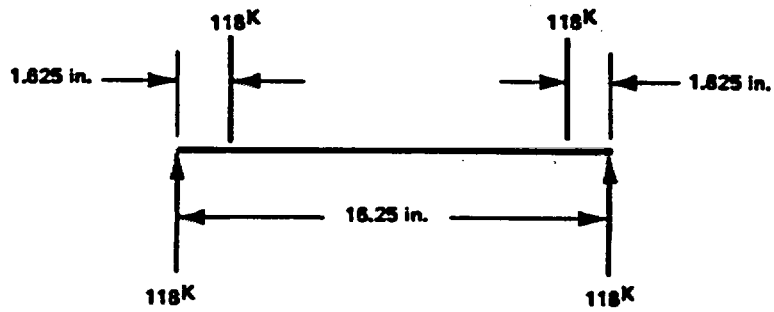


FIGURE V-87. PIN LOADING

$$\text{Assume: } (\sigma_c)_{\text{all}} = \frac{47.4}{0.6} = 79 \text{ ksi}$$

$$\text{SF} = \frac{79}{14.6} = 5.41$$

Stresses in Ring

Check shear stresses:

$$A = 5.84 \text{ in.}^2$$

$$\tau = \frac{102}{5.84} = 17.5 \text{ ksi}$$

$$\text{SF} = \frac{58.4 (0.577)}{17.5} = 1.92$$

Check bearing stresses:

$$\sigma_c = \frac{118}{(3.0)(1.25)} = 31.5 \text{ ksi}$$

$$\text{and SF} = \frac{97.3}{31.5} = 3.1$$

Stresses in Outer Shell and Uranium

The structural model previously used for the tiedown analysis was rerun with the loading scheme shown in Figure V-88.

The computer analysis provided the deflection profile shown in Figure V-89. As before, the negligible interference of the shells demonstrates compatibility of the model.

Stainless steel ring stresses are:

Maximum stress at node 26:

$$M = 196. \text{ in-k (tension on outside)}$$

$$P = 37.0 \text{ k (tension)}$$

FIGURE WITHHELD UNDER 10 CFR 2.390

FIGURE V-88. LIFT WITH CASK IN HORIZONTAL POSITION

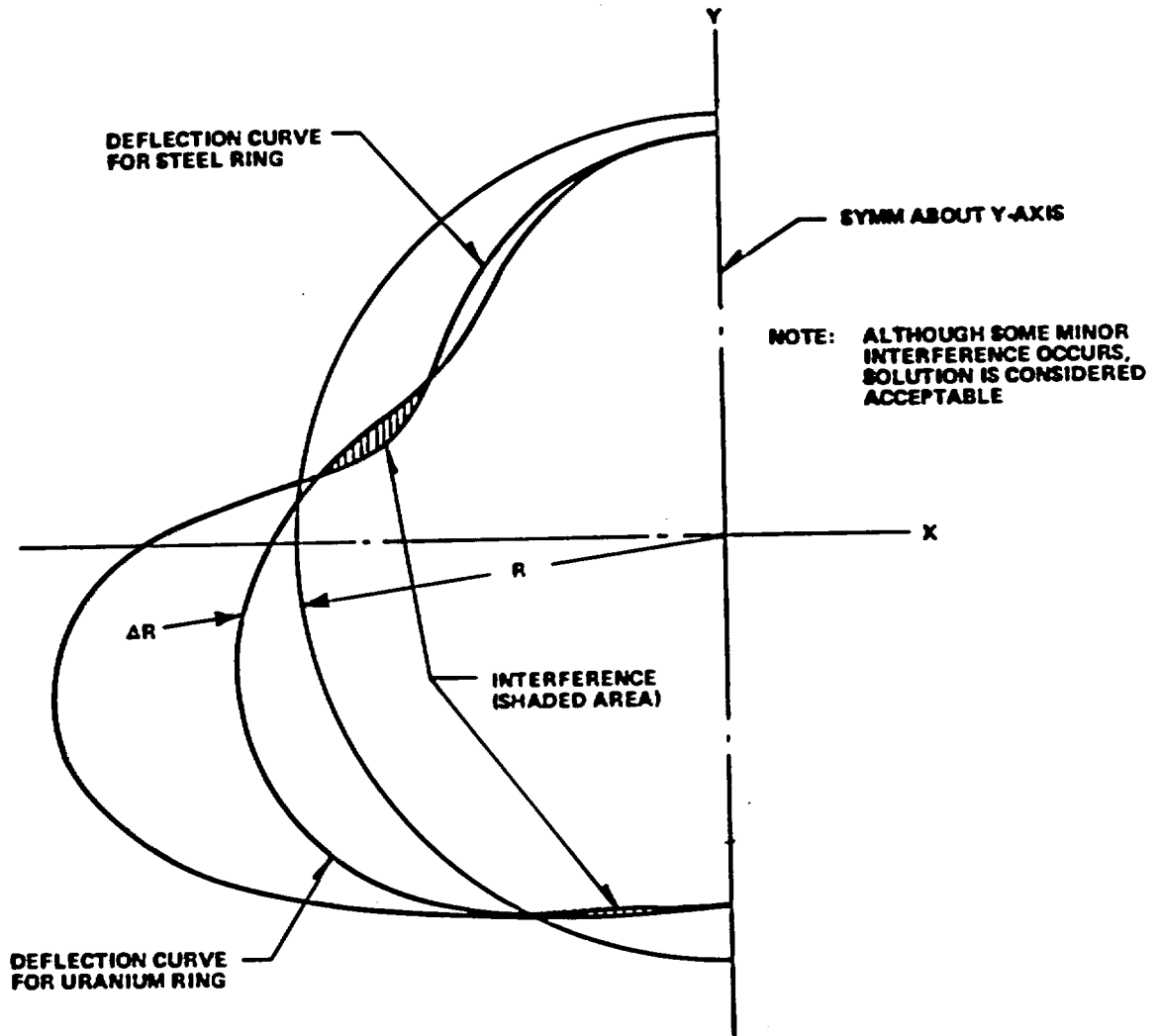


FIGURE V-89. RADIAL DEFLECTION CURVES FOR STEEL AND URANIUM RINGS

$$\sigma_T = \frac{M}{S} + \frac{P}{A}$$

$$S_{\min} = 15.6 \text{ in.}^3; A = 21.88 \text{ in.}^2$$

$$= \frac{(19.6)(12)}{15.6} + \frac{37.0}{21.88}$$

$$= 15.1 + 1.7 = 16.8 \text{ ksi}$$

$$SF = \frac{58.4}{16.8} = 3.5$$

Uranium ring stresses are:

Maximum stress is at node 17:

$$M = 2.9 \text{ in-k (tension on inside)}$$

$$P = 4.11 \text{ k (compression)}$$

$$\sigma_T = \frac{2.9 (12)}{53.35} + \frac{4.11}{80}$$

$$= 0.65 + 0.05 = 0.70 \text{ ksi}$$

$$SF = \frac{30}{0.70} = 42.9$$

5.8.3.2 Cask Vertical

Tipping Cradle

The tipping cradle cross-section is shown in Figure V-78. Figure V-90 shows the reaction at the cradle pivot.

Analyzing the beam action of the 1 in. rib plates:

$$T_o = 6.5 (1.5 W) = 1365 \text{ in-kips} = \text{torque on X-section}$$

$$\tau = \frac{T_o}{2tA} = \frac{1365}{2(1)(4)(23)} = 7.42 \text{ ksi}$$

$$V_1 = \tau A_1 = 7.42 \times 4 = 29.68 \text{ k}$$

$$V_2 = \tau A_2 - \frac{1.5 W}{2}$$
$$= 7.42 \times 23 - 105 = 65.5 \text{ k}$$

$$V_3 = \tau A_3 + \frac{1.5 W}{3}$$
$$= 7.42 \times 23 + 105 = 275.5 \text{ k}$$

$$M_{\max} = 13.5 V_1$$
$$= 13.5 \times 29.68 = 401 \text{ in-kips}$$

$$I \text{ of section} = 100.25 \text{ in.}^4$$

$$\sigma_{\text{bending}} = \frac{401 \times 2.5}{100.25} = 10.0 \text{ ksi}$$

$$\text{and SF} = \frac{38.0}{10.0} = 3.8$$

Analyzing pivot pin stresses:

Figure V-91 below details the loading on one of the cradle pivot pins:

Pin bending:

$$W = 140 \text{ k}$$

$$M_{\max} = 4.25 (1.5 W) = 893 \text{ in.-k}$$

$$\sigma_B = \frac{4M}{\pi R^3} = \frac{4 \times 893}{\pi (3.5)^3}$$
$$= 26.5 \text{ ksi}$$

$$\text{and SF} = \frac{38.0}{26.5} = 1.43$$

NEDO-10084-3
September 1984

FIGURE WITHHELD UNDER 10 CFR 2.390

Pin bearing:

Solving for reactions R_1 and R_2 :

$$R_1 = \frac{8.5 (1.5 W)}{4.25} = 420 \text{ k}$$

$$R_2 = R_1 - 1.5 W = 210 \text{ k}$$

$$\text{then } \sigma_{\text{Brg}} = \frac{R_1}{A_B} = \frac{420}{1.5 \times 7} = 40 \text{ ksi}$$

$$\text{and SF} = \frac{38.0}{0.6 \times 40} = 1.58$$

Thrust plate weld:

$$\text{Load} = \frac{R_1}{3} = 140 \text{ k}$$

$$\begin{aligned} \tau_{\text{Weld}} &= \frac{140}{A_w} \\ &= \frac{140}{10\pi \times 0.375 \times 0.707} \end{aligned}$$

$$= 16.8 \text{ ksi}$$

$$\text{and SF} = \frac{38.0 \times 0.577}{16.8} = 1.31$$

Bearing on thrust plate:

$$\sigma_{\text{Brg}} = \frac{H_c}{A_{\text{BRG}}}$$

$$H_c = 302.4 \text{ k}$$

$$\sigma_{\text{Brg}} = \frac{302.4}{\pi(5.0^2 - 3.5^2)} = 7.55 \text{ ksi}$$

$$\text{and SF} = \frac{38.0}{0.6 \times 7.55} = 8.4$$

Circular loading of cradle:

Figure V-92 below shows the load applied to the cradle structure with the cask in place in the vertical position:

Diameter of load circle = 59.0 in.

W = 140 k

$$w = \frac{3 \times 140}{66.5 \pi} = 2.01 \text{ kips/in.}$$

M = we; e = 3.75 in.

m = 2.01 x 3.75 = 7.54 in.-k/in.

$$\begin{aligned} T_o &= 6.50 (1.5 W) \\ &= 6.50 \times 210 = 1365 \text{ in-k} \end{aligned}$$

Using Reference 7:

$$M_o = \frac{T_o \sin \theta}{2} - wR^2 \left(1.0 - \frac{\pi \sin \theta}{2} \right) + mR$$

(Max. at $\theta = \frac{\pi}{2}$)

$$= 2203 \text{ in.-kips}$$

Using Table V-36 properties:

$$\sigma_B = \frac{2203 \times 12.16}{3125} = 8.58 \text{ ksi}$$

$$\text{and SF} = \frac{38.0}{8.58} = 4.43$$

Also:

$$T_\theta = \frac{T_o \cos \theta}{2} + wR^2 (\theta + 1.5708 \cos \theta - 1.5708)$$

$$T_\theta \text{ is max. when } \frac{dT_o}{d\theta} = 0$$

$$- \frac{T_o \sin \theta}{2} + wR^2 (1 - 1.5708 \sin \theta) = 0$$

Solving for $\sin\theta$:

$$\sin\theta = \frac{wR^2}{\frac{T_0}{2} + 1.5708 wR^2}$$
$$= 0.532$$

$$\theta = 32.14^\circ$$

$$\cos\theta = 0.847$$

Then:

$$T_\theta = 1296 \text{ in-kips}$$

and

$$\tau_{T_\theta} = \frac{T_\theta}{2tA} = 7.05 \text{ ksi}$$

$$V_{\theta=32.14^\circ} = \frac{57.86}{90} (0.75 w) = 67.5 \text{ k}$$

$$\tau_V = \frac{67.5}{57.0} = 1.18 \text{ ksi}$$

$$SF = \frac{38.0 (0.577)}{(7.05 + 1.18)} = 2.66$$

Check on local bending in support lugs:

Figure V-93 is a detail of the lugs upon which the cask rests when in the vertical position.

$$M_{\max} = 26.25 \times 1.75$$

$$= 46 \text{ in-k}$$

$$S = \frac{8 \times 1.0^2}{6} = 1.333 \text{ in.}^3$$

FIGURE WITHHELD UNDER 10 CFR 2.390

FIGURE V-92. VERTICAL LOADING OF PIVOT CRADLE CASK IN VERTICAL POSITION

$$\sigma = \frac{46}{1.333} = 34.5 \text{ ksi}$$

$$\text{and SF} = \frac{38.0}{34.5} = 1.10$$

Cask Body and Trunnions

Section BB of Figure V-85 shows the trunnion loading with the cask in the vertical position.

$$P_V = \frac{3 \times 140}{2} = 210 \text{ k}$$

Check trunnion pin stresses:

$$M_{\text{max}} = 2.5 P_V = 525 \text{ in-k}$$

$$S = 0.7854 \times 2.75^3 = 16.3 \text{ in.}^3$$

$$\sigma_B = \frac{525}{16.3} = 32.2 \text{ ksi}$$

$$\text{and SF} = \frac{38.0}{32.2} = 1.18$$

$$A = \pi \times 2.75^2 = 23.8 \text{ in.}^2$$

$$\tau = \frac{210}{23.8} = 8.83 \text{ ksi}$$

$$\text{and SF} = \frac{38.0 (0.577)}{8.83} = 2.48$$

Check 3 in. ϕ block pin stresses for the symmetrical trunnion.

Figure V-94 shows the load on one of the pins.

Let: T_P = Load on Pin
 T_B = Bearing load on shell

$$T_B = T_P = \frac{(210)(9.25)}{13.0} = 149.2 \text{ k}$$

$$M_{\max} = 134.3 \text{ k} (1.625) = 218 \text{ in-k}$$

$$S = 0.7854 (1.5)^3 = 2.65 \text{ in.}^3$$

$$\sigma_B = \frac{218}{2.65} = 82.3 \text{ ksi}$$

$$\text{and SF} = \frac{125}{82.3} = 1.52$$

$$A = \pi(1.5)^2 = 7.07 \text{ in.}^2$$

$$\tau = \frac{134.3}{7.07} = 19.0 \text{ ksi}$$

$$\text{and SF} = \frac{125(0.577)}{19.0} = 3.80$$

Check bearing on outer shell:

$$A_B = 1.0(8.0) = 8.0 \text{ in.}^2$$

$$\sigma_c = \frac{T_B}{A_B} = \frac{149.2}{8.0} \\ = 18.65 \text{ ksi}$$

$$(\sigma_c)_{\text{all.}} = \frac{47.4}{0.6} = 79.0 \text{ ksi}$$

$$\text{and SF} = \frac{79.0}{18.65} = 4.23$$

Check stresses in ring:

Figure V-95 below is a section of one structural ring.

$$b_1 = 0.78 \sqrt{Rt} \\ = 0.78 \sqrt{(24.0)(1.5)} \\ = 4.68 \text{ in. (use 5.0 in.)}$$

$$b = 1.25 + 2(5.0) = 11.25 \text{ in.}$$

$$\bar{Y} = \frac{16.88 (0.75) + 8.75 (5.0)}{25.63} = 2.2 \text{ in.}$$

$$\begin{aligned} I_x &= \frac{1}{12} \left[(1.25) (7.0)^3 + (11.25) (1.5)^3 \right] \\ &\quad + 16.88 (1.45)^2 + 8.75 (2.8)^2 \\ &= 143 \text{ in.}^4 \end{aligned}$$

$$A = 25.63 \text{ in.}^2$$

Shear:

Figure V-96 below is a view of the 3 in. ϕ pin hole
(Reference 22, Page 291)

$$\begin{aligned} \text{Let } \phi &= \text{Sin}^{-1} \left[\frac{1.5 \text{ Sin } 40^\circ}{31.75} \right] \\ &= 1^\circ - 44.4^{-1} \end{aligned}$$

$$\cos \phi = 0.99954$$

$$L = 31.75 \cos \phi - (28.25 + 1.5 \cos 40^\circ)$$

$$= 2.336 \text{ in.}$$

$$A = 2 L t = 2(2.336) (1.25) = 5.84 \text{ in.}^2$$

$$\tau = \frac{134.3}{5.84} = 23.0 \text{ ksi}$$

$$\text{and SF} = \frac{58.4 (0.577)}{23.0} = 1.47$$

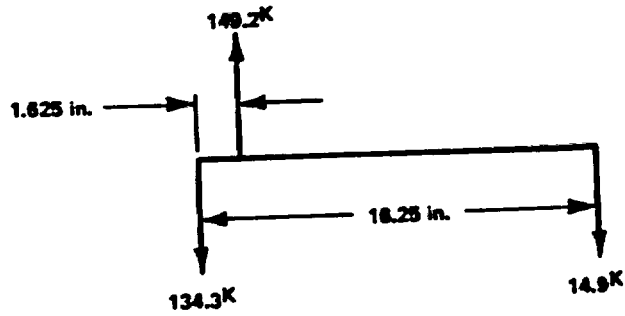


FIGURE V-94. LOADING ON PIN

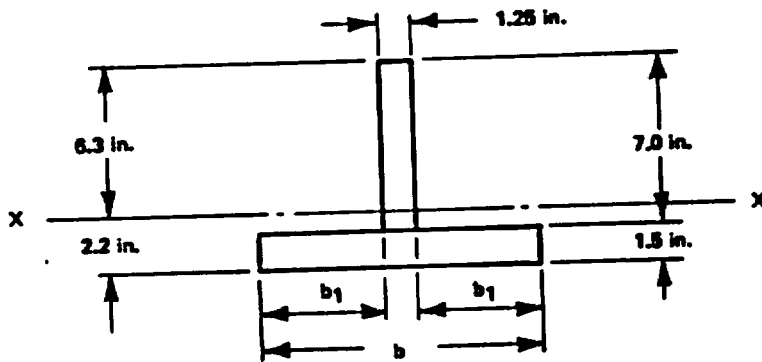


FIGURE V-95. RING SECTION

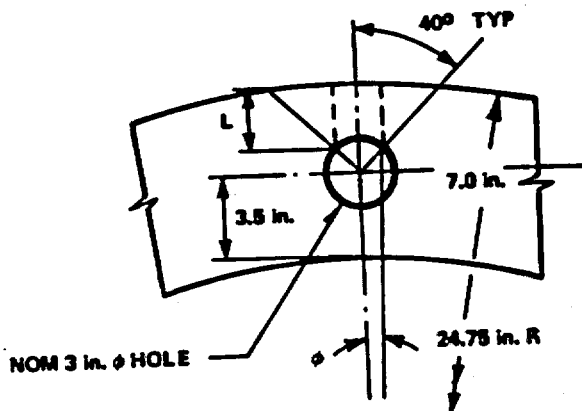


FIGURE V-96. PIN HOLE

Bearing:

$$\sigma_c = \frac{134.3}{(3.0)(1.25)} = 35.8 \text{ ksi}$$

$$(\sigma_c)_{\text{all.}} = \frac{58.4}{0.6} = 97.3 \text{ ksi}$$

$$\text{and SF} = \frac{97.3}{35.8} = 2.72$$

3" Block Pin stresses for the off-set trunnion.

The one (1) inch off-set of the lifting trunnion relative to the 3" pin ζ produces a moment equal to 210,000 in-lbs (assuming 3W for conservatism). This moment is resisted by the 3" dia pin reacting against the trunnion block and the upper pair of structural rings. The direction of the off-set moment, and the reacting forces, is normal to the moment and forces produced in lifting the cask with the symmetrical trunnion as shown above.

Figure V-97 shows the forces on the 3" dia trunnion pin. Forces in the X-X direction are due to the 1" off-set, those in the Y-Y are due to cask lifting (see Figure V-94).

The new pin stresses as a result of the off-set can be determined by examining the resultant of the two normal forces. Following the method for the symmetrical trunnion:

$$T_B \neq T_P = \left[(149.2^k)^2 + (16.15^k)^2 \right]^{1/2} = 150.1^k$$

$$M_{\text{max}} = \left[(134.3^k)^2 + (12.92^k)^2 \right]^{1/2} (1.625")$$

$$= (134.9^k) (1.625") = 219.2 \text{ in-k}$$

NEDO-10084-3
September 1984

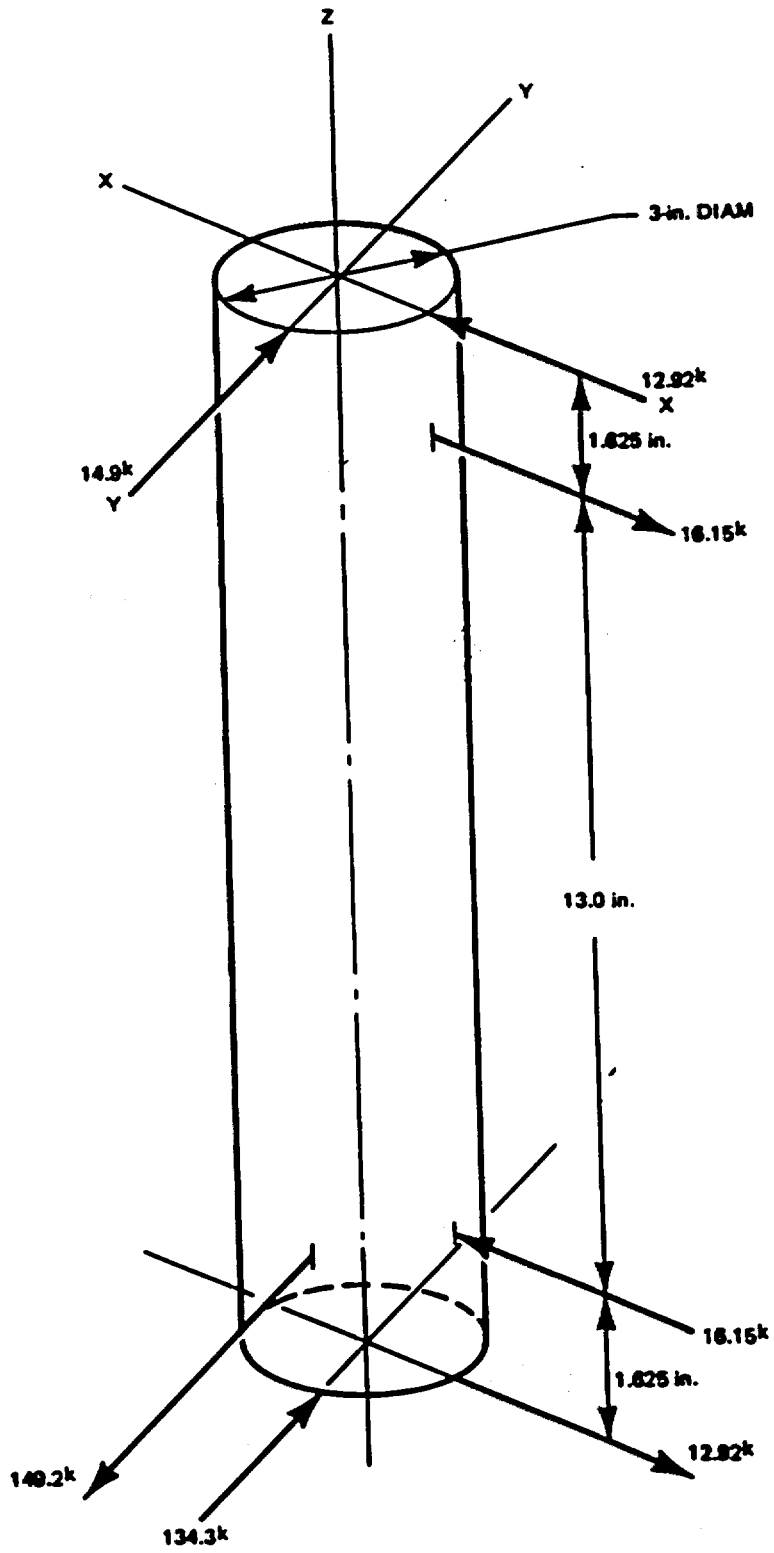


FIGURE V-97. 3" TRUNNION PIN LOADING

And for the 3" pin

$$\begin{aligned}\sigma_B &= \frac{M}{S} \\ &= \frac{219.2}{2.65} = 82.72 \text{ ksi} \\ S_F &= \frac{125}{82.72} = 1.51\end{aligned}$$

Considering shear

$$\begin{aligned}\tau &= \frac{134.9^k}{7.07} = 19.1 \text{ ksi} \\ S_F &= \frac{(125)(0.577)}{19.1} = 3.78\end{aligned}$$

Comparing the above results with those for the symmetrical trunnion, it can be seen that the one-inch trunnion off-set has an insignificant affect on the 3" trunnion pin stresses.

Check bearing stress between lifting block and structural ring:

$$\begin{aligned}\sigma_c &= \frac{P_v}{A} = \frac{210}{(0.5)(8.0)} = 52.5 \text{ ksi} \\ \text{and } SF &= \frac{97.3}{52.5} = 1.85\end{aligned}$$

Check stresses in outer shell and uranium:

Figure V-98 shows a cross-section of the two lifting rings and the underlying uranium segments. The section properties of the rings are shown in a previous section. The uranium section properties are:

$$\begin{aligned}A &= 20(4) = 80 \text{ in.}^2 \\ I &= \frac{1}{12} (20)(4)^3 = 106.7 \text{ in.}^4\end{aligned}$$

FIGURE WITHHELD UNDER 10 CFR 2.390

FIGURE V-98. CASK LIFTING RINGS

$$S = \frac{106.7}{2} = 53.35 \text{ in.}^3$$

$$E = 24 \times 10^3 \text{ ksi}$$

The previously described computer model was run with the appropriate section properties and the loading shown in Figure V-99.

As in the previous models, the deflections of the two rings were co-plotted. The insignificant amount of interference demonstrates the compatibility of the model. The co-plotted results are shown on Figure V-100.

Checking on stainless steel ring stresses:

Max stress is at Node 26

$$M = 65.02 \text{ in.-k (tension on outside)}$$

$$P = 44.11 \text{ k (tension)}$$

Figure V-101 below is the ring section at Node 26.

$$A = 4.0 (1.25) + 1.5 (11.25) = 21.875 \text{ in.}^2$$

$$\begin{aligned} \bar{Y} &= \frac{(2.5)(7.5 + 2.5) + 16.875 (0.075)}{21.875} \\ &= 1.72 \text{ in.} \end{aligned}$$

$$\begin{aligned} I_x &= 2 \left[\frac{1.25 (0.78)^3}{12} \right] + \frac{11.25 (1.5)^3}{12} + 2.5 (5.78)^2 \\ &+ 2.5 (0.78)^2 + 16.875 (0.97)^2 = 105.74 \text{ in.}^4 \end{aligned}$$

$$S_{\min} = \frac{105.74}{6.78} = 15.6 \text{ in.}^3$$

$$S_{\max} = \frac{105.74}{1.72} = 61.5 \text{ in.}^3$$

FIGURE WITHHELD UNDER 10 CFR 2.390

FIGURE V-99. LIFT WITH CASK IN VERTICAL POSITION

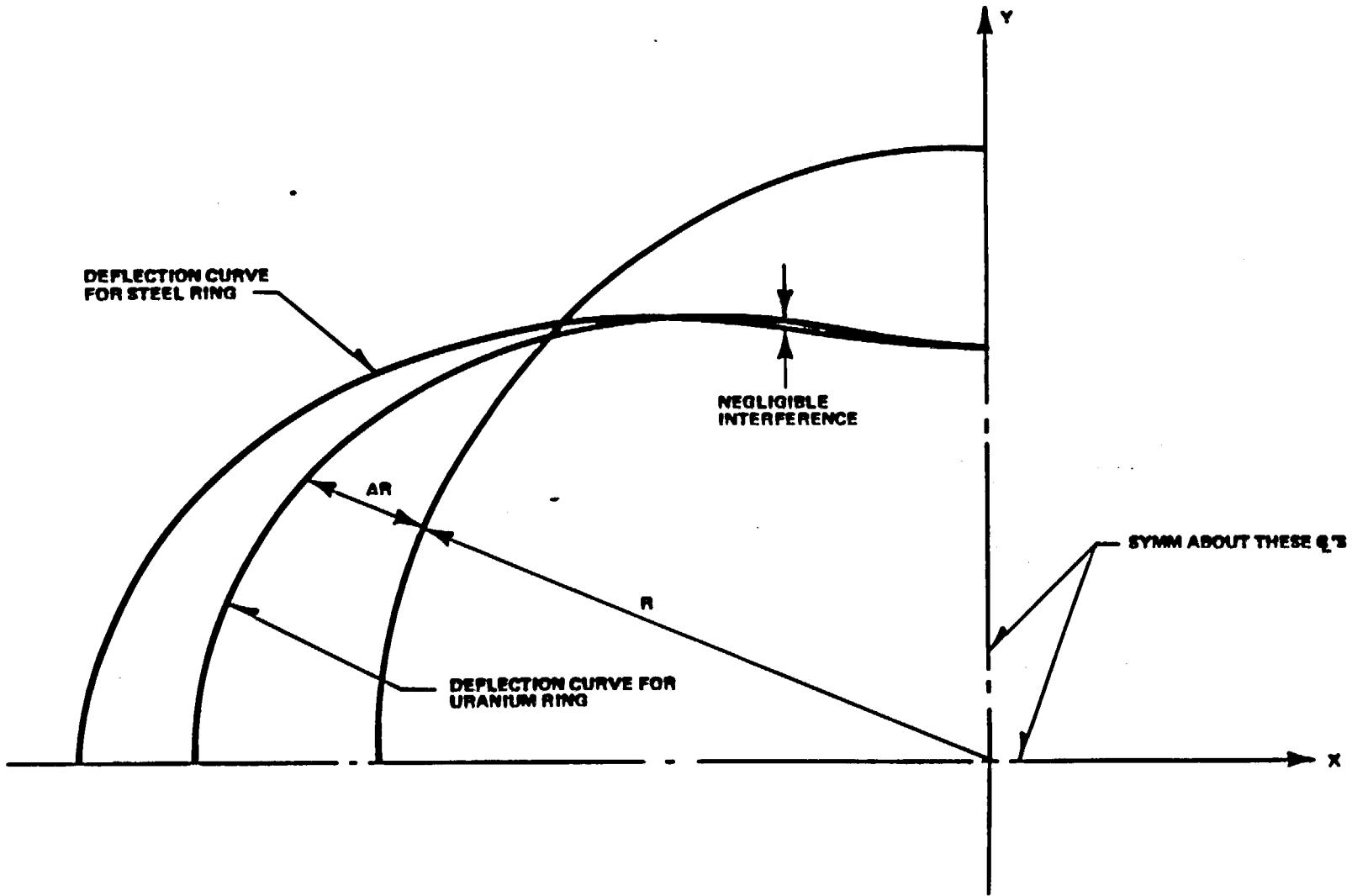


FIGURE V-100. RADIAL DEFLECTION CURVES FOR STEEL AND URANIUM RINGS.

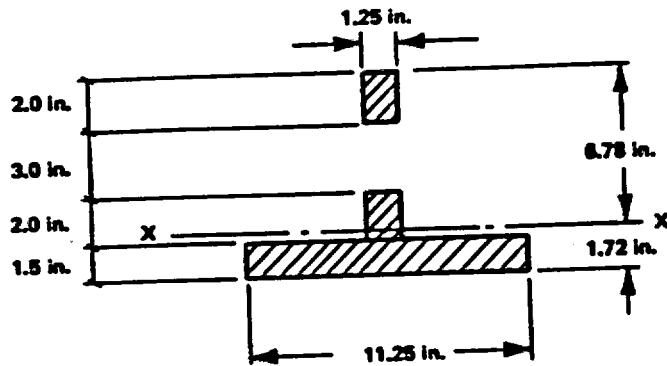


FIGURE V-101. PIN HOLE SECTION

$$\begin{aligned}\sigma_T &= \frac{M}{S} = \frac{P}{A} = \frac{(65.02)(12)}{15.6} + \frac{44.11}{21.88} \\ &= 52.0 \text{ ksi}\end{aligned}$$

$$\text{and SF} = \frac{58.4}{52.0} = 1.12$$

Checking on Uranium Ring Stresses:

@ Node 1

$$M = 29.93 \text{ in.-k (tension on inside)}$$

$$P = 12.26 \text{ k (compression)}$$

$$\begin{aligned}\sigma_T &= \frac{29.93(12)}{53.53} + \frac{12.26}{80} \\ &= 6.88 \text{ ksi}\end{aligned}$$

@ Node 25

$$M = 21.68 \text{ in.-k (tension on outside)}$$

$$P = 39.72 \text{ k (compression)}$$

$$\begin{aligned}\sigma_T &= \frac{21.68(12)}{53.35} + \frac{39.72}{80} \\ &= 5.38 \text{ ksi}\end{aligned}$$

Taking Node 1 Results:

$$\text{SF} = \frac{30}{6.88} = 4.36$$

5.8.4 Conclusion

This section has examined the IF 300 cask-to-skid tiedowns under two conditions: 1) transport, and 2) lifting. The transport cases were analysed under the regulatory 10g, 2g, and 5g combined loading requirements.

The lifting cases were evaluated at 3 times the cask weight, again in compliance with regulations. In all cases, no component safety factor (SF) was less than unity based on the yield strength of the material.

5.9 ENGAGEMENT OF CASK AND TIEDOWNS

When the cask is lowered over the support saddle (Figure V-102), it moves forward out of the pivot cradle to allow for thermal expansion during shipment due to operating and loss-of-coolant conditions. In order for this movement to take place without over-stressing the bottom head fins, saddle ring and saddle lug, the bearing surfaces at the pivot cradle will be coated with lubricant to reduce the coefficient of friction. In order to assure a conservative analysis, the coefficient of friction will be assumed as 0.2 for the pivot cradle and support shoe surfaces and 0.6 for the saddle and lifting ring surfaces. The following equations can be written by the summation of forces = 0 from statics:

$$R_1 (\sin\theta + \mu_1 \cos\theta) + R(\cos\theta - \mu\sin\theta) + P_1 = W$$

$$R_1 (\mu_1 \sin\theta - \cos\theta) + R(\sin\theta + \mu\cos\theta) = 0$$

$$R_1 (78.125\mu + 8.6 \sec\theta + 171.25 \tan\theta - 3) + R(3\mu - 93.125) + 70.625 P_1 \cos \theta = 0$$

solving the conservative case of $\theta = 6^\circ$, $\mu = 0.2$ and $\mu_1 = 0.6$ for R , R_1 , P_1 and μR the saddle ring stress is:

$$\sigma_{\text{Bending}} = \frac{M_c}{I} = 7.03 \text{ ksi}$$

and the saddle lug bending stress is:

FIGURE WITHHELD UNDER 10 CFR 2.390

FIGURE V-102. FREE-BODY DIAGRAM SHOWING FORCES ON CASK UPON ENGAGEMENT WITH SADDLE ;

$$\sigma_{\text{Bend}} = \frac{M}{I} = 19.1 \text{ ksi}$$

The maximum bearing stress at the pivot cradle support shoe (Figure V-103) is conservatively calculated as:

$$\sigma_{\text{Brg}} = \frac{P}{A_{\text{B}}} = 12.15 \text{ ksi}$$

$$\text{where } A_{\text{B}} = 4 \text{ in.}^2/\text{in.}$$

5.10

CORRUGATED EXTERIOR WATER CONTAINMENT

The corrugated cylindrical vessel which surrounds the IF-300 cask exterior is designed to contain a liquid neutron shielding medium. This containment is corrugated to increase the heat transfer area of the cask exterior. These corrugations also strengthen the structure from the effects of internal pressure. The containment is subject to internal pressure and is equipped with pressure relief valves. Filling and draining of the neutron shielding cavities is accomplished through ports normally sealed by pipe plug, blind flange, or valve.

Under normal cooling conditions the internal pressure is only 5 psig. However, under conditions where the cooling system is inoperative the pressure may increase to 157 psig. The containment is designed to have a working pressure of 200 psig. The relief valve setting is 200 psig.

The corrugation configuration is shown in Figure V-104. The structure is comprised of two complete cylinders supported at the ends by heavy structural rings (see Section IV). The material is ASTM A240 Type 304 stainless steel, having a nominal thickness of 1/8 inch. Each cylindrical section has its own vent, drain and pressure relief valve system.

FIGURE WITHHELD UNDER 10 CFR 2.390

FIGURE V-103. LOWER END OF CASK AT CRADLE SHOWING SUPPORT SHOE

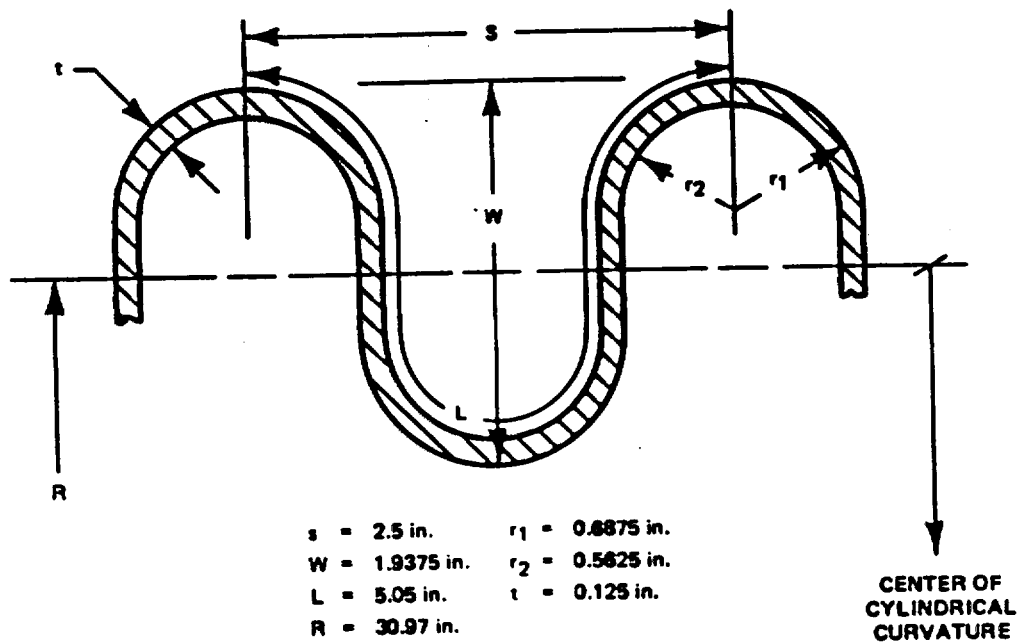


FIGURE V-104. CORRUGATION SECTION

5.10.1 Analysis

The following development describes the stresses in the corrugated containment under 200 psig internal pressure and 350°F conditions (see Figure V-104).

5.10.1.1 Bulging Stress:

$$\sigma_B = \left[\frac{P}{8N_P} \right] \left[\frac{D_o - D_i}{t_P} \right]^2 \quad (\text{Ref. 23})$$

where:

- P = Initial design pressure
- N_P = Number of plies
- D_o = Bellows outside diameter
- D_i = Bellows inside diameter
- t_P = Wall thickness

$$\sigma = \left[\frac{200}{8 \times 1} \right] \left[\frac{63.875 - 60.0}{0.125} \right]$$

= 24,025 psi

From International Nickel Company for 304 stainless steel at 375°F,

$$\sigma_{\text{yield}} = 29,500 \text{ psi}$$

$$SF = \frac{29500}{24025} = 1.23$$

5.10.1.2 Hoop Stress:

$$\sigma_H = \frac{P D_o (L + M_E)}{2N_L D t_P N_P E_j} \quad (\text{Ref. 23})$$

where:

- P = Internal pressure
- D_o = Bellows outside diameter

N = No. of convolutions
L_D = Developed length of one convolution
t_P = Wall thickness
N_P = Number of plys
E_J = Longitudinal weld joint efficiency
L = Free length of bellows
M_E = Movement of bellows in extension beyond free length.

$$\sigma_H = \frac{(200)(63.875)(180 + 0)}{(2)(72)(5.05)(0.125)(1)(1.0)} = 25,297 \text{ psi}$$

$$SF = \frac{29500}{25297} = 1.17$$

5.10.2 Containment Reliability

This corrugated structure has been designed and analyzed following the well-defined practices of expansion joint fabricators. Structures of this type are used in countless applications under high temperature and pressure conditions. Their reliability and ruggedness are well known in the power generation, chemical processing and aerospace industries. The manufacturing process used to form these items have been thoroughly proven over many years.

Stresses generated in the external shielding containment structure under normally encountered transportation and handling loads are only a fraction of those experienced under the conditions above.

"Sloshing" of the shielding liquid is prevented by a number of baffles within the containment. Even a sudden stop, such as encountered in railroad coupling, could not result in significant (> 200 psig) impact-induced pressures, due to this baffling.

5.10.3 30-Foot Drop (Barrel)

The cask has been analyzed in Section 5.4.6 for the effects of a 30-foot free drop as required by federal regulation. The total kinetic energy of the falling cask is 4.2×10^6 foot-pounds. This energy is absorbed by the bending of heavy steel structures, both on the cask ends and sides.

In the case of the side drop, the presence of the thin-walled (0.125 in.) external water containment has no effect in dissipating the cask kinetic energy. The relative metal thickness and the lack of continuous support at the base of the corrugations act to assure that the impact-energy absorbing capability of this thin-walled structure is but a small fraction of that provided by the circumferential rings and fins. Upon impact the outer jacket is assumed to perforate and crumple. The water will be vented; however, the structure will still remain in place around the cask.

5.10.4 Conclusion

The above analyses have demonstrated the ability of the corrugated containment to sustain internal pressures of 200 psig without exceeding yield strength. It has also been shown that the corrugated structure will not materially contribute to the 30-foot drop energy dissipation. This light weight, rugged structure is ideally suited as an external liquid shielding containment.

5.11 CASK RELIABILITY UNDER NORMAL CONDITIONS OF TRANSPORT

5.11.1 Introduction

Subsection 5.4 includes analyses of the cask for stresses and vibrations under normal conditions of transport as defined in 10 CFR 71. This subsection discusses the reliability of the cask components under what could be termed as a broader category of "normal" transport conditions. The one-foot drop criterion is discussed in this section in terms of its applicability to large shipping casks. A discussion of normal conditions of transport not specified in the regulations is also presented.

The principal bases for preventing any release of radioactivity and/or significant increase of external radiation are: (1) initial provision and fabrication of high quality components; (2) inspection and maintenance to assure proper operability for each shipment, and (3) redundant systems, where appropriate, to assure that no single mechanical failure could result in the release of radioactive materials from the cask for conditions that may occur during transport.

5.11.2 Procedures

Procedures are relied upon to assure that the cask and components as initially fabricated and installed meet the required quality criteria, that the cask and components are maintained in good working condition and that, prior to each use of the loaded cask, the cask and components are in proper working order and functioning as intended. These procedures provide a high degree of assurance that there will be no mechanical failure of components during transit.

5.11.2.1 Fabrication and Acceptance Procedures

The fabrication of the IF 300 cask is in accordance with drawings and procedures which provide a level of quality assurance comparable to that required for other nuclear service applications. The procedures are described in a General Electric Company approved manufacturing document which specifies the level of quality control required and forms the basis upon which the detailed quality assurance program is evaluated.

The specification includes material, fabrication and equipment specifications. This document, along with the fabrication drawings forms a package which assures that the cask as fabricated and put into service has the highest level of quality assurance. In addition, those items which can be classified as containment are fabricated following a QA plan based on Appendix B of 10 CFR 50.

To provide further quality control, General Electric has an inspector in the fabricator's shop. General Electric also supplements the resident inspector with periodic audits conducted by personnel from the San Jose, California and/or Morris, Illinois facilities.

Prior to acceptance from the fabricator, the IF 300 cask is given a thermal demonstration test at design basis heat load conditions. These tests are used to verify the normal operating conditions described in Section VI. The thermal demonstration test sequence is described in Section VI. Each cask is functionally tested prior to acceptance by General Electric.

5.11.2.2 Maintenance and Inspection Procedures

The key to maintaining the initial quality and reliability of a system such as the IF 300 is periodic inspection and maintenance of functional areas. In the IF 300 system, these functional areas include:

- a. Corrugated barrel and valving
- b. Cavity closure flange and valving
- c. Cask tiedown structure

The inspection and maintenance plan is discussed in Section X.

5.11.2.3 In-use Procedures

Section X discusses the activities which are performed prior to cask usage. A detailed operating manual exists and is periodically updated with emphasis on proper operation of the items listed in Section 5.11.2.2

For VECTRA-owned casks, VECTRA provides training to all individuals involved in the IF-300 handling operation. VECTRA conducts periodic audits on the condition of the equipment, to assure proper handling. Administrative controls such as sign-off sheets and similar documentation are used to confirm equipment functioning.

Specifically, these procedures require that prior to release to a carrier, the cask and components: (1) are operating properly; (2) temperatures and pressures are within limits for normal operation, and; (3) radiation and contamination levels are within limits. Further, where transshipments are performed, at the time of release to a railroad, the procedures will require that: (1) the mechanical cooling system, if desired, is operating properly, and (2) no package damage has been sustained since leaving the reactor site. These two criteria will assure that there has been no inadvertent damage during the over-the-road portion of the transport. It should be noted that no single failure of a component, including failure due to vandalism, will result in any release of radioactive material to the environment, and that the cooling system is not required for the safe use of the cask.

5.11.3 One-Foot Drop

The regulations include a one-foot drop as part of the conditions of normal transport. Since the IF-300 cask is transported solely in a horizontal orientation, only an analysis of the package (cask and skid) dropped one foot in horizontal orientation is necessary to satisfy the intent of the regulations.

5.11.3.1 1-Foot Drop Analysis - Package

This analysis examines the cask front support, rear support, skid framing, corrugated neutron shielding barrel, barrel water expansion tanks, and the contained fuel rods under one-foot drop conditions. The cask body, cask support, skid framing, and fuel rod were modeled using a spring-mass system (for detailed description of program derivation, see Section 5.6.5 fuel and behavior under 30-foot drop conditions). The barrel was evaluated on a strain-energy basis, and the expansion tanks were examined under the static application of the peak cask deceleration. These calculations demonstrate that all of these components are capable of sustaining this loading without losing package effectiveness. On the cask outer shell some outer fiber strains are slightly in excess of the strain value used to define the yield point (0.002). However, an examination of the outer shell wall cross-section shows this strain to be so small as to be immeasurable.

The shear strain in the cask cradle tipping trunnions is somewhat greater than the yield value. However, the only function of these components during shipping is to resist the 2 g vertical force at the lower end of the cask. The trunnions are more than capable of providing this restraint following the one-foot drop. The indication that some slight yielding occurred in the skid is somewhat questionable because it is loaded in compression and the elevated strength properties of steel in compression over those in tension was not included in the model. Nevertheless, the computed deformations are of the magnitude

associated with local effects at the point of contact with the ground. It should also be noted that in all these computations strain-rate effects (elevated strength) were not considered; such effects would tend to also reduce the amount of permanent strain. The barrel evaluation based on a strain-energy consideration was found to be fully capable of elastically accepting its own one-foot drop kinetic energy. The maximum bending moment in the fuel pin was found to be less than that occurring under the 30-foot drop event and well into the elastic range of material properties.

In summary, the one-foot drop analysis shows that there is no significant affect on any vital package component. Details of the analysis follow:

a. Model for Dynamic Analysis:

Since the bulk of the dropped weight consists of the cask, saddle, pedestals, and cradle, the system will be modeled as shown in Figures V-105 and 106 for purposes of determining the dynamic loading on the cask and its supports.

b. Determination of Spring Properties:

1. Cask

(a) Find moment-curvature relationship using stress-strain curve, Figure V-65.

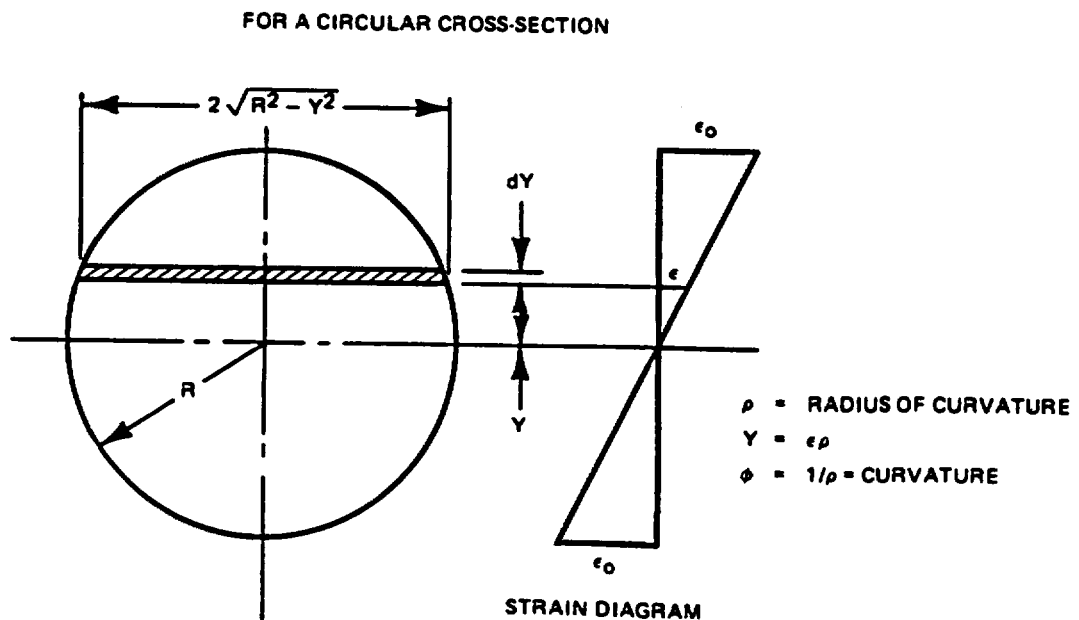


FIGURE WITHHELD UNDER 10 CFR 2.390

FIGURE V-105. ANALYSIS FOR ONE-FOOT DROP

FIGURE WITHHELD UNDER 10 CFR 2.390

FIGURE V-108. MULTI-MASS MODEL

5-274

$$dM = 2\sigma y \sqrt{R^2 - y^2} dy$$

$$dy = \rho d\epsilon$$

$$dM = 2\sigma \rho^2 \epsilon \sqrt{R^2 - \epsilon^2 \rho^2} d\epsilon$$

$$M = 4\rho^2 \int_0^{R/\rho} \sigma \epsilon \sqrt{R^2 - \epsilon^2 \rho^2} d\epsilon$$

$$= 4\rho^3 \int_0^{\epsilon_0} \sigma \epsilon \sqrt{\epsilon_0^2 - \epsilon^2} d\epsilon$$

$$= \frac{4\phi R^4}{\epsilon_0^4} \int_0^{\epsilon_0} \sigma \epsilon \sqrt{\epsilon_0^2 - \epsilon^2} d\epsilon$$

For an annular cross-section,

r = inner radius

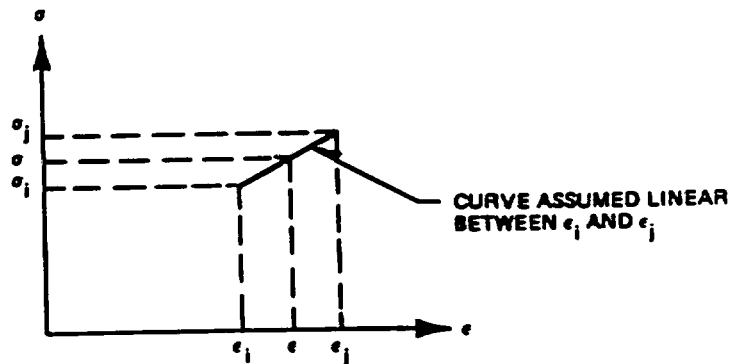
R = outer radius

$$\epsilon_{oi} = r \epsilon_o / R$$

$$\phi = \epsilon_o / R$$

$$\begin{aligned}
 M &= \frac{4\phi R^4}{\epsilon_0} \int_0^{\epsilon_0} \sigma \epsilon \sqrt{\epsilon_0^2 - \epsilon^2} d\epsilon \\
 &\quad - \frac{4\phi r^4}{\epsilon_{oi}} \int_0^{\epsilon_{oi}} \sigma \epsilon \sqrt{\epsilon_{oi}^2 - \epsilon^2} d\epsilon \\
 &= \frac{4 R^3}{\epsilon_0^3} \left[\int_0^{\epsilon_0} \sigma \epsilon \sqrt{\epsilon_0^2 - \epsilon^2} d\epsilon \right. \\
 &\quad \left. - \int_0^{\epsilon_{oi}} \sigma \epsilon \sqrt{\epsilon_{oi}^2 - \epsilon^2} d\epsilon \right]
 \end{aligned}$$

Numerical Integration of Above Equation:



$$\sigma = \sigma_i + \frac{(\epsilon - \epsilon_i)}{(\epsilon_j - \epsilon_i)} (\sigma_j - \sigma_i)$$

Define $E_t = (\sigma_j - \sigma_i) / (\epsilon_j - \epsilon_i)$

$$\sigma = \sigma_i - E_t \epsilon_i + E_t \epsilon$$

$$\begin{aligned}
 & \int_{\epsilon_1}^{\epsilon_j} \sigma \epsilon \sqrt{\epsilon_o^2 - \epsilon^2} \, d\epsilon = (\sigma_1 - E_t \epsilon_1) \\
 & \int_{\epsilon_1}^{\epsilon_j} \epsilon \sqrt{\epsilon_o^2 - \epsilon^2} \, d\epsilon + E_t \int_{\epsilon_1}^{\epsilon_j} \epsilon^2 \sqrt{\epsilon_o^2 - \epsilon^2} \, d\epsilon \\
 & = (\sigma_1 - E_t \epsilon_1) \left[-\frac{(\epsilon_o^2 - \epsilon^2)^{3/2}}{3} \right]_{\epsilon_1}^{\epsilon_j} \\
 & + E_t \left[\frac{-\epsilon(\epsilon_o^2 - \epsilon^2)^{3/2}}{4} + \frac{\epsilon_o^2 \epsilon(\epsilon_o^2 - \epsilon^2)^{1/2}}{8} \right. \\
 & \left. + \frac{\epsilon_o^4}{8} \sin^{-1} \left(\frac{\epsilon}{\epsilon_o} \right) \right]_{\epsilon_1}^{\epsilon_j} \\
 & = (\sigma_1 - E_t \epsilon_1) \left[\frac{(\epsilon_o^2 - \epsilon_1^2)^{3/2} - (\epsilon_o^2 - \epsilon_j^2)^{3/2}}{3} \right] \\
 & + E_t \left\{ \frac{\epsilon_1 (\epsilon_o^2 - \epsilon_1^2)^{3/2} - \epsilon_j (\epsilon_o^2 - \epsilon_j^2)^{3/2}}{4} \right. \\
 & + \frac{\epsilon_o^2}{8} \left[\epsilon_j (\epsilon_o^2 - \epsilon_j^2)^{1/2} - \epsilon_1 (\epsilon_o^2 - \epsilon_1^2)^{1/2} \right] \\
 & \left. + \frac{\epsilon_o^4}{8} \left[\sin^{-1} (\epsilon_j/\epsilon_o) - \sin^{-1} (\epsilon_1/\epsilon_o) \right] \right\}
 \end{aligned}$$

For evaluation of $\int_{\epsilon_i}^{\epsilon_j} \sigma \epsilon \sqrt{\epsilon_{oi}^2 - \epsilon^2} d\epsilon$, substitute

ϵ_{oi} for ϵ_o in above equation.

A computer program was written to evaluate the above integrals for both the inner and outer shells. (See Table V-46). See Figure V-107 for a plot of the results. The following data was used to generate M- ϕ curve:

ϵ	σ	ϵ	σ	Outer shell:
0	0	0.12	90.5	R = 24.75" r = 23.25"
0.002	60	0.16	93.7	
0.01	71.0	0.20	96.0	Inner shell:
0.02	75.0	0.24	97.8	R = 19.25" r = 18.75"
0.03	77.3	0.23	98.8	
0.04	79.3	0.39	99.5	
0.08	87.0	0.31	100.0	

Table V-46

COMPUTER OUTPUT - INTEGRAL EVALUATION

	ϕ	M_{outer}	M_{inner}	M_{total}
2	8.08081E-5	158079.	26123.5	184203.
3	4.0404E-4	232735.	46851.1	279586.
4	8.08081E-4	250794	51207.2	302001.
5	1.21212E-3	259723.	53196.6	312919.
6	1.61616E-3	266215.	54492.6	320708.
7	3.23232E-3	285757.	58073.6	343831.
8	4.84848E-3	300230.	60931.3	361162.
9	6.46465E-3	311068.	63138.8	374207.
10	8.08081E-3	319370.	64879.8	384250.
11	9.69697E-3	325939.	66304.	392243.
12	1.13131E-2	330925.	67480.2	398405.
13	1.29293E-2	334595.	68466.5	403061.
14	1.45455E-2	337404.	69223.2	406627.
15	1.61616E-2	339370.	69824.2	409194.

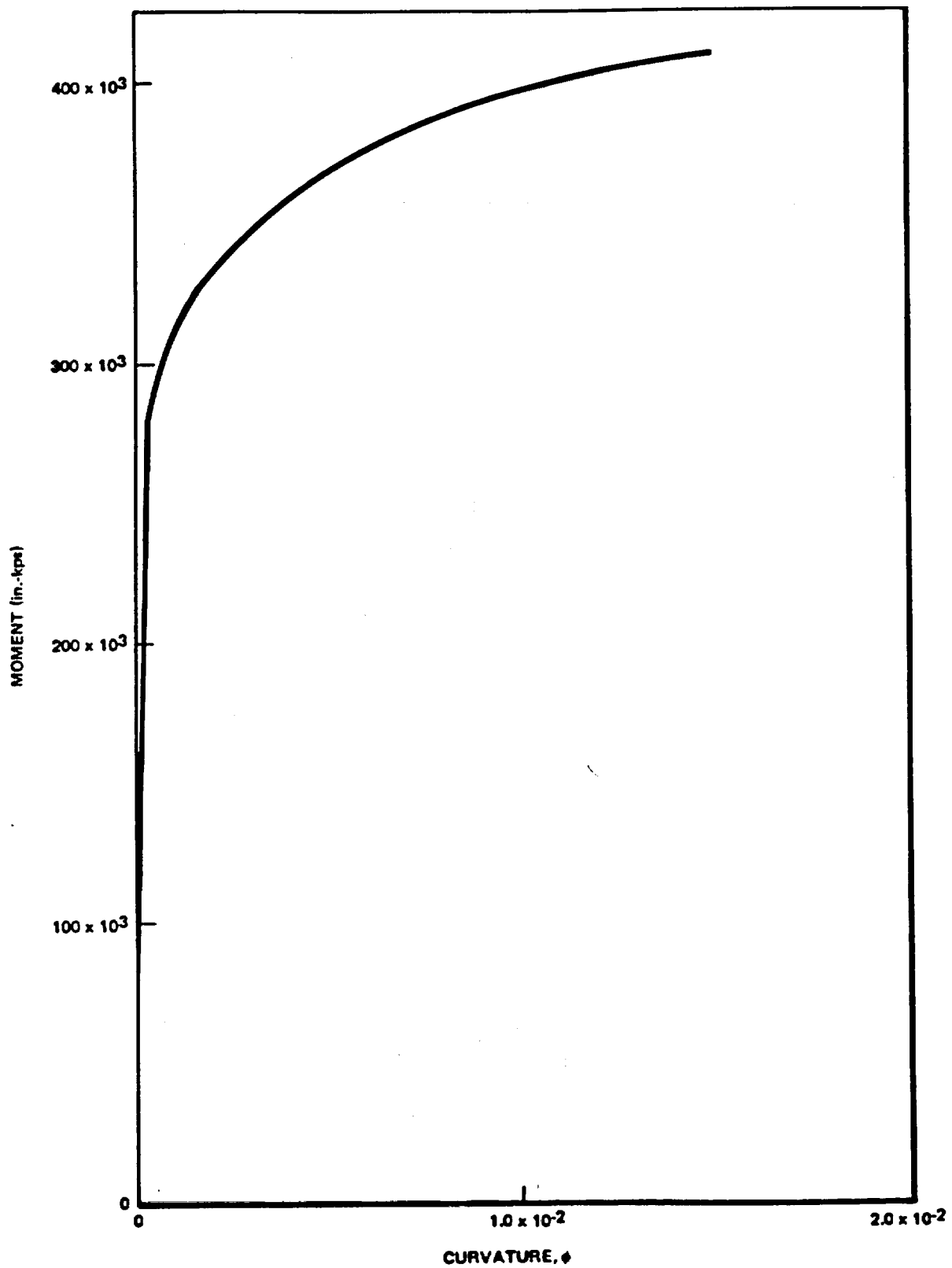
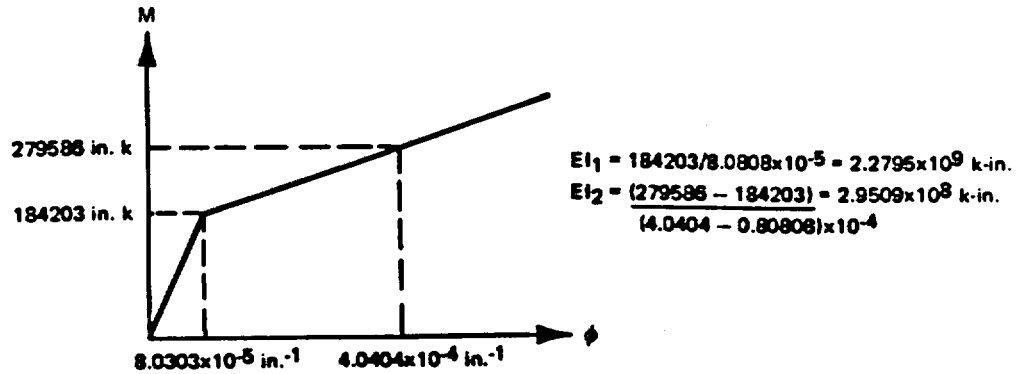


FIGURE V-107. PLOT-CURVATURE VS. MOMENT

Use following bilinear curve:



(b) Shear stiffness of cask:

$$A_s = \frac{\pi}{2} (24.75^2 - 23.25^2 + 19.25^2 - 18.75^2)$$

$$= 142.94 \text{ in}^2$$

$$G = \frac{E}{2(1+\gamma)} = \frac{26500}{2(1+0.28)} = 10352 \text{ ksi}$$

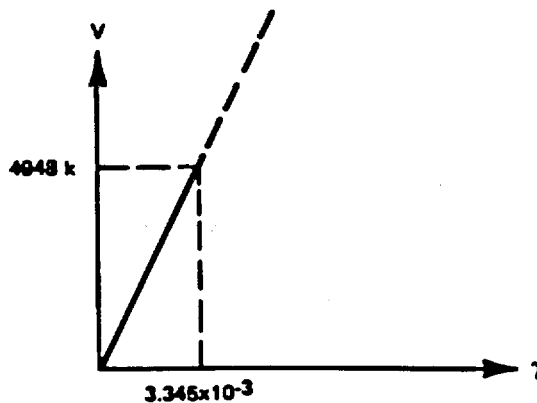
$$A_s G = 142.94 \times 10352 = 1.4797 \times 10^6 \text{ kip}$$

Load to cause yield:

$$\tau_y = 0.577 \times 60 = 34.62 \text{ ksi}$$

$$V_y = 34.62 \times 142.94 = 4948^k$$

Assume cask does not yield in shear during 1 ft drop and use following curve:



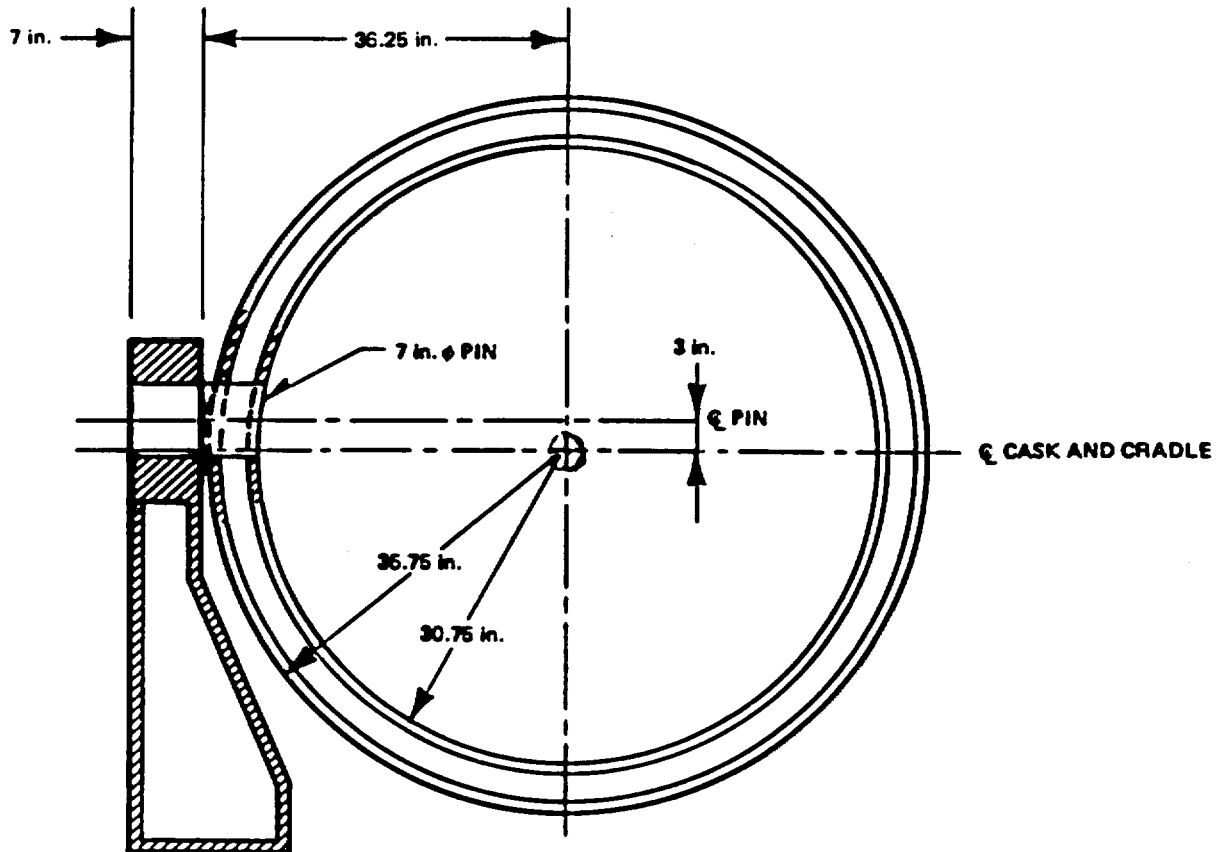
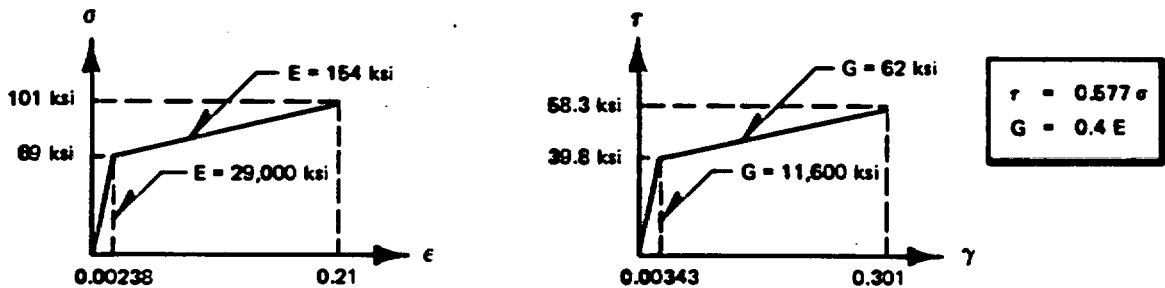
2. Trunnion + Pedestal

(a) Trunnions

Mode of deformation of trunnions is primarily shearing action rather than flexural

Note: Design of trunnions calls for
AISI 4340 steel.

The following assumed stress-strain curves
will be used:



Gap between cradle and pedestal at pin Q_L :

$$l = 36.25 - \sqrt{35.75^2 - 3^2} = 0.626''$$

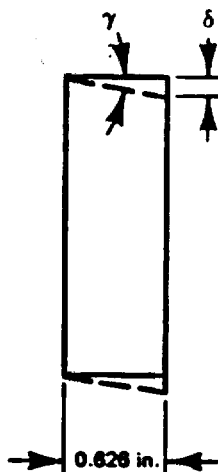
Assume shearing strain constant across pin cross-section.

$$A = \pi \times 3.5^2 = 38.5''^2$$

$$V_y = 38.5 \times 39.8 = 1530^k$$

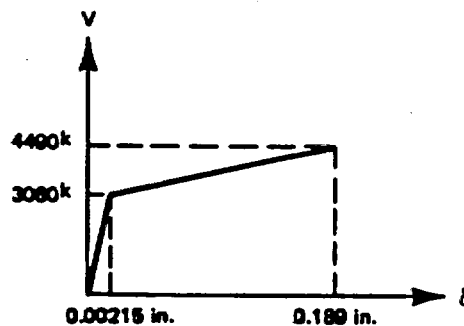
$$V_u = 38.5 \times 58.3 = 2245^k$$

Deformations:



$$\delta_y = 0.00343 \times 0.626 = 0.00215 \text{ in.}$$

$$\delta_u = 0.301 \times 0.626 = 0.189 \text{ in.}$$



V-δ For 2 Trunnions

(b) Pedestal ~ A516 GR 70

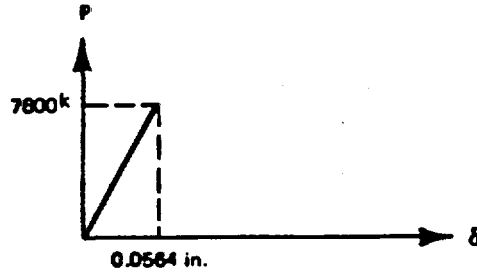
$$\text{Average area} = 100 \text{ in}^2$$

$$\sigma_{yp} = 38 \text{ ksi}$$

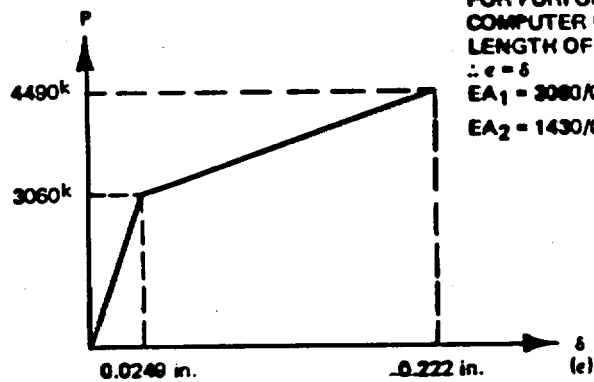
$$\epsilon_y = 38/29000 = 0.00131$$

$$P_y = 100 \times 38 = 3800^k$$

$$\delta_y = 43'' \times 0.00131 = 0.564''$$



P-delta For 2 Pedestals



FOR PURPOSES OF INPUT TO
COMPUTER PROGRAM, USE A
LENGTH OF 1 in. FOR THIS SPRING
 $\therefore \epsilon = \delta$
 $EA_1 = 3060/0.0249 = 1.228 \times 10^5$ kips
 $EA_2 = 1430/0.197 = 7.26 \times 10^3$ kips

Composite Spring
Trunnions + Pedestals

3. Girder Web Underneath Pedestal

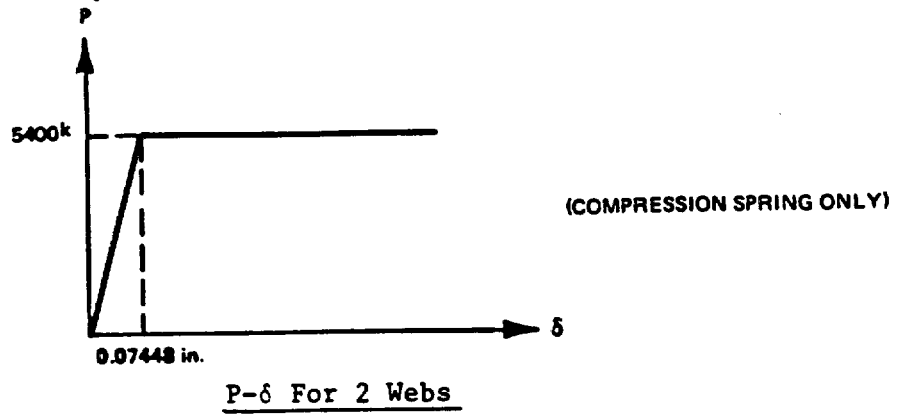
A514 steel $\sigma_{yp} = 90$ ksi

Web thickness = 0.5"

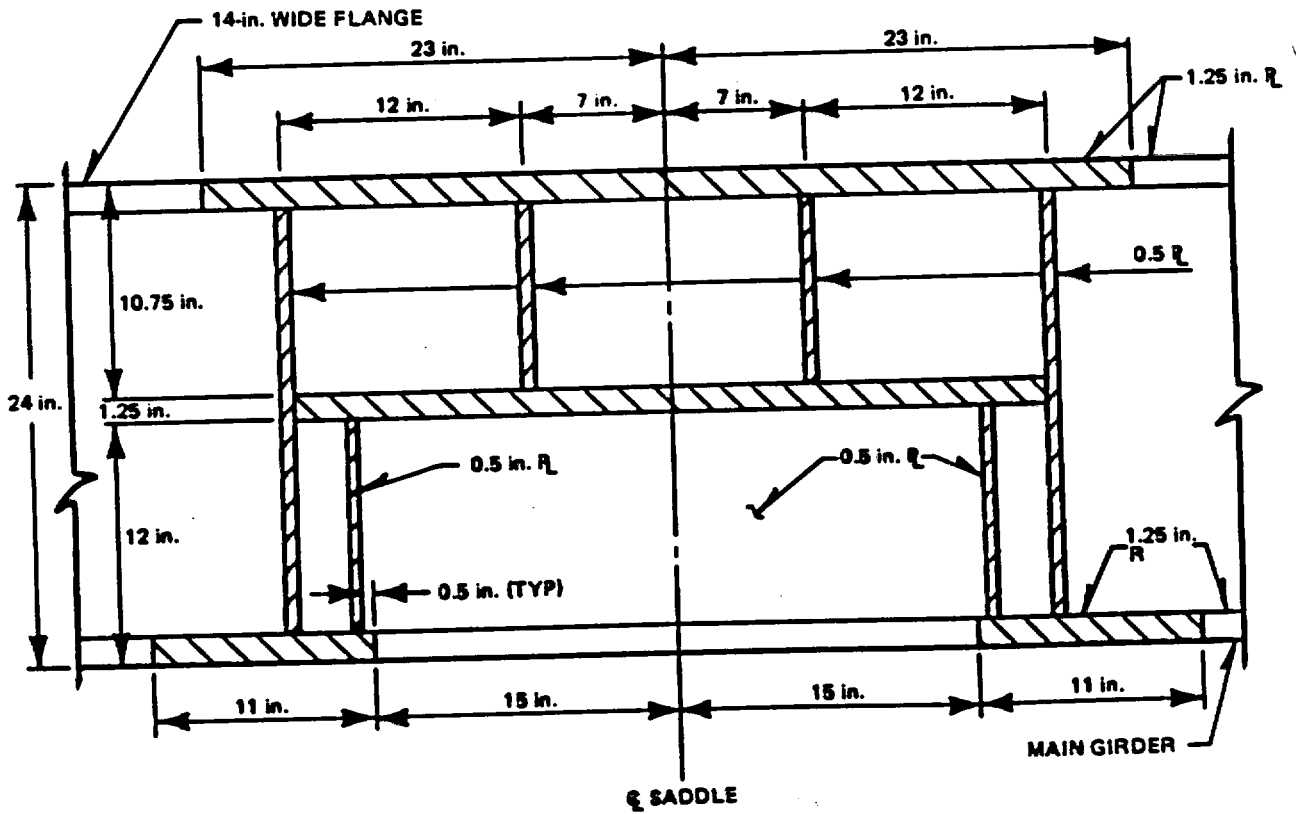
Area @ mid-height = $60 \times 0.5 = 30$ in²

$$P_y = 30 \times 90 = 2700^k$$

$$\delta_y = 24 \times 90 / 29000 = 0.07448''$$



4. Portion of skid underneath front saddle



Section Thru Skid @ Saddle

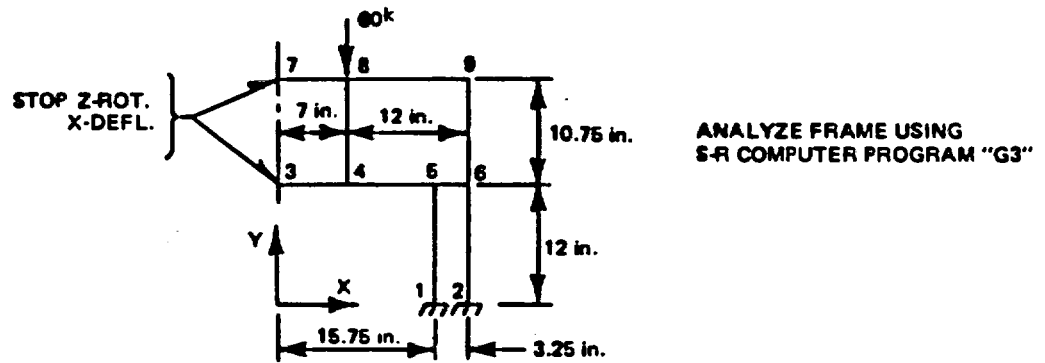
$$\begin{aligned} \text{Wt./Ft of shaded area} &= 0.0034 (1.25 \times 105.5 + 0.5 \times 83.5) \\ &= 0.591 \text{ k/ft.} \end{aligned}$$

$$\text{Center to center spacing of main girders} = 62''$$

$$\text{Total Wt.} = 0.591 \times 5.17 = 3.05^k$$

$$\begin{aligned} \text{Wt. of main beam/ft} &= 0.0034 (1.25 \times 28 + 0.5 \times 21.5) \\ &= 0.1555^k/1 \end{aligned}$$

Determine stiffness of above section:



Member properties: (based on 12" length)

Horizontal members

$$A = 1.25 \times 12 = 15 \text{ in}^2$$

$$A_s = 15/1.2 = 12.5 \text{ in}^2$$

$$I = 12 \times 1.25^3/12 = 1.9531 \text{ in}^4$$

Vertical members

$$A = 0.5 \times 12 = 6 \text{ in}^2$$

$$A_s = 6/1.2 = 5 \text{ in}^2$$

$$I = 12 \times 0.5^3/12 = 0.125 \text{ in}^4$$

$$\text{Stiffness, } k = \frac{2 \times 60}{0.18067} \left(\frac{62}{12} \right) = 3430 \text{ k/in.}$$

Stiffness of girder web:

$$\text{Area @ mid-height} = 0.5 \times 38 = 19 \text{ in}^2$$

$$k = \frac{AE}{l} = \frac{19 \times 29000}{24} = 22958 \text{ k/in.}$$

Increase stiffness by 25% to account for 1/2" diaphragm plates framing into web.

$$k = 1.25 \times 22958 = 28700 \text{ k/in.}$$

$$\text{Total } k = 2 \times 28700 + 3430 = 60830 \text{ k/in.}$$

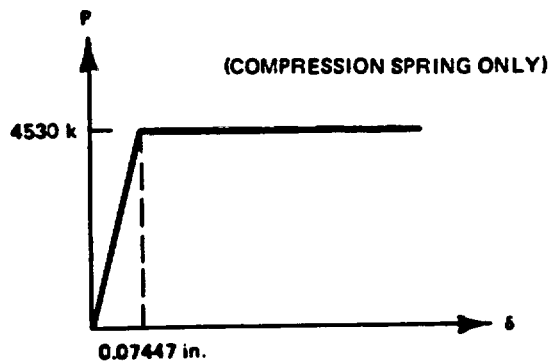
Find equivalent area:

$$60830 = \frac{A \times 29000}{24}$$

$$A = 50.34 \text{ in}^2$$

$$P_y = 50.34 \times 90 = 4530^k$$

$$\delta_y = 4530/60830 = 0.07447''$$



P-δ for Skid Under Saddle

5. Saddle Stiffness (A516 GR 70)

$$A = 60 \times 14 - 57 \times 11 = 213 \text{ in}^2$$

$$k \approx \frac{2900 \times 213}{15} = 412000 \text{ k/in.}$$

This spring will be considered rigid compared to skid.

Translational Masses

$$\text{No. 1: } W = 5^k \quad M = 1.294 \times 10^{-2} \text{ k-sec}^2/\text{in.}$$

No. 2, No. 4 - No. 14:

$$W = 10^k \quad M = 2.588 \times 10^{-2} \text{ k-sec}^2/\text{in.}$$

$$\begin{aligned} \text{No. 3: } W &= 10 + 2.5 + \frac{1}{2} (2 \times 3.17 \times 0.1555 + 3.05) \\ &= 14.5^k \end{aligned}$$

$$M = 3.753 \times 10^{-2} \text{ k-sec}^2/\text{in.}$$

$$\text{No. 15: } W = 5 + 4.25 = 9.25^k$$

$$M = 2.394 \times 10^{-2} \text{ k-sec}^2/\text{in.}$$

$$\begin{aligned}\text{No. 16: } W &= 4.25 + \frac{1}{2} (2 \times 5 \times 0.1555 + 1.25) \\ &= 5.65^k\end{aligned}$$

$$M = 1.462 \times 10^{-2} \text{ k-sec}^2/\text{in.}$$

Rotary Masses

$$M = I\rho\Delta X$$

where I = moment of inertia of cross-section

ρ = mass density

ΔX = spacing of masses

$$\text{Outer Shell: } I = 65208 \text{ in}^4; \rho = 0.284 \text{ lbs./in}^3$$

$$\text{Uranium : } I = 121651 \text{ in}^4; \rho = 0.69 \text{ lbs./in}^3$$

$$\text{Inner Shell: } I = 10776 \text{ in}^4; \rho = 0.284 \text{ lbs./in}^3$$

Masses #2 - #14:

$$\begin{aligned}M &= [(65208 + 10776) \times 2.84 \times 10^{-4} + 121651 \times 6.9 \times 10^{-4}] \\ &= 3.687 \text{ k-in-sec}^2\end{aligned}$$

Masses # 1 and 15:

$$M = 1.8435 \text{ k-in-sec}^2$$

Impact Velocity of Cask:

$$V = \sqrt{2gH} = \sqrt{2 \times 386.4 \times 12} = 96.3 \text{ in/sec}$$

The dynamic analysis will be performed using S-R computer program "Dyrec" which has been developed by Dr. Garry Patterson of Stearns-Roger. See Section 5.6.5.

b. Summary of Results:

1. Cask Outer Shell

$$\text{Max. moment} = 0.98393^{\text{k}} @ t = 0.00605 \text{ sec in members 7-8}$$

$$\phi = 1.289 \times 10^{-4} \text{ in}^{-1}$$

$$E = R\phi = 24.75 \times 1.289 \times 10^{-4} = 0.00319$$

Some slight yielding has occurred on localized outermost fibers. No cross-sectional wall effects.

Max. shear = 4145^{k} @ $t = 0.00554$ sec in members 4-5.
Since $4145^{\text{k}} < 4948^{\text{k}}$, no yielding occurs.

2. Trunnion

$$\text{Max. force} = 3438^{\text{k}} @ t = 0.00807 \text{ sec}$$

$$\tau = 3438/77 = 44.65 \text{ ksi}$$

$$\gamma = 0.00343 + (44.65 - 39.8)/62 = 0.0816$$

Some yielding has occurred.

3. Pedestal

Max. force = 3438^k @ $t = 0.00807$ sec

Since $3438^k < 7600^k$, no yielding occurs.

4. Girder Web Under Pedestal

Max. force = 3946^k @ $t = 0.00121$ sec

Since $3946^k < 5400^k$, no yielding occurs.

5. Skid Underneath Front Saddle

Max. force = 4530^k @ $t = 0.00094$ sec

Skid yields at this force until $t = 0.00368$ sec

$\delta_{\max} = 0.1742''$ small enough to be considered as
localized at point of contact

$\epsilon_{\max} = 0.1742/24 = 0.00725$

Although some yielding has occurred in the system, the max. strains are seen to be small. The analysis was performed for a time duration = 0.12 sec (20 millise). Within this time, the skid has impacted the unyielding surface and rebounded upwards. Any subsequent impacts will be less severe than the initial impact. For this reason, the program was not continued further in time.

c. Neutron Shielding Barrel Under 1' Drop Conditions.

The analysis will examine a single corrugation since the principal stress consideration is circumferential. The methodology is based on the absorption of the barrel and water kinetic energy by elastic deflection of the barrel.

Figure V-108 shows the stressed barrel cross-section in the circumferential direction. For purposes of this analysis, only 270° of the circumference will be assumed to act in absorbing the energy.

The cross-sectional area of one convolution is:

$$A = \pi (0.6875^2 - 0.5625^2) + (1.9375 - 2 \times 0.6875) (0.125)$$

$$= 0.631 \text{ in}^2/\text{convolution}$$

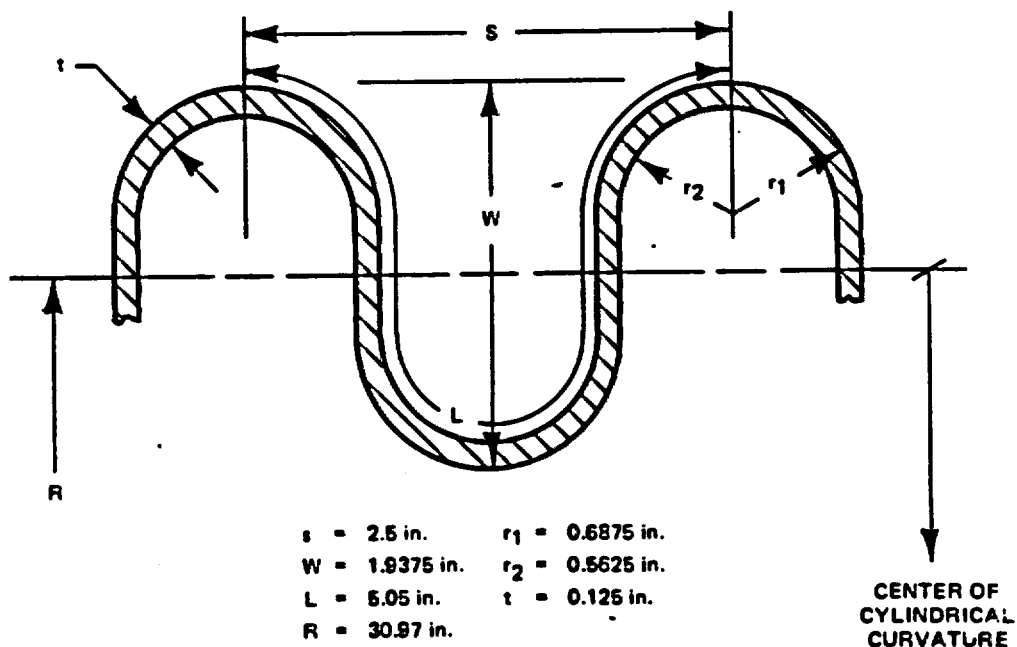


FIGURE V-108. STRESSED BARREL CROSS SECTION

The outer fiber circumference is:

$$\begin{aligned} C &= 2\pi R = 2\pi \left(30.97 + \frac{1.9375}{2} \right) \\ &= (31.94")2\pi \\ &= 200.67 \text{ in.} \end{aligned}$$

Based on actual measurements, the water volume encompassed by one corrugation is:

$$\begin{aligned} V &= \frac{252 \text{ gal}}{58.5 \text{ in}} \times 2.5 \text{ in/corr} - (\text{void vol/corr}) \\ &= 10.8 \text{ gal} - 1.0 \end{aligned}$$

Yielding a water weight of:

$$W_t = (9.8) (8.64) = 75 \text{ lbs.}$$

The barrel weight per corrugation is approximately 35 pounds. This weight will be added to that of the water, since, from a hydrostatic viewpoint, the water is "supporting" the barrel.

Therefore, total effective weight per corrugation length is:

$$W = 75 + 35 = 110\#$$

Thus, the 1' drop kinetic energy per corrugation is:

$$KE = 1 \times 110\# = 110 \text{ ft-lbs.}$$

If the barrel can absorb this amount of kinetic energy elastically, then no reduction in effectiveness will occur due to the 1' drop. The energy absorbing characteristics of the barrel can be obtained by examining the amount

of circumferential elongation available before yield and multiplying this by one-half the product of the stressed area and the yield strength.

$$KE_{ABS} = (\Delta l_c) \left(\frac{1}{2} \times A \times \delta_{yp} \right) \text{ in-lbs.}$$

The Δl_c should be adjusted for any existing barrel strain due to internal pressure.

$$\text{Stress in barrel @ 200 psig} = 24,025 \text{ psi}$$

From this

$$\begin{aligned} \epsilon &= \frac{\delta}{E} = \frac{2.4 \times 10^4}{25 \times 10^6} \\ &= 9.6 \times 10^{-4} \text{ (0.00096)} \end{aligned}$$

For the portion of the barrel under consideration:

Yield point is defined at a strain of 0.002; therefore, the elastic deformation is:

$$\begin{aligned} \Delta l_c &= (0.002 - 0.00096) \left(\frac{200.67 \times 270^\circ}{360^\circ} \right) \\ &= 0.157 \text{ in} \end{aligned}$$

Computing the energy absorbing capabilities

$$\begin{aligned} KE_{ABS} &= (0.157) \left(\frac{1}{2} \right) (0.631) (29,500) \frac{1}{12} \text{ ft-lbs} \\ &= 122 \text{ ft-lbs} \end{aligned}$$

Thus, the barrel is capable of elastically absorbing the 1' drop kinetic energy. The safety factor is

$$SF = \frac{122}{110} = 1.11$$

d. IF-300 Cask Barrel Expansion Tanks Under 1-foot Drop Conditions

1. Discussion:

The descriptive drawings show the stainless steel tanks which are mounted on the IF-300 cask to accommodate shielding water expansion. The barrel itself has been evaluated under 1-foot drop conditions and found to be capable of sustaining such loads. This analysis examines the expansion tanks under similar loading conditions.

Previous sections contain the details of a dynamic spring-mass model of the IF-300 cask. As discussed, the response of the cask under the 1-foot drop is best described as vibratory. The peak deceleration was 210 g's with the total time from zero to peak and back to zero being about 0.0005 second this is shown on Figure V-110 for node 7. For simplicity in analysis, the barrels were examined assuming a static load of 210 g's. Yield strength of the material will be used as the basis of the safety factor. Figure V-109 is from the International Nickel Company Stainless Steel Handbook for 304 SST under Compressive Loading. Tensile yield of 304 SST is taken as 34000 psi.

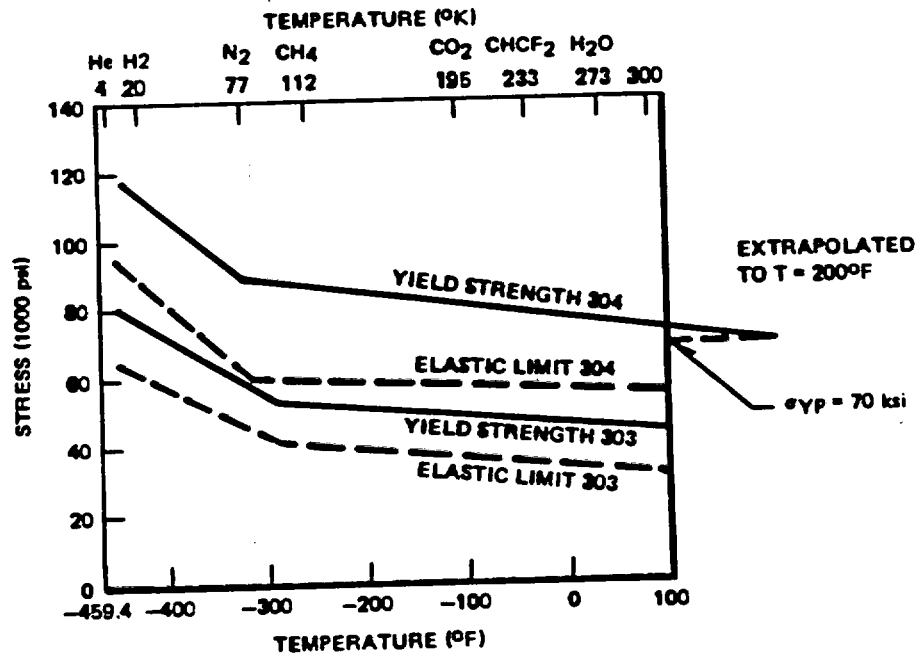


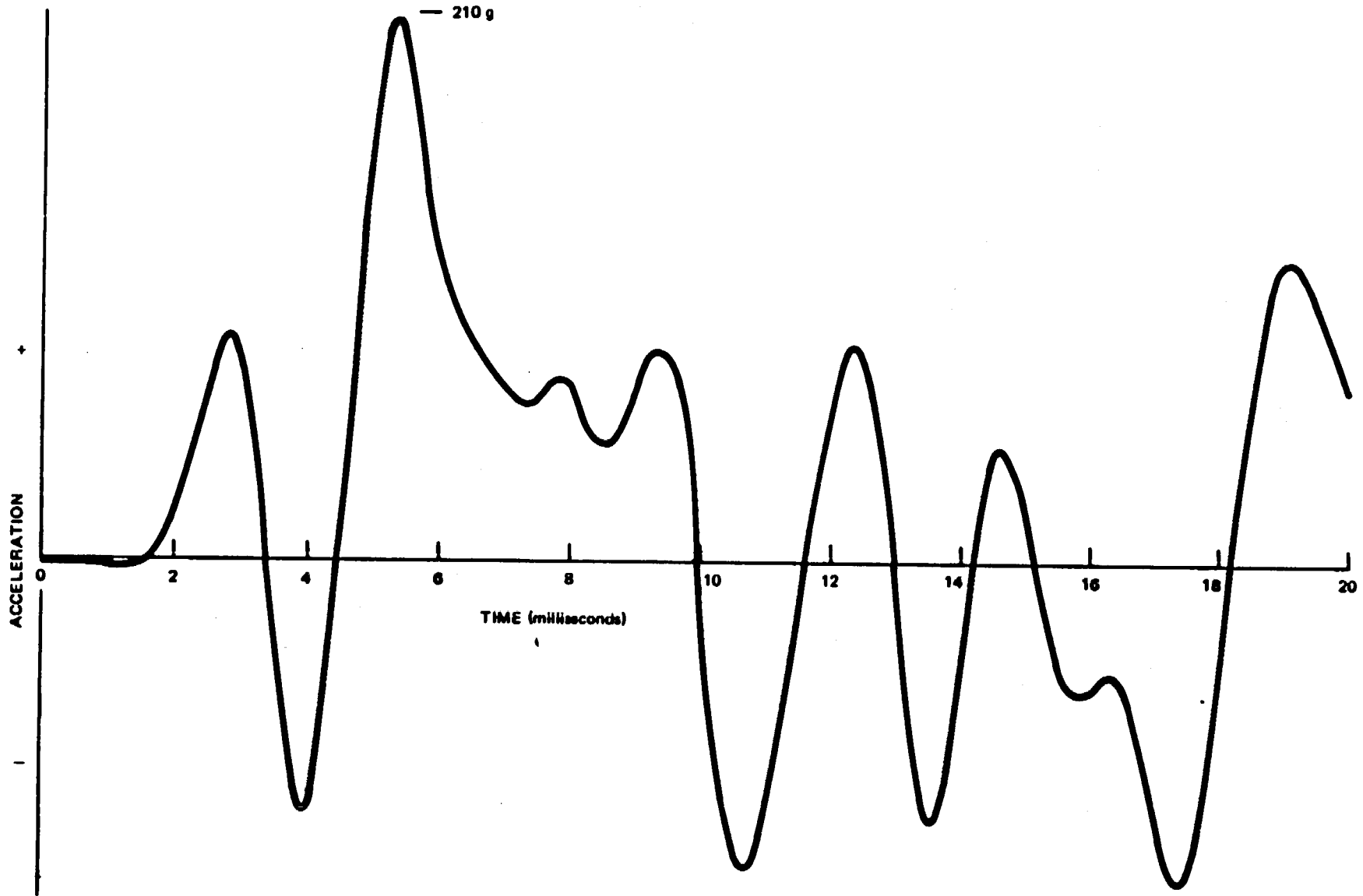
FIGURE V-109. COMPRESSIVE YIELD STRENGTHS AND ELASTIC LIMITS OF TYPES 303 AND 304 STAINLESS STEELS

2. Analysis:

The following calculations are based on the lower expansion tank shown on Sheet 8 of the reference drawings 159C5238. This tank, or tank pair, is the heavier of the two. The mounting brackets for either set of tanks are identical. Critical areas are examined

(a) Force applied to the tank:

$$\begin{aligned}
 F &= (\text{tank} + \text{water WT}) \times g \\
 &= 250 \text{ lbs} \times 210 \text{ g} = 52500 \text{ lbs}
 \end{aligned}$$



NEDO-10084-3
September 1984

FIGURE V-110 ACCELERATION Vs. TIME FOR NODE 7 - EXPANSION TANK ELEVATION
(ANALYSIS FOR 1 FOOT DROP)

(b) Bracket-to-tank weld

The bracket circumference is welded to the tank head.

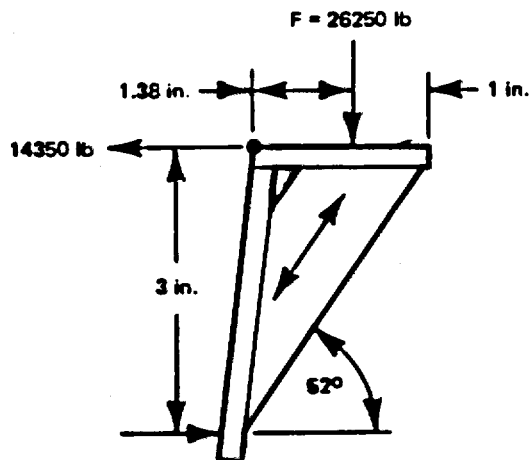
$$\begin{aligned} A_W &= (2 \times 8'' + 2 \times 2'') \times 0.25 \times 0.707 \\ &= 3.535 \text{ in}^2 \end{aligned}$$

Since there are two brackets:

$$A_{WT} = 2 \times 3.535 = 7.07 \text{ in}^2$$

$$\begin{aligned} \text{Stress in weld} &= \frac{F}{A} = \frac{52500}{7.07} \\ &= 7426 \text{ psi} \end{aligned}$$

(c) Front bracket stresses



The bracket-to-fin weld area is greater than the bracket-to-tank weld area, therefore it is acceptable. The bracket itself will be analyzed as a truss.

NEDO-10084-3
September 1984

$$F = \frac{1}{2} (52500 \text{ lbs}) = 26250 \text{ lbs}$$

Compressive force in the rib will be

$$@52^\circ F_C = \frac{26250}{\sin 52^\circ} = 33500 \text{ lbs}$$

Area of the three ribs:

$$A = 2(1.0 \times 0.25) + 1.0 \times 0.5 = 1.0$$

$$\therefore \text{Compressive stress} = \frac{33500}{1.0} = 33500 \text{ psi}$$

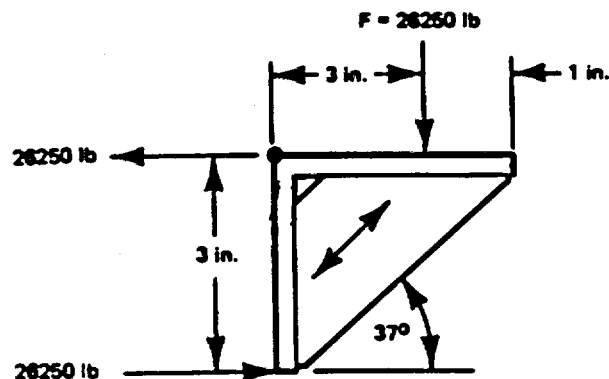
Compressive yield strength = 70,000 (304SST)

$$SF = \frac{70000}{33500} = 2.09$$

The tension stress in the horizontal member is

$$\begin{aligned} \sigma &= \frac{F}{A} = \frac{14350 \text{ lbs}}{0.25 \times 8.0} \\ &= 7175 \text{ psi} \end{aligned}$$

(d) Rear bracket stresses



The bracket-to-valve box weld area is greater than the bracket-to-tank weld area, therefore it is acceptable. As with the front bracket, the rear bracket will be treated as a truss.

$$F = \frac{1}{2} (52500) = 26250 \text{ lbs}$$

Compressive force on rib is

$$F_C = \frac{26250}{\sin 38^\circ} = 43750 \text{ lbs}$$

Area of three ribs:

$$A_R = 2 (1.5 \times 0.25) + 1.5 \times 0.5 = 1.5$$

Compressive stress in rib

$$\sigma = \frac{43750}{1.5} = 29,167 \text{ psi}$$

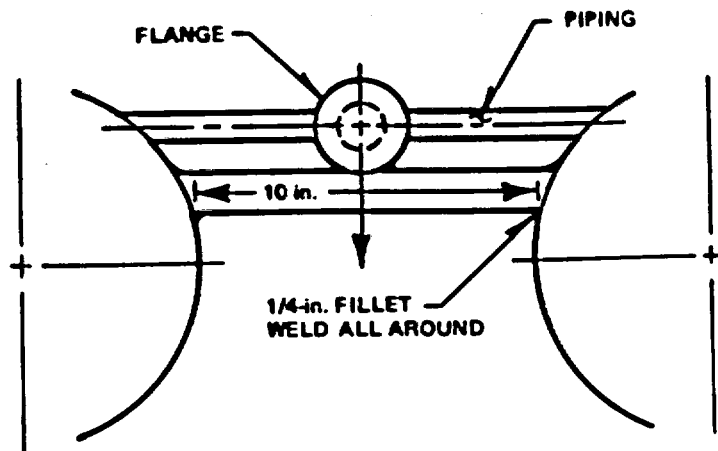
$$SF = \frac{70000}{29167} = 2.4$$

Tension in horizontal member

$$\sigma = \frac{F}{A} = \frac{26250}{(0.25 \times 8)} = 13125 \text{ psi}$$

$$SF = \frac{34000}{13125} = 2.6$$

(e) Stress in the relief valve support bar



The relief valve support bar runs between the two surge tanks directly beneath the valve attachment flange. This bar prevents the valve from applying any torque or force on the cross-over piping.

Support bar 1" x 0.5" x 10" lg. 304 SST.

Yield strength = 34000 psi

Bending:

Wt of valve and flange = 3 lbs.

$F = 210g \times 3 \text{ lbs} = 630 \text{ lbs}$ applied at midspan

$$\text{Built-in beam } M_{\max} = \frac{FL}{8} = \frac{(610)(10)}{8}$$
$$= 762.5 \text{ in-lbs.}$$

$$I = \frac{bh^3}{12} = \frac{(0.5)(1.0)^3}{12} = 0.0417 \text{ in}^4$$

$$c = 0.5$$

$$\therefore \text{Max bending stress} = \frac{Mc}{I} = \frac{(762.5)(0.5)}{0.0417}$$
$$= 9150 \text{ psi (LOW)}$$

Shear at welds

Weld size = 1/4"

Min weld thickness = $(0.707)(0.25) = 0.177 \text{ in.}$

Weld length = $2[2 \times 0.5 + 2 \times 1.0] = 6 \text{ in.}$

$$\begin{aligned}\text{Weld area} &= 6 \text{ in} \times 0.177 \text{ in} \\ &= 1.06 \text{ in}^2\end{aligned}$$

$$\text{Shear in weld} = \frac{F}{A}$$

$$V_w = \frac{630 \text{ lbs}}{1.06} = 594 \text{ psi (LOW)}$$

Shear in bar

$$F = 610$$

$$A = 0.5 \times 1.0 = 0.5$$

$$V_B = \frac{610}{0.5} = 1220 \text{ psi (LOW)}$$

The presence of the support bar prohibits movement of the relief valve assembly and hence no loading is transmitted to the cross-over piping. The stress levels in the support bar and attachment welds are low even under a static 210g deceleration.

e. Conclusion

This analysis under the very conservative assumption of a 210g static loading of the tanks demonstrates that the brackets and valve piping are more than capable of sustaining the one-foot drop without damage.

5.11.4 Penetration Protection

This section deals with the vulnerability of cask components to missile damage. First the various missiles are defined, then the vulnerable cask areas are identified. Finally, the effects of missile damage are examined.

5.11.4.1 Missiles

There are three categories of missiles to be considered here, those thrown from the side, those dropped from above, and those fired from the side.

a. Thrown Object

The thrown object would be a rock and might be considered as a five-inch diameter sphere of concrete weighing approximately five pounds. This represents about the heaviest object which an individual can throw a short distance. Several such objects can be considered.

b. Dropped Object

The dropped object could be handled by two individuals and does not require propelling. The maximum weight of this object is assumed to be 150 pounds and is in the form of a six-inch diameter by 1-1/2-foot long steel cylinder. The six-inch diameter pin was chosen because it corresponds to the 40-inch drop puncture peg of 10 CFR 71. The dropped height is considered to be 15 feet, yielding 2250 ft-lb of energy. A single such object can be considered.

c. Fired Object

The fired object is quite difficult to define. An upper limit would appear to be a 30 caliber rifle as used for deer hunting, with soft-nosed ammunition. A single such object can be considered.

It is assumed that the package is in motion when the objects are projected at it. Furthermore, it is assumed that the incidents are random occurrences against a train rather than specific attacks

directed at the IF 300 cask. On this basis, the probability of occurrence is quite low.

5.11.4.2 Protection Provided by Enclosure

The primary purpose of the enclosure is personnel exclusion. However, with solid, braced ends and roof and braced, expanded metal sides, penetration of the enclosure from side-thrown objects is virtually impossible. Penetration is more probable from the dropped object. The ductility of the panels and the braces will absorb some of the kinetic energy and the mere presence of the roof will tend to deflect the dropped object, particularly when the cask is in motion.

The enclosure offers little penetration protection from the fired object. However, two events could occur, a deflection of the projectile and/or a deformation (flattening) of the projectile. Both of these tend to protect the cask.

5.11.4.3 Vulnerability of Equipment

Before discussing the inherent ruggedness and redundancy of the shipping cask and support equipment, it is necessary to identify those areas which are the most vulnerable to damage by the missiles defined in 5.11.4.1 above. From the argument of 5.11.4.2, there are only two objects, dropped and fired, which are capable of penetrating the screened enclosure.

The areas most vulnerable to penetration are the cask water jacket and the mechanical cooling system. The cooling system has no effect on safety and is not discussed.

The corrugated water jacket surrounding the cask provides neutron shielding as well as heat removal area. The structure is 1/8-inch thick 304 stainless steel. It is fabricated to ASME code specifications and has a pressure rating of 200 psig. The corrugations which provide

an increased surface area also lend strength to the cylindrical structure. On the basis of the shell penetration correlation recommended in NSIC-68, Cask Designer's Guide, the water jacket is capable of absorbing a minimum of 14,000 ft-lb without puncturing. Since the dropped object kinetic energy is only 2250 ft-lb, the water jacket cannot be penetrated. Furthermore, this analysis ignores the strengthening effect of the corrugations.

The fired object is the only one which has a possibility of penetrating the water jacket. If the missile strikes the surface at an angle, there is a good chance that it will deflect without puncturing. However, in the event there is penetration, only half of the water can be lost. The barrel has been partitioned at the cask midlength such that a loss of water in one half will not result in a loss of the remaining half.

Heat transfer calculations (See Section 6) considering one neutron shielding cavity empty indicate that the other half is capable of dissipating the added heat load without raising either the cask inner cavity temperature or the remaining shielding water temperature beyond acceptable limits.

Table V-47, compares the normal and 50% shielding water loss temperatures and dose rates under 262,000 Btu/hr, wet shipment conditions.

Table V-47
TEMPERATURES AND DOSE RATES

<u>Event</u>	<u>Coolant Temperature</u>	<u>Six-Foot Total Dose Rate</u>
Normal Cooling	302°F	9.42 mRem/hr
50% Loss of Shield Water	409°F	20 mRem/hr

5.11.4.4 Integrity of Corrugated Water Jacket

The resistance of the corrugated water jacket to missile penetration was discussed in Subsection 5.11.4.3. This section will outline the fabrication quality assurance program pertaining to the barrel and the in-service inspections which are instituted to check on integrity.

a. Design and Fabrication

The corrugated structure provides a significant amount of additional strength and resistance to damage over a flat-sided cylinder of comparable diameter, evidenced by applications in roofing, frameless trailers, culvert pipes and other structural uses. Thus, the corrugated water jacket is an extremely rugged structure. It is designed and fabricated by an established expansion joint manufacturer to ASME specifications. Expansion joints of this size have been used for years in chemical and power generation applications under severe thermal conditions with an excellent record of reliability. The structure is made of 304 stainless steel having a wall thickness of 1/8 inch. The barrel is rated at 200 psig design pressure.

To assure the highest quality structure, the water jacket fabrication is done using the ASME code, where applicable. All material is certified as meeting minimum strength requirements. Each weld is non-destructively tested by accepted non-destructive testing methods. This includes both barrel fabrication and barrel attachment welds. Once the water containment is attached to the cask body, it is hydrostatically tested to 200 psig as an acceptance test, in addition to the other NDT methods.

b. In Service

Once in service, the barrel is hydrotested at least annually at 80 psig. Visual inspection for leakage or cracking is performed prior to every shipment. Repairs, if required, are performed and inspected under the same standards as the original fabrication.

The flexible nature of the expansion joint makes it less susceptible to vibratory and handling stresses than a flat-sided cylinder under similar conditions. Flat-sided cylinders of comparable size (tank cars, etc.) have been used for years for the railroad transport of liquids with few failures. Thus, there is only an exceedingly remote possibility that any leak could develop in the barrels during the course of transportation.

5.11.5 Summary on Reliability

The IF 300 spent fuel shipping package has been designed in full accordance with the intent of 10 CFR 71. All parts are of the highest quality and the fabrication follows the strictest standards for workmanship.

The design has carefully considered all aspects of equipment performance. The system is fully redundant, as no single event except the hypothetical accident will result in any release of radioactive materials from the cask. The events considered are:

1. 1 foot drop of the cask/skid in its normal transport orientation
2. Fired missile penetration of the corrugated water jacket or ducting
3. Dropped object penetration of the corrugated water jacket or ducting
4. Thrown missiles

The basis of the reliability of such a shipping package is the degree of preventive maintenance and inspection performed in service. All vital components of the system are periodically checked in accordance with written procedures. Procedural controls are strictly enforced to ensure that the equipment will be performing as designed each time it is dispatched to a reactor site and each time a loaded container is released to a carrier for transport.

In summary, the IF 300 shipping package will provide years of safe, dependable service in the movement of irradiated fuel assemblies.

5.12

SECTION CONCLUSION

This section has examined the IF 300 shipping package design under normal and accident conditions. Under even the most conservative assumptions, the cask and associated equipment totally comply with the requirements of 10 CFR 71.

5.13

REFERENCES

The references listed below, one through 20, are those referenced in the text. Under Section 5.13.1 are listed other references that have been used at various times throughout the history of the IF-300 cask.

1. "Reactor Handbook, Vol. I - Materials," 2nd Edition, C.R. Tipton, Jr.
2. "Strength of Materials," Parts I and II, 3rd Edition, Timoshenko.
3. "Formulas for Stress and Strain," 4th Edition, Raymond J. Roark.
4. "Theory of Elastic Stability," S. Timoshenko, 1st Edition.
5. C.E. Coleman, D. Mills, J. Van Der Kuur. "Deformation Parameters of Neutron-Irradiated Zircaloy-4 at 300°C", Canadian Met. Quart. 11 (1), 1972, p. 91.

6. A.A. Wells. "Application of Fracture Mechanics at and Beyond General Yielding", British Welding Journal, November 1968, p. 563.
7. R.C. Hoagland and R.G. Rowe, "Fracture of Irradiated Zircaloy-2", J. Nucl. Mats. 30, 1969, p. 179.
8. H.T. Corten and A.K. Shoemaker. "Fracture Toughness of Structural Steels as a Function of the Rate Parameters $\dot{T}ln(A/\dot{c})$ ", J. Basic Eng. Trans. ASME 89, 1967, p. 86.
9. J.M. Krafft and A.M. Sullivan. "Effects of Speed and Temperature on Crack Toughness and Yield Strength in Mild Steel." Trans ASM 56, 1963, p. 160.
10. B. Watkins, A. Cowan, G.W. Parry and B.W. Pickles. "Embrittlement of Zircaloy-2 Pressure Tubes" ASTM-STP-458, 1968, p. 141.
11. A. Cowan and W.J. Langford. "Effects of Hydrogen and Neutron Irradiation on the Fracture of Flawed Zircaloy-2 Pressure Tubes", J. Nucl. Mats. 30, 1969, p. 271.
12. J.H. Schemel. "Tension Testing Variables in Zirconium", ASTM-STP-458, 1968, p. 347.
13. J.B. Melehan. "Yankee Core Evaluation Program, Final Report", WCAP-3017-6094, January 1971.
14. D. Lee. "The Strain Rate Dependant Plastic Flow Behavior of Zirconium and Its Alloys, Met. Trans. 1, 1970, p. 1607.
15. D.S. Clark. "The Influence of Impact Velocity on the Tensile Characteristics of Some Aircraft Metals and Alloys", NACA Technical Note No. 868.

16. W.K. Anderson, C.J. Beck, A.R. Kephart and J.S. Theilacker. "Reactor Structural Materials: Engineering Properties as Affected by Nuclear Service", ASTM-STP-314 (1962), p. 62.
17. R.L. Knecht and P.J. Panakaskie. "Zircaloy-2 Pressure Tubing", USAEC Report BNWL-746, Dec. 1968.
18. G.T. Hahn and A.R. Rosenfield. "Mechanics and Metallurgy of Brittle Crack Extension", BMI Progress Report to Ship Structure Committee, Project SR-165, September 12, 1966.
19. D.G. Hardy. "The Effect of Neutron Irradiation on the Mechanical Properties of Zirconium Alloy Fuel Cladding on Uniaxial and Biaxial Tests", ASTM-STP-484, 1979, p. 215.
20. "Elasto-Plastic Response of Timoshenko Beams", R.K. Wen and N. Beylerian, Journal of the Structural Division, ASCE, June, 1967.
21. "Irradiated Fuel Shipping Cask Design Guide," L.B. Shappert, ORNL-TM-2410, January 1969.
22. "Aircraft Structures," David J. Perry, McGraw-Hill, 1950.
23. "Single Bellows Design Analysis," Pathway Bellows Incorporated, June 22, 1971.
24. "Fundamentals of Earthquake Engineering", N.M. Newmark and E. Rosenblueth, p. 109.
25. T. Ishizaki and K.J. Bathe. "On Finite Element Large Displacement and Elastic-Plastic Dynamic Analysis of Shell Structures", Computers and Structures, Vol. 12, pp. 309-318, 1980.

26. K.J. Bathe, E. Ramm and E.L. Wilson. "Finite Element Formulations for Large Deformation Dynamic Analysis", International Journal for Numerical Methods in Engineering, Vol. 9, pp. 353-386, 1975.
27. K.J. Bathe and H. Ozdemir. "Elastic-Plastic Large Deformation Static and Dynamic Analysis", Computers and Structures, Vol. 6, pp. 81-92, 1976.
28. K.J. Bathe and S. Bolourchi. "Large Displacement Analysis of Three-Dimensional Beam Structures", International Journal for Numerical Methods in Engineering, Vol. 14, pp. 961-986, 1979.

5.13.1 Other References

The following references have also been used during design and development of the IF-300, but are not specifically referenced in this test.

- "ASME Boiler and Pressure Vessel Code," 1968, Section II and Section III.
- "Elements of Strength of Materials," 4th Edition, Timoshenko and Young.
- NRC "10 CFR Part 71."
- "General Notes," FRO 028, General Electric Company.
- "Rings and Arcuate Beams," Alexander Blake, Product Engineering, January 7, 1968.
- "Behavior of Stainless Steel Columns and Beams", A.L. Johnson and C. Winter, Transactions, ASCE, Vol. 92, No. ST5, Oct. 1966, Pages 97-118.

- "Structural Analysis of Shipping Casks, Vol. 6 - Impact Testing of a Long Cylindrical Lead-Shielded Cask Model," B.B. Klima, L.B. Shappert, and W.C.T. Stoddart, ORNL-TM-1312, March 1968.
- "Resistance of Materials," 4th Edition, Seely and Smith.
- "Pressure Vessel and Piping Design," Collected Papers of the ASME, 1927-1959.
- "Design of Maching Elements," 3rd Edition, V.M. Faires.
- AISC "Manual of Steel Construction," 6th Edition.
- "Bulletin 06-158," April 1969; "Bulletin 06-065," December 1967; and "Selection Guide to Molycote Solid Film Lubricants," Form No. 06-144, Engineering Products Division, Dow-Corning Corporation, Midland, Michigan.
- "Structural Design for Dynamic Loads," C.H. Norris, et al.
- "Demonstration Fuel Element Shipping Cask from Laminated Uranium Metal-Testing Program," C.B. Clifford.
- "The Railroad Environment - A Guide to Shippers and Railroad Personnel," Technical Research Department, New York Central Railroad Company, 1966.